ROLE OF INHIBITORY NEURON TYPES OF THE TRN IN AUDITORY PROCESSING

Solymar Rolón Martínez

A DISSERTATION

in

Neuroscience

Presented to the Faculties of the University of Pennsylvania

in

Partial Fulfillment of the Requirements for the

Degree of Doctor of Philosophy

2023

Supervisor of Dissertation

Maria N. Geffen, PhD
Associate Professor of Otorhinolaryngology

Graduate Group Chairperson

Joshua I. Gold, PhD
Professor of Neuroscience

Dissertation Committee:
(Chair) Dr. Minghong Ma, PhD, Professor of Neuroscience
Dr. J. Nicholas Betley, PhD, Associate Professor of Biology
Dr. Diego Contreras, MD, PhD, Professor of Neuroscience
(External) Dr. Julie Haas, PhD, Associate Professor of Biological Sciences, Lehigh University

This thesis is dedicated to my family: my mom & dad, sister, and nephews.

To Chane: may this serve as an example that you can accomplish anything you ever dream of. Tití te ama.

ACKNOWLEDGMENTS

The work presented in this dissertation could not have been done without the help and support of so many people. Firstly, I would like to acknowledge all the animals that were sacrificed for this work. Thank you for always behaving, I think I only got bit once or twice, and for that I am grateful. May your lives during the length of my experiments have been full of treats and proper care. Secondly, I want to acknowledge and thank Dr. Maria N. Geffen, my mentor. Maria, you opened your lab doors to me, a bright-eyed eager graduate student with zero experience in the auditory neuroscience world. You gave me the tools to dive into this field with optimism, hope, and tenacity. We worked together to make what seemed like an impossible project at times, an incredible body of work. I would not be the scientist I am today without having been in your lab. I respect and admire your strong presence as a female scientist in a male-dominant field; I have learned so much from just watching you navigate these spaces. You have been a kind and understanding mentor; one that has given me the space to handle the emotions that come from being in graduate school without ever losing hope in me. I am forever grateful for your mentorship.

I would like to thank my fellow Geffen lab members, past and current. I want to especially thank Dr. Katherine Wood. You taught me everything that I know from surgical techniques to code. I knew that I could always come to you with any questions I had. I am glad I was able to continue and finish this journey with you in the lab. Secondly, I want to thank Dr. Jennifer Blackwell, one of my fellow Geffen Lab graduate students. You taught me just about everything on how to navigate grad school, and for that I am forever grateful. Not only did you teach me the ins and outs of Penn and lab, but you also rekindled my love for reading and teaching. I cannot express how much those day-day conversations about books, the state of the world and academia, helped me grow as a human. I am forever grateful to you for always listening and giving me advice, and I am so happy to see you grow as an educator, a passionate advocate, and just an awesome

human being. To Dr. Christopher Angeloni, I do not know how to summarize how grateful I am for your help, guidance, and support during my thesis years. You are one of the humblest human beings I have ever met, and I was blessed to be able to work with you for so long. I am forever grateful for all the times you dropped whatever you were doing to help me with anything I needed help with, even to find objects that were right next to me. You were always patient when I would come to you speaking in what you coined as the Solymar-language. I truly could not have done any of this work without your support, all the fun conversations and laughter, and silly little fights about music, math, art, and just about everything. I wish you nothing but the best, and I cannot wait to see what the future has in store for you (PS: math sux ;)). I want to thank Dr. Alexandria Lesicko, another gem of a human that I have had the privilege of working alongside. Thank you for always listening to me rant while you did surgeries, especially during my last year of grad school, and for your words of encouragement during the writing of this dissertation. Your genuine love of science and humbleness towards your awesomeness has and always will be something I will admire forever. Thank you, and I am excited to see what you do next! Last but certainly not least, to everyone else in the lab: thank you for listening to my ideas, offering advice and for being genuinely awesome human beings, keep at it!

I would like to thank the members of my committee and the Neuroscience Graduate Group. Drs. Minghong Ma, Diego Contreras, Nick Betley, and Julie Haas, thank you for serving on my thesis committee and for being the most supportive group of people I could have asked for. Minghong, you were such a strong advocate for me, and I am eternally grateful. To Julie, thank you for being a part of this journey, always providing such great feedback and ideas. To the NGG, especially Dr. Joshua Gold, thank you for your immense amount of support during the toughest parts of my graduate training. To the past and present administrative powerhouses of the NGG, Christine Clay, Tom Hindman, Keyana Moody, Mariel Featherstone, and Dominic Homac, you have run NGG like a well-oiled machine, always knowing the answer to every question we have.

Thank you for being such a big support during graduate school. I could not have asked for a better department. To those friends and colleagues of the NGG, thank you for teaching me how to become a better and more holistic scientist. The NGG is truly a special place, and I will continue to sing praises of you whenever I can. The support and camaraderie during my time here will be something I cherish forever. Keep being the best grad group ever!

To my 2016 NGG cohort: thank you for being the best cohort I could have asked for. Every one of you made an impact in my life in one way or another, and I would not be writing this dissertation had I not had this amazing group of humans to tackle graduate school with. With all our silly little events, we became more than just a cohort. Thank you for all the laughs and support during these years. We have made it a long way since our first journal club in 2016, and I cannot wait to see what everyone accomplishes!

A mis puertorriqueños en Penn: gracias por darme la oportunidad de ser parte de una comunidad cuando pensé que no la tendría más. Sufrimos, lloramos y perseveramos juntos y me enorgullece verlos lograr todo lo que se han propuesto. No es fácil irse de la isla para navegar mares nuevos, pero poder tener un grupo de personas que nos haga sentir en casa, es algo sumamente especial. Al Dr. Arnaldo Diaz, gracias por ser nuestro líder y mentor siempre. Por darnos el espacio de poder ir a desahogarnos y hablar de lo que no podíamos con personas que no entendían. Durante los momentos más fuertes estando lejos de nuestro Puerto Rico, fuiste tú quien nos tomó de la mano y nos llevaste a seguir adelante. Gracias.

To the special lifelong friends I made through my time at the NGG: Daniel Schonhaut, Alex Wei, Logan Fickling, Maria (Mafe) Navarro, and Jared Zimmerman. Thank you for your support through this time; for always listening to me rant about lab and everyone in it and for all the laughs and memories we have shared. I look forward to seeing what we all become. A huge shoutout to Logan, one who never says no to anything, and one that always grounds me with your presence. Thank you for being a phenomenal friend through this time.

I want to especially thank Mafe, for being such a huge support system during grad school. From editing emails and resumes to helping me move, you have always been there. I am excited to see where we end up, hopefully close, perhaps me living in your basement if the offer still stands. Thank you for everything you have ever done for me. We are indeed getting out Mafe, it is happening! I also want to especially thank Jared. Words fail to describe how thankful I am for your presence in my life during grad school. For all your support and advice during these years, for all the Ryle pictures and videos that never failed to cheer me up, and for all the words of encouragement when I doubted myself the most. I of course have so much more to say, but it would take up too much space, so I will leave it at this: I am truly blessed to have you be a part of my life and thank you for everything.

A mi mejor amiga, Yarel: gracias por estar. Esas palabras nos las decimos todo el tiempo, pero realmente dicen tanto. Gracias por estar en todos esos momentos difíciles y esos momentos llenos de dudas del futuro. Gracias por estar en los momentos llenos de felicidad y optimismo por lo que viene. Soy afortunada de poder tenerte en mi vida. Un ser lleno de amor, paciencia, tenacidad y optimismo, que nunca falla en decirme “Sol, vamos lejos”. Y ahora te digo a ti: Yarel, vamos lejos. Gracias por ser parte de esta loca aventura, por estar al cien desde aquel día en un restaurante en el 2015 que te dije que me quería ir a hacer un doctorado en los estados. Nunca dudaste en mí y por eso mis infinitas gracias.

A mi patria, Puerto Rico, le doy gracias por formarme en la persona quien soy. Me fui con una esperanza de hacer patria, y espero que lo haya logrado y que siempre pueda seguir haciéndolo. I want to also thank all the amazing dogs in my life: Blizzy (RIP), Rebel, Luna and Ryle, thanks for all the snuggles and cuddles.

To my sister, my biggest role-model, Dr. Maria V. Rolón Martínez, thank you for always being a support system. I will forever admire your work ethic, your passion for your profession, and your drive to always do more, while still staying grounded and present. A mi papá, José D.

Rolón Roquet, por darme las herramientas para haberme convertido en lo que soy. Por escucharme y darme consejos, por nunca decir que no y por el amor incondicional. A mi mamá, Marilyn Martínez Alicea, gracias por escucharme por teléfono todas las tardes de camino a mi apartamento, por darme consejos y por siempre calmarme, recordándome que todo esto era pasajero. Por ser un ejemplo para seguir de amor y compasión. Gracias infinitas a ustedes tres, que me han dado el espacio para llegar a lograr esto, por no ponerme peros en el camino, por siempre apoyarme en cualquier loquera que se me haya ocurrido. Sin su sacrificio, jamás hubiese llegado a escribir estas palabras ni esta tesis. He sido bendecida. No puedo escribir todo aquí porque me quedaría sin páginas así que, en fin: los amo.

Finally, I want to acknowledge myself, for finding ways to accomplish what I wanted to accomplish. For learning to navigate grad school and for finishing what I said I would finish. It took time and patience, but I did it. This is a lesson for anyone reading this: acknowledge yourself, be kind to yourself, give yourself space and time to figure things out, and always remind yourself that you are awesome.

ABSTRACT

ROLE OF INHIBITORY NEURON TYPES OF THE TRN IN AUDITORY PROCESSING

Solymar Rolón Martínez

Maria N. Geffen

Sensory perception requires a set of complex feedforward and feedback processes between the periphery, subcortical pathways, and the sensory cortices. For most sensory systems synapses within the thalamic sensory nuclei play a key role in fine-tuning sensory information. The thalamic reticular nucleus (TRN), a thin sheet of GABAergic neurons encapsulating the thalamus, is the primary source of inhibition to the thalamic nuclei. Through its inhibitory projections to thalamic relay cells, it filters relevant sensory information between the thalamus and cortices. Two dominant subclasses of inhibitory neurons are found in the TRN: parvalbumin (PV) and somatostatin (SST) neurons, neuron types that play differential roles in auditory processing. Although the TRN is necessary for the transfer of important acoustic information to higher-order structures, little is known of the function of the TRN and its inhibitory neuronal subtypes in the auditory pathway. In chapter 2 we tested how arising auditory information is relayed from the basolateral amygdala (BLA) to the auditory cortex; two functionally important areas for fear related behaviors. We found that activation of direct projections from the BLA to the TRN decreases spontaneous activity but amplifies auditory responses to pure tones in the auditory cortex and thalamus. This suggests that the BLA-TRN circuit is crucial for relaying behaviorally relevant signals to auditory cortex. To further understand the TRNs contributions to auditory processing, in chapter 3 we explored the circuit mechanisms between the TRN and the auditory thalamus, the medial geniculate body (MGB). Via anatomical tracing we found that PV neurons of the TRN project to the ventral MGB, which relays sensory information to primary auditory areas, and that SST cells of the TRN project to dorsal and medial MGB, which relay information

to secondary auditory association areas. Furthermore, through optogenetic inhibition of PV and SST neurons of the TRN we find that responses to pure tones in excitatory relay cells of the MGB are both facilitated and suppressed. Together, these results establish a nuanced yet crucial role of the TRN in auditory processing.

TABLE OF CONTENTS

LIST OF FIGURES

CHAPTER 1:

INTRODUCTION

Our ability to enjoy our everyday interactions and encounters in an acoustically rich world depends on the perception of the sounds that surround us. From the sound of a dog barking in a dog park signaling a joyful outing, to the siren of a fire truck signaling an emergency, the perception of the sounds going on around us is essential for providing cues on how we should react at any moment. Sound reaches our peripheral auditory system via sound waves produced in our environment. These waves reach our ears and cause the small bones housed within them to vibrate, converting the air waves into mechanical signals; these signals are then converted to electrical signals by mechanoreceptors in the hair cells of the inner ear. The electrical signals ascend from the hair cells through the auditory nerve to the cochlear nucleus, then to the superior olivary nucleus in the brainstem, reaching the lateral lemniscus and inferior colliculus (IC) in the midbrain. The IC then sends ascending projections to the medial geniculate body (MGB) in the thalamus, which relays encoded auditory information to the auditory cortex (AC). Auditory information goes through multiple steps of processing, with the most direct route including at least 6 synapses, prior to being encoded by the higher-association areas like AC (**Figure 1.1**-Butler & Lomber, 2013).

The AC is a hub for encoding complex and behaviorally relevant signals; however, information reaching the AC must go through a series of fine-tuning steps to filter out irrelevant information (Aizenberg et al., 2015; Aizenberg & Geffen, 2013; Wood et al., 2022). The auditory system mediates auditory information with a set of complex excitatory-inhibitory circuits within different relay centers of the pathway and connections with other association areas of the brain

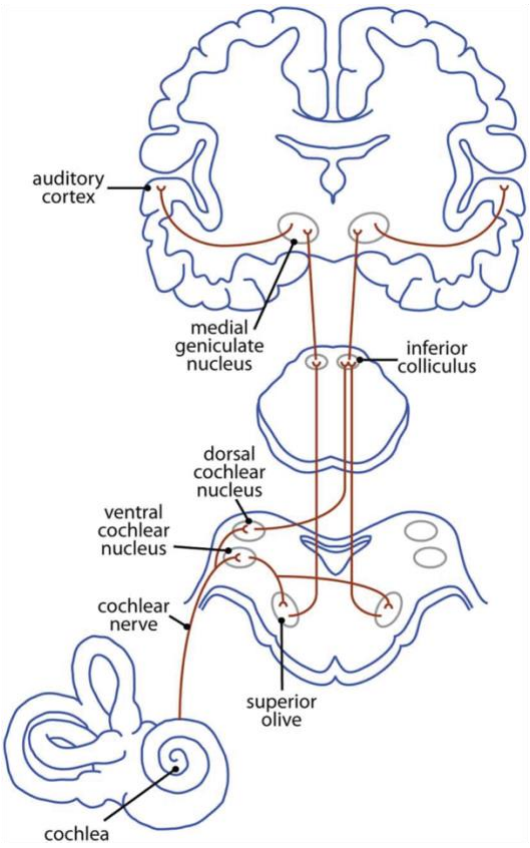

Figure 1.1. The ascending auditory pathway. (Adapted from: Butler & Lomber, 2013)

(Blackwell & Geffen, 2017). The goal of our work is to address whether and how these excitatory-inhibitory circuits along the auditory pathway modulate auditory information to contribute to filtering behaviorally relevant auditory information at the cortical and subcortical level. I asked the following questions: *1) Through which circuit mechanisms does auditory information get filtered and relayed to the AC?* The AC is a critical brain region for encoding behaviorally relevant sounds (Aizenberg & Geffen, 2013). It receives input from various regions of the brain, including the basolateral amygdala (BLA), canonically known to be the "fear center" of the brain, where the formation or expression of fear memories is associated with the presented sensory stimuli (Janak & Tye, 2015). The BLA sends direct projections to the AC, and AC exhibits plastic changes in sound encoding that is selective to fear-related sounds (Yang et al., 2016). However, how these two

critical association areas exchange auditory information provides an example for how areas of the auditory pathway transform sound representation for behaviorally relevant stimuli. Through anatomical and physiological experiments, we identify a novel thalamic excitatory-inhibitory circuit that mediates auditory information between the AC and the BLA. *2) What is the anatomical distribution of specific inhibitory cell-types of the thalamic nuclei within the auditory pathway?* The thalamic nuclei are the relay centers for sensory information processed in downstream subcortical regions to surrounding sensory cortices (Guillery & Sherman, 2002; Murray Sherman, 2016). The MGB is the primary auditory relay center to the AC, it is primarily excitatory and receives direct inhibitory inputs from the surrounding reticular nucleus of the thalamus (TRN), a structure rich in different sub-classes of neurons (Bartlett, 2013; Crabtree, 1998; He, 2003). We use viral tracing and immunohistochemical techniques to establish the cell-type specific anatomical inputs of the TRN to the MGB. *3) How does cell-type specific inhibitory thalamic circuit mechanisms affect processing of auditory information?* The auditory pathway is comprised of complex circuit mechanisms, which depend on interactions between excitatory cells in relay nuclei such as the MGB and inhibitory cells in feedforward and feedback source areas such as the IC and the TRN. Using optogenetics and *in-vivo* electrophysiological recordings of awake mice, we show a novel role of inhibitory cell-types of the TRN on auditory information processing in the thalamus.

Learning how excitatory-inhibitory circuits of the thalamus work together to process and filter auditory information is essential for understanding how higher-order cortical regions encode behaviorally relevant auditory information. Therefore, it is important to review the role of the auditory thalamus in behaviors such as fear expression, the anatomical and physiological contributions of inhibitory cell types within the auditory pathway and contributions of the TRN in sensory modalities.

Role of the thalamus in regulation of auditory related behaviors.

Neuronal and behavioral responses to sensory stimuli in everyday acoustic environments are shaped not only by the stimulus itself, but also by the experience during which the sensory stimulus occurs. Associating an emotional response with a sensory cue redirects the nervous system to enhance sensory responses (Phelps et al., 2006). Some neuropsychiatric diseases, including schizophrenia and post-traumatic stress disorder are characterized by abnormal emotional responses associated with abnormalities in processing of sensory stimuli (Ohman et al., 2001; M. L. Phillips et al., 2003). Several studies have identified changes in sensory processing following fear conditioning in rodents and humans (Aizenberg & Geffen, 2013; W. Li et al., 2008). The BLA plays a critical role in fear behaviors; it exhibits robust responses following aversive cues and is involved in the formation of fear memories in the presence of sensory stimuli (Ghosh & Chattarji, 2015; Grewe et al., 2017; Paré & Quirk, 2017; Quirk et al., 1997). Lesions to the amygdala in humans and rodents led to a decrease in fear responses to aversive stimuli (Adolphs et al., 1994; A. K. Anderson & Phelps, 2001; LeDoux et al., 1990). Fear behaviors are typically studied through an association learning paradigm of classical fear conditioning. During conditioning, a conditioned stimulus (CS) is paired with an aversive stimulus (US); those commonly used are a tone and a foot-shock, respectively. Conditioning causes a CS-evoked increase in firing rates of neurons in the BLA to tones that are associated to the foot-shock, suggesting that these neurons are involved in forming and extinguishing the fear response to the tone (Quirk et al., 1995, 1997). Indeed, neurons in BLA tend to maintain an excitatory response to a tone paired with the aversive stimuli (Collins & Paré, 2000; Maren, 2000; Quirk et al., 1995, 1997). This finding demonstrates potentiation of sensory inputs in BLA neurons, following an increase in long-term potentiation, a form of synaptic plasticity, following CS and US pairings (Clem & Huganir, 2010; McKernan & Shinnick-Gallagher, 1997; Rogan et al., 1997). Sensory inputs are important for fear learning; optogenetically activating BLA neurons with inputs from auditory areas in the presence of a tone

(CS) increased conditioned freezing, serving as a US (Johansen et al., 2010; Nabavi et al., 2014). The process of fear learning therefore requires sensory input, specifically inputs converging in the auditory pathway.

Stimulus convergence in AC is required for learning to associate fear with complex tones, and this process relies on an interneuron-mediated disinhibition within AC (Letzkus et al., 2011). Our lab has shown that following differential auditory fear conditioning (DAFC), a variation of classical fear conditioning in which a foot shock is presented at the end of one tone (CS+) but not with another tone (CS-), mice could specialize or generalize learning (Aizenberg & Geffen, 2013). In specialized learning, mice have a significant fear response to CS+ but not to CS-, while in generalized learning mice significantly freeze to both CS+ and CS-. This distinction between specialized and generalized learning was independent of AC; inactivation of AC with muscimol, a $GABA_A$ agonist, led to no changes in fear learning. Optogenetic suppression of inhibitory parvalbumin (PV) interneurons in AC increased generalization of fear responses, whereas activation of PV neurons had no effect on specialized learning (Aizenberg et al., 2015). Inactivation of AC is crucial for frequency discrimination, however, was not necessary for fear learning. However, these results provide evidence that interneuron mediation in AC is required for proper stimulus convergence and fear expression.

There is evidence of a functional connection between AC and BLA, such that AC drives BLA activity in fear memory retrieval and expression (Aizenberg & Geffen, 2013; Cambiaghi et al., 2016; Ghosh & Chattarji, 2015; Grewe et al., 2017; Yang et al., 2016). Initial studies determined that interactions between the BLA and AC could be involved in transmission of stimulus information during fear conditioning through several pathways. One proposed pathway is through a direct projection between the MGB and the BLA (Turner & Herkenham, 1991). An alternative pathway is a multi-synaptic feedback pathway between the thalamus, AC and the BLA (Mascagni et al., 1993; Romanski & Ledoux, 1993). Indeed, neuroanatomical studies in non-

human primates found direct projections from the BLA to TRN, a structure entirely composed of GABAergic neurons in the thalamus (Zikopoulos & Barbas, 2012). This result suggests that the latter of the proposed pathways serve as a functional connection between AC and BLA.

Several studies show that the TRN facilitates or suppresses sensory stimuli before reaching the sensory cortices, highlighting its role as an important structure for processing sensory cues (Ahrens et al., 2015; Halassa et al., 2014, p. 20; Nakajima et al., 2019; Schmitt et al., 2017; Wimmer et al., 2015). The TRN experiences cortex-mediated changes that are subject to relevant sensory inputs; TRN networks therefor work together to respond appropriately to sensory inputs as a way of sensory gain (Wimmer et al., 2015). Studies of attention, using sensory selection in a two-alternative forced choice task (2AFC), have demonstrated that a thalamocortical circuit amplifies cortical connectivity to sustain attentional control (Schmitt et al., 2017). Studies on the effects of TRN inhibition during these tasks show optimization in sensory selection providing further evidence of TRN gain of sensory information (Halassa et al., 2014). Disruption of a receptor tyrosine kinase essential for inhibitory synapses, ERB4, in somatostatin-expressing TRN neurons led to an increase in sensory discrimination between auditory stimuli and a decrease in the ability to switch between two conflicting cues (Ahrens et al., 2015). These results further provide evidence of the role of TRN in enhancing sensory information in a modality dependent way. Overall, these findings suggest that TRN might gate auditory fear cues from the BLA to the auditory pathway to drive plastic changes in cortical responses to aversive sounds.

In chapter 2 we explore the role of the BLA-TRN projection in auditory processing of pure tones. Using anatomical tracing, optogenetics and *in-vivo* electrophysiology we focus on understanding how activation of the BLA-TRN projection affects tone-evoked activity in the relay cells of the MGB and pyramidal neurons of the AC. To further understand how these structures functionally interact with each other, we will continue to discuss the anatomical and functional contributions of TRN and its relation to the auditory pathway.

Anatomical characterization of the TRN.

The thalamic nuclei are made up of glutamatergic thalamocortical relay cells and GABAergic interneurons. These relay centers receive bottom-up and top-down sensory information from subcortical and cortical regions, respectively (**Figure 1.2-**Antunes & Malmierca, 2021). Encapsulating the thalamic nuclei is the TRN, a thin sheet of GABAergic cells, that provides most of the inhibition to thalamocortical relay cells (Houser et al., 1980; Oertel et al., 1983). The TRN receives feedback projections from L5 and L6 corticothalamic neurons as well as axon collaterals from thalamocortical cells (Carroll et al., 2022; Crabtree, 2018; Gentet & Ulrich, 2003, 2004; Guo et al., 2017; Lam & Sherman, 2005, 2005, 2011, 2011). Canonically, the TRN has been anatomically subdivided by its function in individual sensory modalities; the caudo-dorsal TRN is referred to as the visual TRN (visTRN), the ventro-central TRN as the somatosensory TRN (ssTRN), the rostral TRN as the motor TRN, and the caudo-ventral TRN as the auditory sector of the TRN (audTRN) (Pinault, 2004). However, recent studies show the TRN is a multimodal structure, responding to different sensory stimuli across all sectors of the TRN (Kimura, 2014).

Whereas canonical anatomical studies have documented a homogenous expression of GABAergic markers throughout the neurons of the TRN (Houser et al., 1980; Pinault & Deschênes, 1998), more recent studies show a more complex molecular makeup of the neurons within the TRN. The TRN is primarily composed of calbindin (CB), parvalbumin (PV) and somatostatin (SST) expressing neurons (Clemente-Perez et al., 2017; Martinez-Garcia et al., 2020). In the ssTRN, cells are distinctly organized within zones of the TRN; PV cells are found throughout the entirety of the TRN, SST cells are primarily clustered in edge zones and CB cells are clustered in the central zones (Martinez-Garcia et al., 2020). Interestingly, TRN cells can co-express each of these molecular markers, though the proportion of co-expression remains unclear.

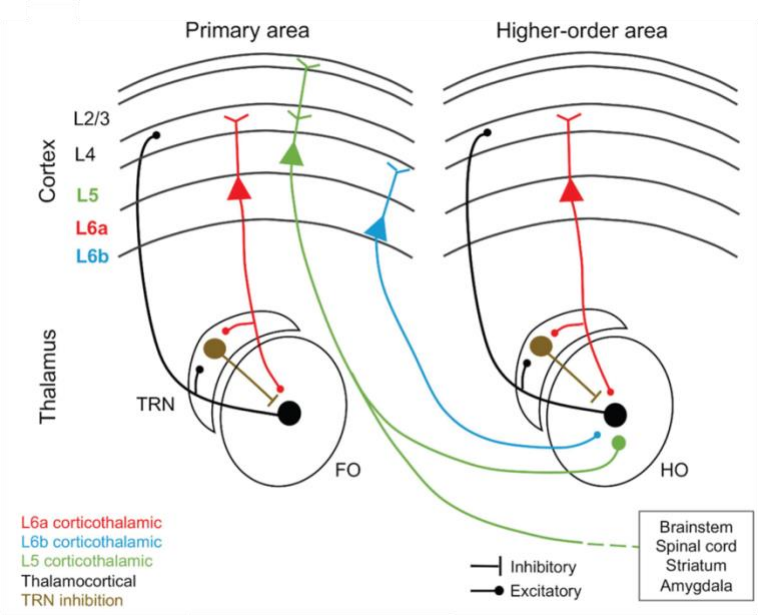

Figure 1.2.Auditory corticothalamic circuitry (Adapted from: Antunes & Malmierca, 2021)

In one study, the proportion of SST and CB cells in the ssTRN co-expressing with PV is at 1:1 (Martinez-Garcia et al., 2020), whereas another study shows that the proportions of co-expression between SST and PV are location dependent and at much lower values (~0.2:1- 0.3:1) (Clemente-Perez, et al., 2017). These diverging results can be due to technical differences in the way experiments were conducted, but nonetheless show the anatomical complexity of the TRN and patterns of protein expression in different cell classes. Moreover, it raises important questions like what are the functional implications of TRN cells that co-express PV and SST? More recently, a single-cell transcriptomic analysis shows that this described distinct expression of cell-types within the TRN can be a result of an expression of negatively correlated transcriptomic genetic profiles (Y. Li et al., 2020). This study identifies expression of two marker genes *Spp1*$^{+}$ (secreted phosphoprotein 1) and *Ecel1*$^{+}$ (endothelin converting enzyme like 1). Consistent with the previous anatomical studies described, *Spp1*$^{+}$ and *Ecel1*$^{+}$ showed similar edge and core zone expression patterns; with *Ecel1*$^{+}$ cells located in the edge zones and *Spp1*$^{+}$ cells located in the core zones. The

findings described here indicate a complex anatomical distribution of cell types that coexist within the TRN.

These distinct expression profiles of cells within the TRN extend to how they project to their anatomical targets and who they collect information from. First-order thalamic nuclei (FO) are those who directly drive information to primary sensory areas, whereas to higher-order (HO) thalamic nuclei are defined as those who receive input from cortical regions and drive information to secondary association areas (Bickford, 2016; Sherman & Guillery, 1998). The MGB is anatomically subdivided into three main nuclei: the ventral division (vMGB), the medial division (mMGB), and the dorsal division (dMGB). The vMGB makes up part of the lemniscal auditory pathway (FO-MGB), which directly modulates primary auditory areas such as primary auditory cortex (A1), meanwhile the dMGB and mMGB make up part of the non-lemniscal auditory pathway which modulates secondary auditory areas such as the secondary auditory cortex (A2) and other auditory association areas (HO-MGB) (L. A. Anderson & Linden, 2011; Kimura et al., 2003; Lee, 2015; Oliver & Huerta, 1992; Winer, 1992, 2005). The projections of cells within the audTRN target and envelop the MGB in its entirety and the TRN receives direct input from AC and from collaterals of relay cells of the MGB (Bartlett, 2013; Guillery & Sherman, 2002; Hirsch et al., 2015; Kimura et al., 2005; Pinault, 2004; Pinault & Deschênes, 1998). Furthermore, PV neurons of the ssTRN project primarily to FO somatosensory thalamic nuclei and SST neurons of the ssTRN primarily project to HO somatosensory thalamic nuclei (Clemente-Perez, et al., 2017). *Spp1*$^{+}$ and *Ecel1*$^{+}$ cells follow these projection distinctions as well, with *Spp1*$^{+}$ neurons projecting to FO thalamic nuclei and *Ecel1*$^{+}$ neurons primarily projecting to HO nuclei (Y. Li et al., 2020). As described above, different types of cells of the TRN project to either FO-MGB or HO-MGB, however, it remains unknown whether and how the projections of PV and SST cell types of the TRN project to the MGB and if they follow the projection patterns to FO and HO auditory thalamus.

In chapter 3 we explore whether and how PV and SST neurons of the audTRN project to the MGB. Using anatomical tracing and immunohistochemistry techniques we focus on understanding how these two regions anatomically organize. These distinct anatomical projection patterns of cells in the TRN to the surrounding thalamic nuclei provide an informational framework to begin to understand whether and how the TRN functionally modulates sensory information. We therefore will continue to explore the physiological functions and behavioral relevance of TRN cells within sensory modalities.

Functional role of inhibitory neurons of the thalamus and sensory processing.

There is little evidence for local GABAergic neurons in the auditory thalamus of rodents, which has been found to be entirely glutamatergic (Ito et al., 2011). The TRN is therefore considered to be the primary source of inhibition to the MGB. The TRN receives excitatory information from collateral projections from the MGB and from corticothalamic inputs from AC and it also sends inhibitory projections back to MGB, these processes serve as feedback mechanisms to modify sensory information within the MGB (Guo et al., 2017; Shosaku & Sumitomo, 1983). The TRN is known as the "gatekeeper" structure of the thalamus (Crick, 2006; Makinson & Huguenard, 2015). It contributes to sensory information filtering and supports optimal behavioral performance in sensory attentional tasks (Nakajima et al., 2019; Wimmer et al., 2015). It has been functionally tied to roles in attention, upkeep of sleep spindles, sensorimotor behaviors like whisking, and sensory information filtering (Clemente-Perez, et al., 2017; Halassa et al., 2014; Iavarone et al., 2023; J. Liu et al., 2023; P.-F. Liu et al., 2022; Schmitt et al., 2017; Visocky et al., 2022; Wimmer et al., 2015). The TRN is crucial for tasks requiring attention and for filtering relevant sensory information. In studies in which animals were tasked with appropriately responding to a stimulus in the presence of a conflicting cue, suppression of the TRN impaired the ability of mice to correctly identify the stimulus they had to pay attention to (Nakajima et al., 2019; Wimmer et al., 2015). The TRN experiences functional changes based

off top-down information from the cortex, making it one possible way in which the TRN networks select appropriate inputs as a way of sensory information gain.

Stimulation of the TRN modulates tone-evoked responses of the MGB; in the anesthetized rat preparation, responses to auditory stimuli in MGB were suppressed when TRN neurons were activated by an electrical pulse in presence of varying auditory stimuli (Shosaku & Sumitomo, 1983). Furthermore, inactivation of the TRN also results in increases of "signal to noise ratio" (SNR) in MGB neurons (Nakajima et al., 2019). Neurons of the TRN that project differentially to subdivisions of the MGB also exhibit distinct bursting properties in presence of white noise (Kimura & Imbe, 2015). TRN cells that directly project to FO-vMGB, show an increased number of spikes and shorter interspike-intervals than those that project to the HO-dMGB. TRN neurons differentially modulate thalamic relay nuclei based on their intrinsic bursting properties, with cells that burst at higher levels causing stronger levels of inhibition on thalamic relay cells (Kim et al., 1997). Cell-type specific neurons of the ssTRN show similar distinct intrinsic properties. PV and SST neurons of the ssTRN show differential bursting properties; PV neurons in the ssTRN burst at higher levels compared to the SST neurons, and also have higher intra-burst frequencies (Clemente-Perez, et al., 2017). Furthermore, central-zone cells of the TRN receiving inputs from the FO somatosensory thalamus have more varied intrinsic bursting properties than edge zone cells receiving input from HO somatosensory thalamus (Martinez-Garcia et al., 2020). These central-zone cells are more likely to fire rebound-bursts following hyperpolarization, whereas edge-zone cells failed to fire any rebound bursts (Martinez-Garcia et al., 2020). Similarly, among the genetically distinct *Spp1*$^{+}$ and *Ecel1*$^{+}$ cells, *Spp1*$^{+}$ cells that project to FO thalamus–as previously described–had a higher tendency of firing rebound bursts while *Ecel1*$^{+}$ cells were less likely to do so (Y. Li et al., 2020).

These findings suggest that distinct cell populations within the TRN mediate thalamic nuclei in an information-dependent manner, with central zone cells mediating primary sensory

information and edge cells propagating more complex associated auditory information. Within the auditory system, specifically AC, inhibitory interneuron types also show differential functions. Excitatory-inhibitory interactions between inhibitory interneurons and excitatory pyramidal cortical neurons shape sound responses. The two major types of inhibitory interneurons in the AC are PV and SST neurons, which anatomically synapse onto different areas of the pyramidal cells. PV interneurons synapse onto the cell body of pyramidal cells and SST neurons synapse onto the distal dendrites (Blackwell & Geffen, 2017; Rudy et al., 2011). Manipulation of these population of cells lead to differential effects on sound responses in AC. Activating PV or SST interneurons in AC led to a decrease in frequency selectivity and an overall increase in tone responsiveness of cortical excitatory neurons (Aizenberg et al., 2015; Hamilton et al., 2013; E. A. Phillips & Hasenstaub, 2016; Seybold et al., 2015). Furthermore, PV and SST neurons demonstrate differential effects on frequency tuning. Activating PV interneurons had subtractive and divisive effects in frequency tuning of AC cells but inactivation of PV interneurons led to an additive and multiplicative effect on frequency tuning after adaptation; however, inactivation or activation of SST interneurons led to a multiplicative effect on frequency tuning (Aizenberg et al., 2015; E. A. Phillips & Hasenstaub, 2016; E. A. K. Phillips et al., 2017; Seybold et al., 2015). Beyond affecting frequency tuning, PV and SST interneurons also play a critical role in modulating a phenomenon that occurs in the auditory pathway called stimulus-specific adaptation (SSA). SSA is a phenomenon in which neurons are responding less to a tone that is presented more frequently (standard tone) than when a tone is presented rarely (deviant tone) (Farley et al., 2010; Fishman & Steinschneider, 2012; Natan et al., 2015; Taaseh et al., 2011; Ulanovsky et al., 2003). SST interneurons, but not PV interneurons contribute to SSA generation in the AC (Natan et al., 2015, 2017). Inactivation of SST interneurons increased responses to standard tones but not to the deviant tones, whereas inactivation of PV neurons led to a general decrease of responses to both the standard and the deviant tone (Natan et al., 2015).

Furthermore, SST suppression in the cortex leads to an increase in frequency tuning to a specific stimulus following adaptation, whereas PV suppression increased frequency tuning across all stimulus repetitions (Natan et al., 2017). SSA and deviance detection take place in AC, IC, and the vMGB (L. A. Anderson et al., 2009; Antunes et al., 2010; Antunes & Malmierca, 2011; Polterovich et al., 2018). Limited evidence shows that neurons in the non-lemniscal MGB and the TRN encode deviance detection (Grimm & Escera, 2012), an enhanced response to a deviant tone, or a tone not presented frequently (Grimm & Escera, 2012; Ulanovsky et al., 2003). Inactivation of the TRN leads to enhanced neuronal responses to deviant tones in the MGB (Yu et al., 2009). Together these results show that PV and SST neurons are key players in auditory processing along the auditory pathway. They also show that PV and SST neurons have differential functions within the AC and TRN and that their functions are likely dependent on their input-output circuit mechanisms.

Suppression of the TRN leads to the inability to properly perform attention tasks, has effects on sensory related behaviors, and affects critical auditory processes like deviance detection. This leads to the hypothesis that PV and SST neurons of the TRN play a crucial role in auditory processing at the level of the thalamus. In chapter 3 we continue to explore whether and how suppression of PV and SST neurons of the TRN affect tone-evoked activity and frequency tuning of excitatory thalamic relay cells of the MGB. We use a combination of optogenetics, *in vivo* electrophysiology to record neuronal response of MGB cells to further understand the role of the TRN in shaping auditory information.

CHAPTER 2:

PROJECTION FROM THE AMYGDALA TO THE THALAMIC RETICULAR NUCLEUS AMPLIFIES CORTICAL SOUND RESPONSES.

This chapter is in press as: Aizenberg M, Rolón-Martínez S, Pham T, Rao W, Haas JS, Geffen MN. Projection from the Amygdala to the Thalamic Reticular Nucleus Amplifies Cortical Sound Responses. Cell Rep. (2019);28(3):605-615.e4. doi:10.1016/j.celrep.2019.06.050. My contributions as second author to this published work includes conducting anatomical tracing studies, electrophysiological experiments, data analysis and writing of the manuscript.

ABSTRACT

Many forms of behavior require selective amplification of neuronal representations of relevant environmental signals. Emotional learning enhances sensory responses in the sensory cortex, yet the underlying circuits remain poorly understood. We identify a novel pathway between the basolateral amygdala (BLA), an emotional learning center in the mouse brain, and the inhibitory nucleus of the thalamus (TRN). Optogenetic activation of BLA suppressed spontaneous, but not tone-evoked activity in the auditory cortex (AC), amplifying tone-evoked responses. Viral tracing identified BLA projections terminating at TRN. Optogenetic activation of amygdala-TRN projections further amplified tone-evoked responses in the auditory thalamus and cortex. The results are explained by a computational model of the thalamocortical circuitry, in which activation of TRN by BLA primes thalamo-cortical neurons to relay relevant sensory input. This novel circuit mechanism shines a neural spotlight on behaviorally relevant signals and provides a potential target for treatment of neuropsychological disorders.

2.1 INTRODUCTION

In our everyday experience, we encounter the same sensory stimuli under different behavioral and emotional contexts, which can modify their behavioral relevance. If a stimulus is repeatedly encountered in an emotionally salient context, sensory resources are reallocated to preferentially encode that stimulus (Öhman et al., 2001; Phelps et al., 2006). This is particularly important for dangerous, fear-evoking stimuli. Behaviorally, the link between emotional learning, such as fear conditioning, and changes in sensory processing, has been established in humans and other mammals. Recently, we found that differential fear conditioning can lead to an impairment or an improvement in sensory discrimination, depending on the generalization of learning, and that the auditory cortex is required for expression of these perceptual changes (Blackwell & Geffen, 2017). Similar effects were found following fear conditioning in humans (Li et al., 2008; Resnik and Paz, 2015; Resnik et al., 2011). Many neuropsychological disorders are characterized by inappropriate emotional weighting of sensory stimuli, including schizophrenia (Ferrarelli and Tononi, 2011; Young and Wimmer, 2017) and anxiety disorders (Öhman et al., 2001; Phillips et al., 2003). Untangling the mechanisms that govern emotion-driven control of sensory perception is important not only for basic understanding of sensory processing in everyday environments, but also for identifying potential treatment targets characterized by abnormal emotional responses to benign sensory stimuli.

The baso-lateral amygdala (BLA) is a critically important hub for the formation and expression of fear memories associated with sensory stimuli (for review see LeDoux, 2000). Aversive stimuli drive strong responses in the BLA (Ghosh and Chattarji, 2015; Quirk et al., 1997; Resnik and Paz, 2015) (although they can be heterogeneous Grewe et al., 2017), and fear conditioning evokes plastic changes in neuronal responses to conditioned sounds in the sensory cortex (Grosso et al., 2015; Kumar et al., 2012; Sacco and Sacchetti, 2010; Weinberger, 2004). BLA has been proposed to drive plasticity in the auditory cortex for signals associated with fear

(Li et al., 2008; Padmala and Pessoa, 2008). While changes in the auditory cortex following fear conditioning have been extensively documented (for review see (Weinberger, 2004)), it is not clear whether and how BLA modulates cortical responses to sensory stimuli (Chavez et al., 2009; Letzkus et al., 2011).

Lateral amygdala (LA) sends direct projections to the AC, as evidenced by imaging of LA axons in AC (Yang et al., 2016). However, recent studies in the primate brain revealed an additional pathway from the BLA to the primary inhibitory nucleus in the thalamus, the thalamic reticular nucleus (TRN) (Zikopoulos and Barbas, 2012). This finding raises the possibility that TRN facilitates gating of signals in the sensory cortex from the BLA. TRN is a layer of inhibitory GABAergic neurons located between neocortex and thalamus, which does not send direct projections to the neocortex but provides inhibition for the sensory thalamocortical relay cells (Steriade et al., 1985). At the same time, TRN receives excitatory collaterals from cortex and thalamus (Pinault, 2004). These projections position TRN as a gatekeeper, controlling sensory information flowing from thalamus to cortex, and potentially suppressing irrelevant stimuli, offering an opportunity to reweigh sensory responses based on their behavioral saliency (Ahrens et al., 2015; Halassa et al., 2014; Wimmer et al., 2015).

Here, we first tested the effects of activation of BLA on tone-evoked responses in AC. We found that activating BLA suppressed spontaneous activity in AC, leading to an increase in tone-evoked response amplitude. By examining the connectivity between BLA and the thalamus using viral anterograde and retrograde viral tracing techniques in the mouse, we identified direct projections from BLA to TRN. We found that activating this connection selectively suppressed spontaneous activity in the auditory thalamus, similar to the effects of activating BLA on AC. Through a computational model of thalamocortical circuitry, we found that activating BLA inputs to TRN could account for the reduction in spontaneous thalamic activity, and this reduction acted to prime the thalamocortical relay response to sensory input. Together, these findings suggest

that the amygdala-TRN pathway amplifies responses to sensory input by suppressing spontaneous activity of relay neurons, a process that could underlie fear-driven changes in auditory and other forms of sensory discrimination.

2.2 RESULTS

Photo-activation of BLA amplifies tone-evoked responses in the AC.

We first tested the effect of optogenetic activation of BLA on spontaneous and tone-evoked activity in AC. To manipulate the level of activity of excitatory neurons in the amygdala, we expressed Channelrhodopsin (ChR2) using targeted viral delivery to BLA of mice expressing Cre recombinase in neurons under the CamKIIα promoter (CamKIIα-Cre mice, **Figure 2.1A** – for data, for all figures here and below, see doi.org/10.6084/m9.figshare.8226329). Injection of a modified adeno-associated virus (AAV), which carried the antisense code for ChR2 under the FLEX cassette resulted in efficient and specific expression of ChR2 (flex-ChR2) in excitatory neurons in BLA of CamKIIα-Cre mice (**Figure 2.1B**).

We measured spontaneous and tone-evoked activity of neurons in the auditory cortex (AC), targeting the primary auditory cortex (A1), by recording from awake, head-fixed mice during acoustic presentation of a random tone sequence consisting of 50 ms tone pips at 50 frequencies ranging from 1 to 80 kHz (70 dB SPL). BLA was activated by shining blue laser light (473 nm, 3.5 mW/mm^2 intensity at the fiber tip) through implanted optic cannulas. Photo-activation of BLA significantly reduced overall spontaneous firing rate (FR_{base}, computed during the baseline period, 0–50 ms prior to tone onset, N = 190, p = 8.15e-7, df = 189, tstat = 5.10) in AC (**Figures 2.1C, 2.1D and 2.1G**). While peak tone-evoked firing rate in the AC (FR_{tone}, computed 0–50 ms after tone onset) was not significantly affected by BLA activation (**Figures 2.1C, 2.1D and 2.1H,** n.s.), the amplitude of responses to tones compared with spontaneous firing rate increased (**Figures 2.1D and 1I,** N = 190, p = 2.12e-10, tstat= 6.72). Activation of BLA did not significantly

affect the tuning bandwidth of neurons in AC, quantified by sparseness of tuning curve (**Figures 2.1E, 2.1F and 2.1J,** n.s.). Thus, by reducing the spontaneous firing rate, but not increasing the tone-evoked response, activation of BLA amplified tone-evoked responses in the auditory cortex.

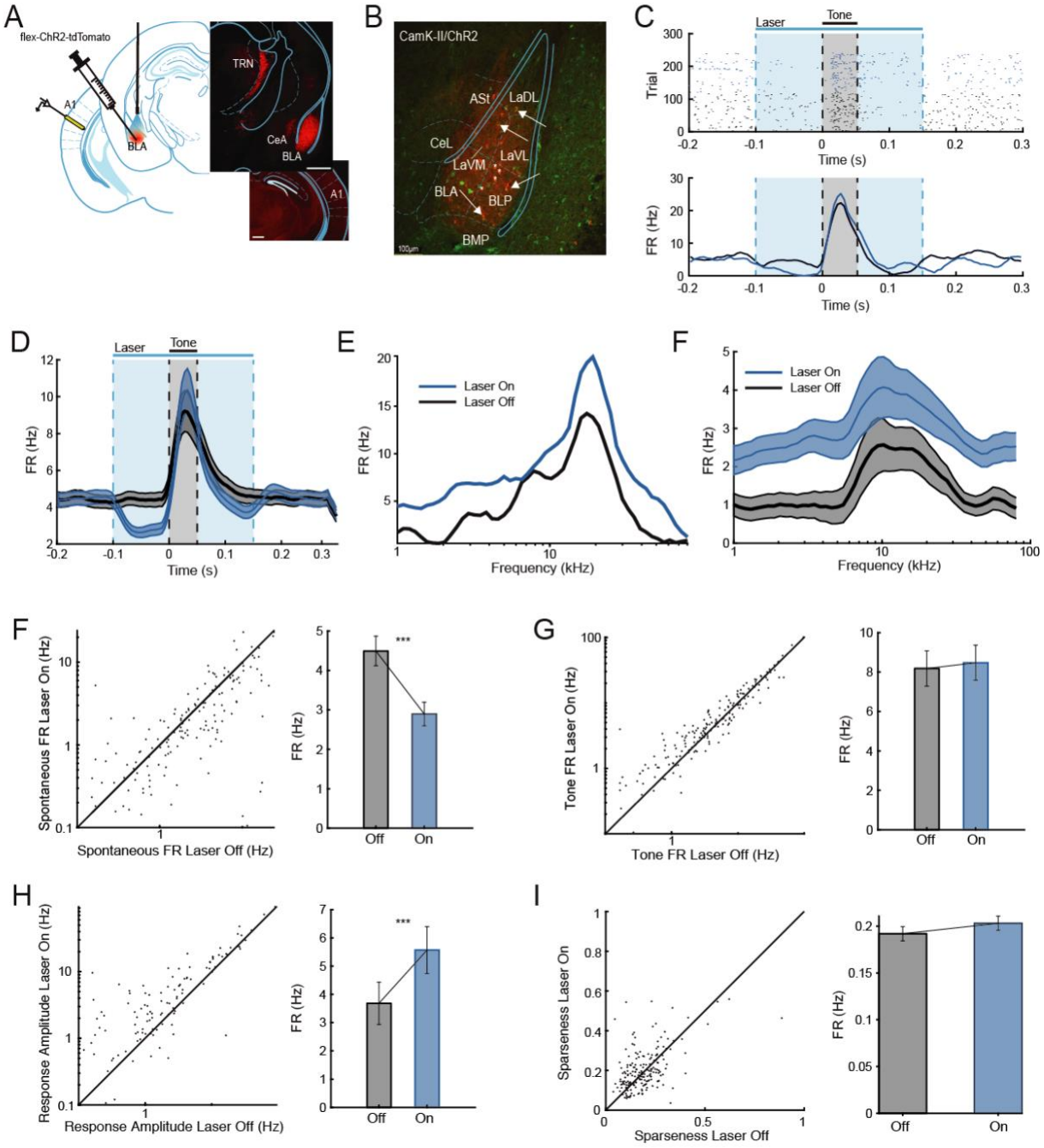

Figure 2.1. Photo-activation of BLA increases tone-evoked responses in the AC.

A. *Left panel*. CamK-cre mice were injected bilaterally with AAV-FLEX-ChR2-tdTomato into BLA. Animals were implanted with optical fibers bilaterally targeting BLA. Putative excitatory

neurons in BLA were activated by blue light (473 nm) while neuronal activity in AC was recorded using either a multi-tetrode micro-drive or multichannel silicon probe. *Right panel.* Top. Micrograph showing expression of injected virus in BLA and its projections to thalamus. Bottom. Micrograph showing little labelling in AC. Scale bar = 0.5 mm. AC: primary auditory cortex; BLA: basolateral amygdala; CeA: central nucleus of amygdala; TRN: thalamic reticular nucleus. **B.** Immunohistochemistry demonstrating co-expression of ChR2-tdTomato in putative excitatory neurons in the BLA of a CamKIIα-Cre mouse. Red: tdTomato. Green: antibody for CamKIIα. Scale bar = 100 microns. **C.** Responses of a representative AC neuron to optogenetic stimulation of BLA. Light was presented from 0 to 0.25 s (blue rectangle). Tone was presented from 0.1 to 0.15 s (grey rectangle). Top: Raster plot of spike times. Bottom. Corresponding peristimulus time histogram (PSTH) of neuronal response in light-On (blue) and light-Off (black) conditions. **D.** PSTH of the AC neurons in response to a tone (grey rectangle) during light-On (blue line) and light-Off (black line) trials. Time of photo-activation of BLA is outlined by a blue rectangle. Plot shows data from all recorded AC neurons (N=190 single units) from 7 mice. Mean ± SEM. **E-F** (E) Frequency response function of the neuron from (B) and mean frequency response function (F) in the absence of photostimulation (Off trials) and during photostimulation of BLA (On trials). **G-J** Optogenetic activation of BLA suppressed spontaneous firing rate (FR_{base}, G, paired ttest, t_{189}=5.10, p=8.15e-7), but not tone-evoked activity of neurons recorded from AC (FRtone, H, paired ttest, n.s.). Therefore, the amplitude of tone-evoked response was increased (I, paired ttest, t_{189}=6.72, p=2.12e-10). Activation of BLA did not affect sparseness of tuning of neurons in AC (J, paired ttest, n.s.). *Left panel*: Scatter plot of firing rate (G-I) or sparseness (J) on light-On plotted versus light-Off trials. Each circle represents a single unit (red) or multi-unit (black). *Right panel*: Mean ± SEM of measures from the *left panel*. ***: p < 0.001 (paired t-test).

BLA sends projections to TRN.

Suppression of spontaneous firing in cortical neurons during BLA activation is most likely due to an inhibitory synapse. Recent studies identified direct projections from the BLA to the TRN, an inhibitory nucleus in the thalamus (Zikopoulos and Barbas, 2012). The TRN in turn projects to the MGB, and therefore activation of BLA could drive suppression of spontaneous activity in AC by activating inhibitory TRN to MGB projections. We observed that AAV injected in the BLA resulted in labeling of projections in the TRN (**Figure 2.1A**). To confirm the existence of BLA-TRN pathway, we injected rAAV encoding GFP in the TRN as well as retrograde CAV2-Cre vector in the TRN of AI14 reporter mice, in which tdTomato is conditionally expressed in the cells transfected with Cre recombinase. We identified retrograde labeling of neurons in the basolateral and central nuclei of amygdala (**Figure 2.2A, S1**), confirming the existence of a direct pathway from the BLA to the TRN.

Photo-activation of BLA-TRN pathway increases amplitude of tone-evoked responses in the AC.

To test whether BLA-TRN pathway underlies the amplification of tone-evoked responses caused by BLA activation (**Figure 2.1**), we injected either a vector expressing hChR2 under CAG promoter in the BLA of WT mice, or flex-ChR2 vector into the BLA of CamKIIα-Cre mice. We then shined blue laser light onto the TRN through implanted cannulas, while recording neural responses in AC using multichannel silicon probes (**Figure 2.2B**). This allowed us to test the effect of selective activation of neurons that project from BLA to TRN on neuronal activity in AC. Activation of BLA terminals in TRN led to a significant suppression of spontaneous neuronal activity in AC (**Figure 2.2C, 2.2D and 2.2G**, N = 216, p = 0.0067, df = 215, tstat = 2.74), whereas absolute tone-evoked firing rate was significantly increased (**Figure 2.2D and 2.2H,** N = 216, p = 0.0048, df = 215, tstat = 2.85). Hence, average amplitude of responses to tones increased

significantly (**Figure 2.2D and 2.2I,** N = 216, p = 5.0e-8, df = 215, tstat = 5.65). Sparseness of tuning curves increased as result of TRN activation (**Figure 2.2E, 2.2F and 2.2J,** N = 216, p = 2.73E-10, df = 215, tstat = 6.62).

These effects persisted when we also blocked activity of BLA neurons by focal application of TTX (Supplemental figure S2 A-F, with TTX: N = 75, decrease in spontaneous activity, p = 3.03e-11, df = 74, tstat = 7.8; increase in response amplitude, p = .0061, df = 74, tstat = 2.82; Supplemental figure S2 G, H; without TTX: N = 74, decrease in spontaneous activity, p = 1.49e-10, df = 73, tstat = 7.45; increase in response amplitude, p = 7.01e-6, df = 73, tstat = 4.84). This control ensured that our stimulation of BLA-TRN terminals did not lead to activation of another pathway originating from the cell bodies in the BLA (Jhang et al., 2018; Lerner et al., 2016; Znamenskiy and Zador, 2013). Combined, these results demonstrate that selective activation of BLA-TRN projections evokes similar effects to those observed with general BLA activation on activity in the AC.

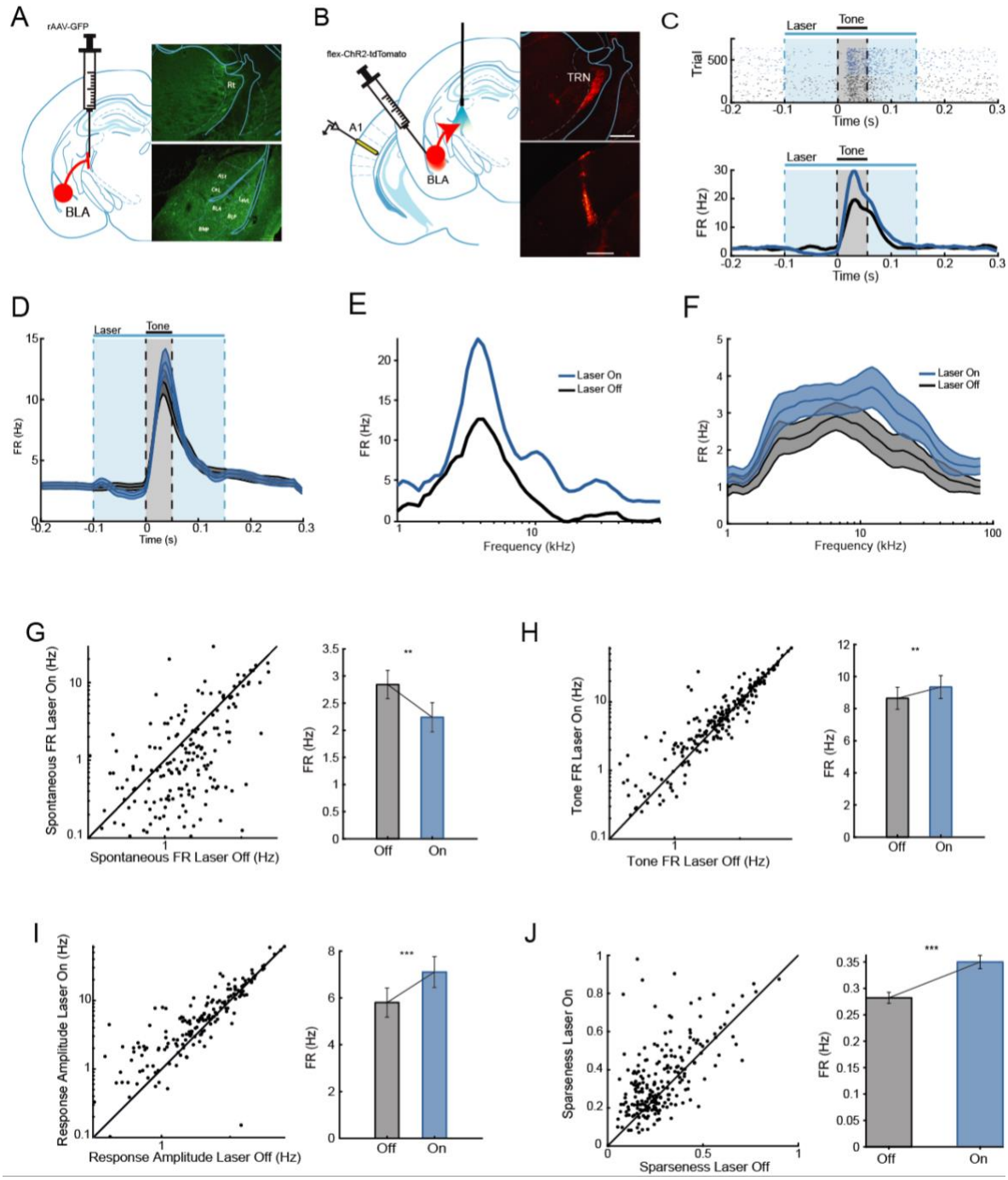

Figure 2.2. Photo-activation of projections from BLA to TRN increases amplitude of tone-evoked responses in AC.

A. *Left Panel*. Retrograde tracing of the BLA projections to TRN. AI14 mice were injected with CAV2-cre in TRN. *Right panel*. Top: Micrograph showing expression at the viral injection site in TRN. Scale bar = 0.5mm. Bottom: Retrograde expression of tdTomato in neurons in BLA and

CeA. Scale bar = 0.1mm. **B.** Anterograde tracing of the BLA projections to TRN. *Left panel*. Mice were injected bilaterally with the virus expressing ChR2 into BLA. Animals were implanted with optical fibers bilaterally targeting TRN. BLA-TRN projections were activated by blue light (473 nm) on the TRN while neuronal activity in AC was recorded using a multichannel silicon probe. *Right panel*. Top: Micrograph showing projections in TRN. Bottom: Fluorescent trace from recording silicon probe. Scale bar = 0.5 mm. **C.** Responses of a representative AC neuron to optogenetic stimulation of TRN. Light was presented from 0 to 0.25 s (blue rectangle). Tone was presented from 0.1 to 0.15 s (grey rectangle). Top: Raster plot of spike times. Bottom. Corresponding PSTH of neuronal response in light-On (blue) and light-Off (black) conditions. **D.** Mean PSTH of the AC neurons in response to a tone (grey rectangle) on light-On (blue line) and light-Off (black line) trials. Time of photo-activation of TRN is outlined by a blue rectangle. Plot shows data from all recorded AC neurons (N=216) from 5 mice. Mean ± SEM. **E.** Frequency response function of a representative neuron in the absence of photostimulation (Off trials) and during photostimulation of TRN (On trials). **E-F.** Frequency response function of a representative neuron (E) and mean response function (F) in the absence of photostimulation (Off trials) and during photostimulation of TRN (On trials). **G-J.** Optogenetic activation of BLA-TRN projections suppressed spontaneous firing rate (FRbase, G, paired ttest, t_{215}=2.74, p=0.0067), but increased tone-evoked activity of neurons recorded from AC (H, FRtone, paired ttest, t_{215}=2.85, p=0.0048). Amplitude of tone-evoked response was increased (I, paired ttest, t_{215}=5.65, p=5.0e-8). Activation of BLA-TRN projections increased sparseness of tuning of neurons in AC (J, paired ttest, t_{215}=6.62, p=2.73e-10). *Left panel*: Scatter plot of firing rate (G-I) or sparseness (J) on light-On plotted versus light-Off trials. Each circle represents a single unit. *Right panel*: Mean ± SEM of measures from the *left panel*. ***: p <0.001 (paired t test).

Photo-activation of BLA-TRN pathway increases amplitude of tone-evoked responses in the auditory thalamus.

There is extensive evidence that TRN inhibits sensory processing in the sensory thalamus (Ahrens et al., 2015; Shosaku, 1986). Therefore, we hypothesized that effect of BLA-TRN pathway on the AC activity is the result of inhibition that auditory thalamus receives from TRN (**Figure 2.3A left**). We tested whether activation of BLA-TRN terminals drives similar effects to those observed in AC in the auditory thalamus (Medial Geniculate Body, MGB). We tested this hypothesis by optogenetically activating BLA-TRN pathway as described above, while simultaneously recording from MGB (**Figure 2.3A and 2.3B**). Similarly to previous results, photo-activation of amygdalar terminals in TRN led to significant suppression of spontaneous firing rate of neurons in MGB (**Figure 2.3C and 2.3F,** N = 126, p = 8.97e-10, df = 125, tstat = 6.63). In contrast, mean tone-evoked activity was not affected by photo-stimulation (**Figure 2.3C and 2.3G,** n.s.), resulting in increased amplitude of tone-evoked responses (**Figure 2.3H**, p = 9.6e-7, df = 125, tstat = 5.16). Similarly to AC recordings, photo-activation of BLA-TRN pathway increased the sparseness of tuning curve (**Figure 2.3D, 2.3E and 2.3I,** p = 8.65 e-5, df = 125, tstat = 4.06). Combined, our findings are consistent with the hypothesis that BLA-TRN pathway acts on the AC through MGB.

To verify that effect of light on the activity in auditory thalamus and cortex is specific to action of ChR2, we injected control group of mice with viral vector that encoded only fluorescent protein. In control mice, shining blue light on BLA projections in TRN did not cause any significant change in the firing rates of neuron either in AC (Supplemental Figure S3) or in MGB (Supplemental Figure S4).

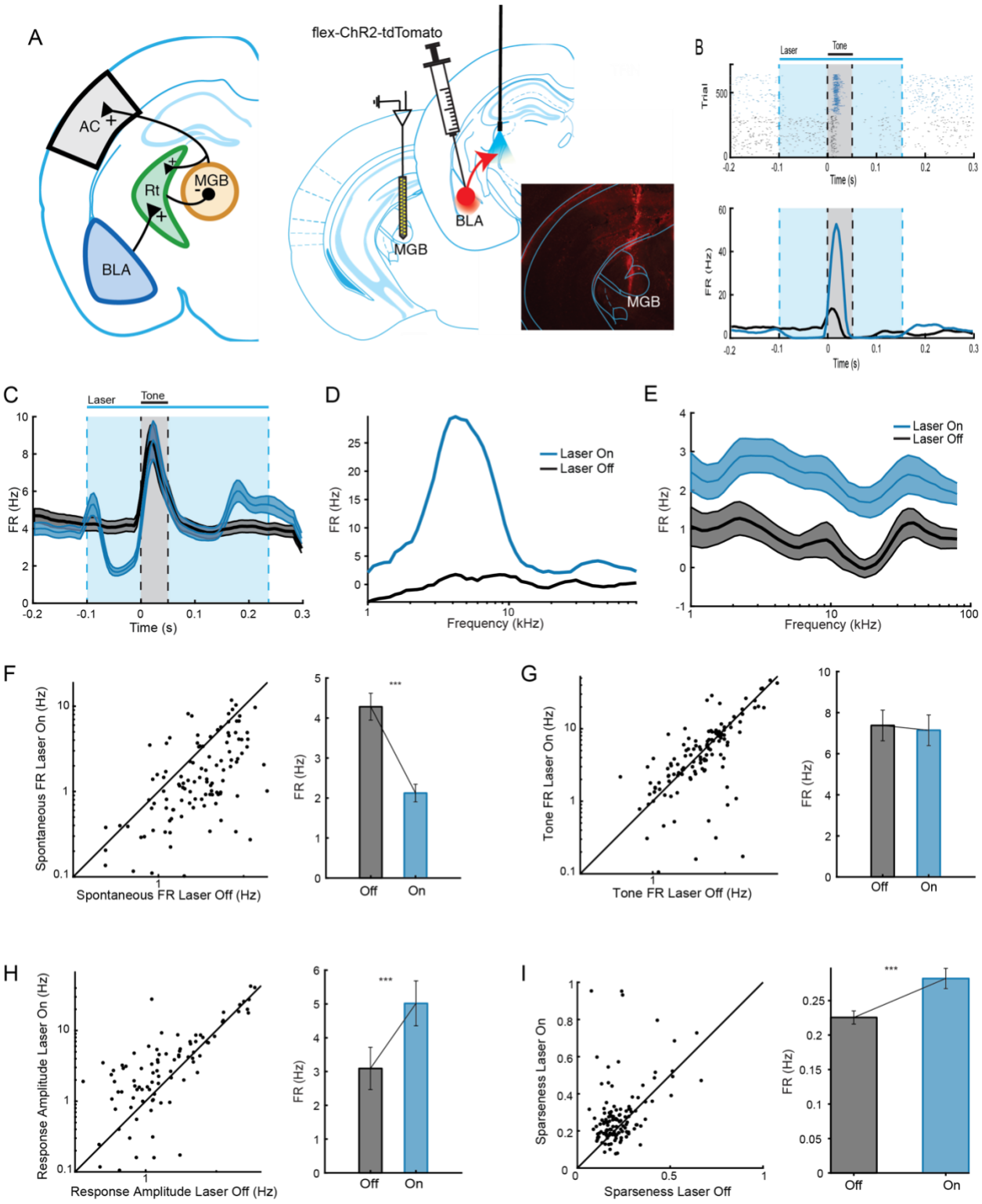

Figure 2.3. Photo-activation of projections from BLA to TRN increases amplitude of tone-evoked responses in the MGB.

A. Left: Diagram showing proposed circuit underlying the effects of the amygdala-TRN pathway

on auditory processing. Photo-activation of BLA-TRN projections ('+' synapses onto the TRN) leads to inhibition of spontaneous activity and amplification of the amplitude of tone-evoked activity of MGB neurons as result of inhibition from TRN ('- 'synapses onto MGB). This, in turn, amplifies auditory responses in the auditory cortex ('+' synapses onto AC). Inserts: representative tone-evoked responses in MGB and AC. Blue lines: during BLA-TRN activation. Black lines: baseline. Gray: tone; blue: laser on. **Right:** *Left panel*. Mice were injected bilaterally with a virus expressing ChR2 into BLA. Animals were implanted with optical fibers bilaterally targeting TRN. BLA-TRN projections were activated by blue light (473 nm) while neuronal activity in MGB was recorded using a multichannel silicon probe. *Right panel*. Micrograph showing fluorescent trace from the recording silicon probe. Scale bar = 0.5 mm. **B.** Responses of a representative MGB neuron to optogenetic stimulation of TRN. Light was presented from 0 to 0.25 s (blue rectangle). Tone was presented from 0.1 to 0.15 s (grey rectangle). Top: Raster plot of spike times. Bottom. Corresponding PSTH of neuronal response in light-On (blue) and light-Off (black) conditions. **C.** PSTH of the MGB neurons in response to a tone (grey rectangle) during light-On (blue line) and light-Off (black line) trials. Time of photo-activation of TRN is outlined by a blue rectangle. Plot shows data from all recorded MGB neurons (N=126) from 5 mice. Mean ± SEM. **D.** Frequency response function of the neuron from (B) in the absence of photostimulation (Off trials) and during photostimulation of TRN (On trials). **E.** Mean frequency response functions of neurons from C in the absence of photostimulation (Off trials) and during photostimulation of TRN (On trials). **F-I.** Optogenetic activation of BLA-TRN projections suppressed spontaneous firing rate (FRbase, F, paired ttest, t_{125}=6.63, p=8.97e-10), but did not significantly change tone-evoked activity of neurons recorded from MGB (FRtone, G, paired ttest, n.s.). The amplitude of tone-evoked response was increased (H, paired ttest, t_{125}=5.16, p=9.6e-7). Activation of BLA-TRN projections increased the sparseness of tuning of neurons in MGB (I, paired ttest, t_{125}=4.06, p=8.65e-5). *Left panel*: Scatter plot of firing rate (F-H) or sparseness (I) on light-On plotted

versus light-Off trials. Each circle represents a single unit. *Right panel*: Mean ± SEM of measures from the *left panel*. ***: $p < 0.001$ (paired t test).

A bursting model of TRN and MGB produces enhancement in tone-evoked responses in TRN and A1 due to BLA-TRN activation.

How does the enhanced responsiveness to tones square with the decreased spontaneous activity upon BLA-TRN activation? These dual effects may be explained by the feedback connectivity between the bursting neurons in TRN and MGB. We constructed a three-cell model of MGB, TRN and CAC neurons (**Fig. 2.4**). As all thalamic neurons exhibit bursts of spikes resulting from T currents (Gribkova et al., 2018; Huguenard, 1996; Willis et al., 2015), we used a bursting neuron model for our TRN and MGB neurons (Haas and Landisman, 2011; Traub et al., 2005a). Our simulation code is available at https://github.com/jhaaslab/trn_aud. Spontaneous spiking was elicited by Poisson-distributed inputs to the MGB and AC neurons. We delivered a 100-ms long pulse of input to the TRN neuron to represent optogenetic activation of BLA terminals in TRN, and a shorter 10-ms input to MGB to represent the tone input. BLA activation initiated a burst in TRN neurons, with regular tonic firing following the burst for increased strengths of BLA activation (**Fig. 2.4B**, first column). For weak BLA input, the initial burst in TRN was late and elicited fewer spikes, providing only weak inhibition of the spontaneous firing in MGB and of the MGB response when the tone arrived (second row in **Fig. 2.4B and C**). For moderate values of BLA activation, a quicker and stronger burst in TRN delivered stronger and earlier inhibition in MGB and AC (third row in **Fig. 2.4B and C**). This inhibition terminated spontaneous firing in MGB, and the timing of the TRN burst resulted in stronger rebound from inhibition in the MGB neuron. Together, these effects allowed MGB and AC to produce an amplified response when the tone arrived. Overactivation of BLA (bottom row in **Fig. 2.4B and C**) led to overactivation of TRN and correspondingly stronger and persistent inhibition of MGB

and AC. These effects of strength and timing of TRN bursts on firing rates in MGB and AC are summarized in **Fig. 2.4D**. Consistent with the experimental results, the suppression of spontaneous MGB spiking allowed for an increased ability to respond to the auditory input and relay it to AC. Together, these results provide a link between the suppression of spontaneous activity to amplified AC response by demonstrating that a moderate activation by BLA of TRN, such as those used in our experiments, increase the readiness of MGB neurons to respond. As a result, peak-to-peak firing rates in MGB and AC increased during BLA activation (**Fig. 2.4E**).

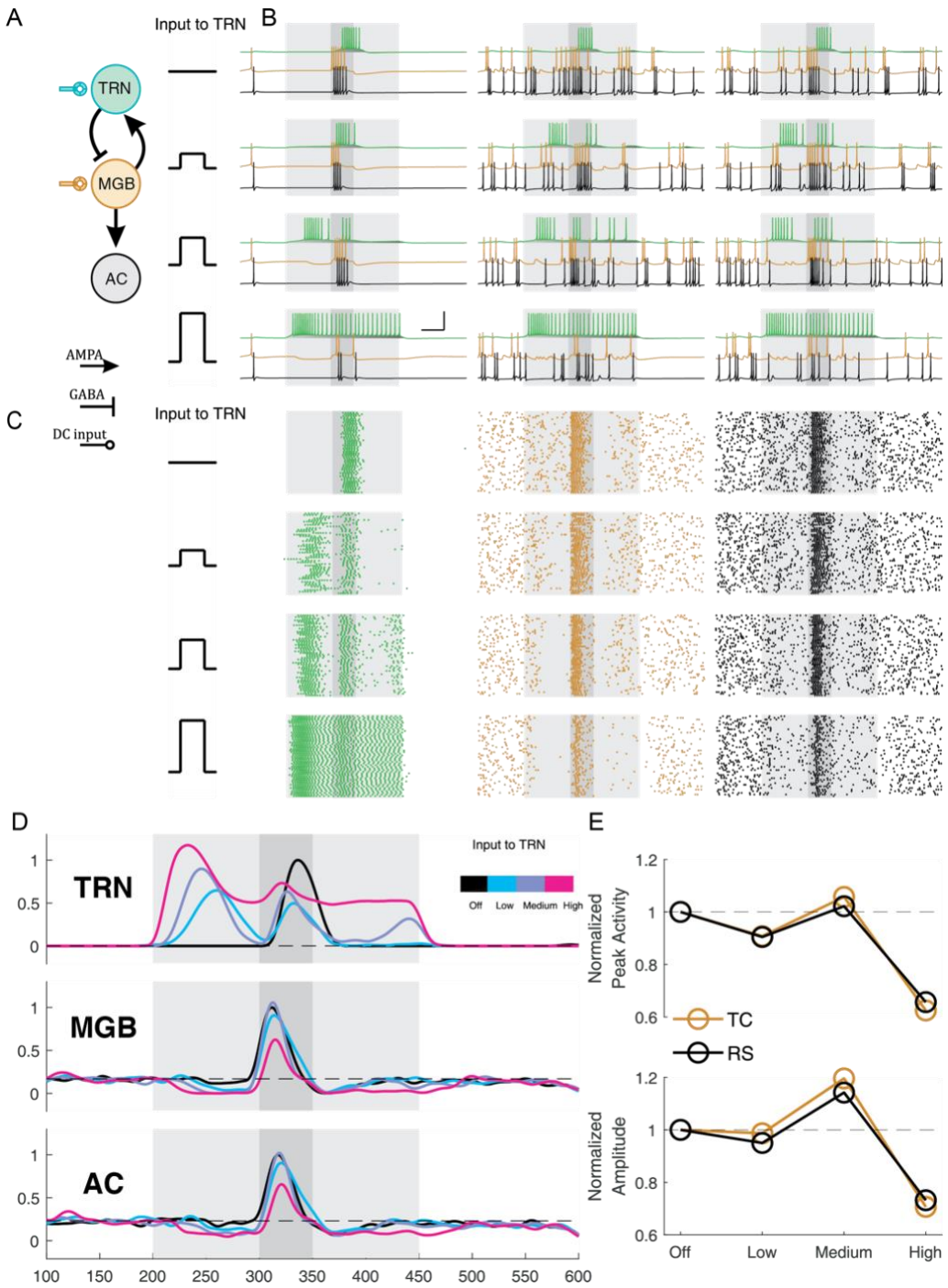

Figure 2.4. Possible mechanism for BLA enhancement of tone-evoked MGB and AC responses.

A. Simulated network, including TRN, MGB and AC cells (see Methods). A 100-ms input to TRN represented optogenetic activation of BLA. The tone was a 10-ms pulse to MGB during light stimulus. **B.** Simulations of the network for no spontaneous inputs (left column) and for two

simulations with spontaneous input to MGB and AC (middle and right columns), in the absence of BLA activation (top row) and with increasing strengths of BLA activation (lower rows). **C.** Spike rasters for 25 repeated simulations in **B. D**. Spiking rates in the TRN, MGB and ACAC neurons, shown for control conditions (black) and for the three strengths of BLA activation of TRN (shades of blue), each normalized to zero-input values. **E.** Maximum firing rates in MGB and AC during the tone (top), and peak-to-peak amplitudes of the tone response (bottom) shown for the varied strengths of BLA activation.

2.3 DISCUSSION

The basolateral amygdala is a critically important brain area for auditory fear conditioning (for review see (LeDoux, 2000), where conditioned and unconditioned stimuli converge (Romanski and Ledoux, 1993; Romanski and LeDoux, 1992). Lesions of the BLA (Campeau and Davis, 1995; Goosens and Maren, 2001) or either the lemniscal or non-lemniscal auditory inputs to the BLA, impair acquisition and expression and discrimination of conditioned fear responses (Antunes and Moita, 2010; Boatman and Kim, 2006); whereas paired activation of the BLA with an auditory cue is sufficient to induce a conditioned fear response (Johansen et al., 2010). Recent studies found that sensory fear conditioning can modulate sensory discrimination acuity (Li et al., 2008; Resnik et al., 2011), and we demonstrated that in the auditory system this modulation requires the auditory cortex (Aizenberg and Geffen, 2013). Therefore, in the present study, we examined whether and how activating BLA affects tone-evoked responses in AC. We first found that activating BLA increases tone-evoked response amplitude in AC by suppressing spontaneous activity, but not affecting tone-evoked responses. We identified a mechanism by which this suppression can occur: via the projections from the BLA to the inhibitory nucleus of the thalamus, the TRN. Consistent with established anatomy, we did not find significant direct projections from TRN to AC. Therefore, we hypothesized that the TRN controls responses in AC via the MGB of the

auditory thalamus (Kimura et al., 2007). Indeed, specifically activating BLA-TRN projection neurons drove an increase in tone-evoked response amplitude in both MGB and AC. The effects were stronger in MGB than AC further suggesting that the MGB serves as a relay for cortico-collicular control. These effects could be accounted for by a three-cell model of the TRN-MGB-AC connections (**Fig. 2.3A, 2.4**), with the critical effect provided by the difference in timing and magnitude of the inhibition that TRN delivered to MGB, consistent with previous thalamo-cortical models (Gribkova et al., 2018; Haas and Landisman, 2011; Pham and Haas, 2018; Willis et al., 2015). Our study thus establishes an important pathway connecting the emotional and sensory processing centers that potentially drives changes in auditory perception as result of emotional learning.

The thalamic reticular nucleus is a thin sheet of GABAergic neurons surrounding dorsal thalamus, which exhibits sectorial anatomical organization, such that each sector of the TRN is specific to a sensory modality (Guillery et al., 1998; Jones, 1975). Although the TRN does not send direct projections to sensory cortical areas, it can control the flow of auditory and other sensory information to the cortex by inhibiting or disinhibiting thalamic projection neurons (Kimura et al., 2007; Kimura et al., 2012; Pinault and Deschênes, 1998; Villa, 1990). The unique anatomical and functional organization of TRN gave rise to the "attentional searchlight" hypothesis (Crick, 1984), which proposed that the TRN drives attention toward salient stimuli by inhibiting sensory responses to irrelevant information. Our results imply that that BLA is one of the controls of that searchlight, control that is exerted by inhibiting spontaneous activity in the relay cells. Our parameters also suggest that fear driven BLA activation that is too weak, or conversely overwhelming, fails to control the spotlight. We suggest that this simple mechanism may apply to multiple arising senses as they pass through the thalamocortical circuit.

Communication across the TRN (Landisman et al., 2002) or by convergence and divergence of TRN-thalamic connections offers the possibility for the activation of one specific

sense, or sensory modality, to affect the thalamic relay of another sense (Brown et al., 2019; Willis et al., 2015). Recently, the TRN was experimentally shown to selectively amplify processing of task-relevant stimuli and attention-guided behaviors. Either genetic (knockout or knockdown of the ErbB4 receptor in TRN neurons) or optogenetic perturbation of neuronal activity in the TRN diminished attentional switching between conflicting sensory cues in a two-alternative choice task (Ahrens et al., 2015; Wimmer et al., 2015). Similarly, optogenetic activation of the TRN during the window of elevated attention to a visual cue interfered with performance in a visual detection task (Halassa et al., 2014). Our present results showing that TRN activity is modulated by its inputs from BLA suggest that emotional responses generated in the amygdala may also modulate sensory interactions within and through the TRN, particularly during fear learning.

Auditory fear conditioning drives plastic changes to tone-evoked responses in auditory thalamus (Lennartz and Weinberger, 1992) and auditory cortex (Weinberger, 2004; Weinberger et al., 1993). Multi-neuronal recording in AC demonstrated that tone-evoked responses to the conditioned stimulus are increased following fear conditioning (Bakin and Weinberger, 1990), with individual neurons exhibiting heterogeneous but sustained changes in their tuning properties (Weinberger et al., 1993). Auditory fear conditioning promotes formation of dendritic spines in AC (Moczulska et al., 2013), pointing to plastic changes in neuronal connectivity. Direct amygdala-cortical projections are thought to underlie the facilitation of responses to emotionally salient stimuli (Amaral and Price, 1984; Yang et al., 2016; Yukie, 2002), as fear conditioning leads to an increase in the post-synaptic spines and pre-synaptic boutons specific to BLA-AC neuronal pairs (Yang et al., 2016). Here, we demonstrate that a parallel processing pathway to cortex from the BLA, via the TRN and MGB (**Fig. 2.3A**). This pathway may potentially play a regulatory role during the acquisition and recall of auditory fear memories. These two pathways may complement each other in enhancing responses to the conditioned stimulus by strengthening amygdala-cortical connectivity. In future studies, it will be important account for the interactions between

these pathways in interpreting the effects of fear conditioning and learning on sensory responses in the cortex.

We previously found that generalized auditory fear learning led to an impairment in frequency discrimination acuity, whereas specialized learning led to an improvement in acuity (Aizenberg and Geffen, 2013). Similar bi-directional changes in auditory discrimination were achieved by manipulating the activity of inhibitory interneurons in the cortex (Aizenberg et al., 2015). The existence of parallel pathways for controlling tone-evoked responses after activation of BLA may be useful for enabling bi-directional changes in sensory processing. In particular, top-down control of inhibition early in sensory processing is particularly useful in gating incoming sensory information. The connection that we identified here may be a manifestation of a more general principle of control of behavioral performance via inhibitory-excitatory interactions (Wood et al., 2017).

2.4 METHODS

Experimental model and subject details

All experiments were performed in adult female (n=5) or male (n=14) mice (supplier: Jackson Laboratories) between 7–15 weeks of age weighing between 17–27 grams. Strains: CamKIIα-Cre: B6.Cg-Tg(CamKIIα-Cre)T29-1Stl/J; wild-type mice: C57BL/6J), AI14: Rosa-CAG-LSL-tdTomato-WPRE::deltaNeo housed at 28°C on a 12 h light – dark cycle with water and food provided ad libitum, with fewer than five animals per cage. In CamKIIα-Cre mice, Cre was expressed in excitatory neurons. All animal work was conducted according to the guidelines of University of Pennsylvania IACUC and the AALAC Guide on Animal Research. Anesthesia by iso-fluorane and euthanasia by carbon dioxide were used. All means were taken to minimize the pain or discomfort of the animals during and following the experiments.

Surgery and Virus Injection

At least 10 days prior to the start of experiments, mice were anesthetized with isoflurane to a surgical plane. The head was secured in a stereotactic holder. For recordings targeting AC, the mouse was subjected to a small craniotomy (2 x 2 mm) over left AC under aseptic conditions (coordinates relative to Bregma: −2.6 mm anterior, 4.2 mm lateral, +1 mm ventral). For recordings targeting MGN, the mouse was subjected to a small craniotomy (0.5 x 0.5 mm) over left MGN (coordinates relative to Bregma: −3.2 mm anterior, 2.0 mm lateral). For optogenetic activation of BLA neurons, a small craniotomy (0.5 x 0.5 mm) was performed bilaterally over amygdala (coordinates relative to Bregma: 1.5 mm posterior, ±3.0 mm lateral). Fiber-optic cannulas (Thorlabs, Ø200 μm Core, 0.39 NA) were implanted bilaterally over the craniotomy at depth of 4.4 mm from the Bregma. For optogenetic activation of BLA projections to TRN, a small craniotomy (0.5 x 0.5 mm) was performed bilaterally over TRN (coordinates relative to Bregma: −1.1 mm anterior, ±2.0 mm lateral). Fiber-optic cannulas were implanted bilaterally at depth of 2.7 mm from Bregma. Viral constructs were injected using a syringe pump (Pump 11 Elite, Harvard Apparatus) either in BLA (200-400 nl, 4.6 mm depth from Bregma) or in TRN (200 nl, 3.4 mm depth from Bregma). Craniotomies were covered with a removable silicon plug. A small head-post was secured to the skull with dental cement (C&B Metabond) and acrylic (Lang Dental).

For postoperative analgesia, Buprenex (0.1 mg/kg) was injected intraperitonially, and lidocaine was applied topically to the surgical site. An antibiotic (0.3% Gentamicin sulfate) was applied daily (for 4 days) to the surgical site during recovery. Virus spread was confirmed postmortem by visualization of fluorescent protein expression in fixed brain slices, and its co-localization with excitatory neurons, following immuno-histochemical processing with the anti-CAMKIIα antibody.

Viral Vectors

Modified AAV vectors were obtained from Penn VectorCore. Modified AAV encoding ChR2 under FLEX promoter (Addgene plasmid 18917 AAV-FLEX-ChR2- tdTomato) was used for activation of excitatory neurons in CamKIIα-Cre mice. hChR2 was used for activation of neurons in WT mice (Addgene 20938M AAV5-CAG-hChR2(H134R)-mCherry-WPRE-SV40). Modified AAV vectors encoding only tdTomato under a FLEX cassette were used as a control for the specific action of ChR2 on the neuronal populations. Cav2-cre virus (Viral Vector Production Unit) was used for retrograde tracing of BLA-TRN projections in AI24 mice that express tdTomato under FLEX cassette.

Histology

Brains were extracted following perfusion of 0.01 M phosphate buffer pH 7.4 (PBS) and 4% paraformaldehyde (PFA), postfixed in PFA overnight and cryoprotected in 30% sucrose. Free-floating coronal sections (40 μm) were cut using a cryostat (Leica CM1860). Sections were washed in PBS containing 0.1% Triton X-100 (PBST; 3 washes, 5 min), incubated at room temperature in blocking solution (10% normal horse serum and 0.2% bovine serum albumin in PBST; 1h), and then incubated in primary antibody diluted in carrier solution (1% normal horse serum and 0.2% bovine serum albumin in PBST) overnight at 4°C. Anti-CAMKIIα antibody was used to stain excitatory neurons (abcam5683 rabbit polyclonal, 1:500, abcam). The following day sections were washed in PBST (3 washes, 5 min), incubated for 2 hours at room temperature with secondary antibodies (Alexa 488 goat anti-rabbit IgG; 1:750), and then washed in PBST (4 washes, 10 min). Sections were mounted using fluoromount-G (Southern Biotech) and confocal or fluorescent images were acquired (Leica SP5 or Olympus BX43)

Photostimulation of Neuronal Activity

Neurons were stimulated by application of five 25 ms-long light pulses (25 ms inter-pulse interval) of blue laser light (473 nm, BL473T3-150, used for ChR2 stimulation), delivered through implanted cannulas. Timing of the light pulse was controlled with microsecond precision via a custom control shutter system, synchronized to the acoustic stimulus delivery. Prior to the start of the experiment, the intensity of the blue laser was adjusted to 3.5 mW/mm^2 as measured at the tip of the optic fiber.

Electrophysiological Recordings

All recordings were carried out as previously described (Aizenberg et al., 2015) inside a double-walled acoustic isolation booth (Industrial Acoustics). Mice were placed in the recording chamber, and their headpost was secured to a custom base, immobilizing the head. Activity of neurons was recorded either via a 32-channel silicon multi-channel probe (Neuronexus), or custom-made Microdrive housing multiple tetrodes lowered into the targeted area via a stereotactic instrument following a durotomy. Electro-physiological data were filtered between 600 and 6000 Hz (spike responses), digitized at 32kHz and stored for offline analysis (Neuralynx). Spikes belonging to single neurons were sorted using commercial software (Plexon).

Acoustic Stimulus

Stimulus was delivered via a magnetic speaker (Tucker-David Technologies), calibrated with a Bruel and Kjaer microphone at the point of the subject's ear, at frequencies between 1 and 80 kHz to ± 3 dB. To measure the frequency tuning curves, we presented a train of 50 pure tones of frequencies spaced logarithmically between 1 and 80 kHz, at 70 dB, each tone repeated twice in pseudo-random sequence, counter-balanced for laser presentation. The full stimulus was repeated 5 times. Each tone was 50 ms long, with inter-stimulus interval (ISI) of 450 ms. Laser

stimulation occurred during every other tone, with an onset 100 ms prior to tone onset. Laser stimulation on each trial consisted of five 25 ms-long pulses with 25 ms-long inter-pulse intervals.

Neuronal Response Analysis

The spontaneous firing rate (FRbase) was computed from the average firing rate 50 ms before tone onset for light-On and light-Off trials. The tone-evoked firing rate (FRtone) was computed as the average firing rate from 0 to 50ms after tone onset. To examine frequency selectivity of neurons, sparseness of frequency tuning was computed as:

$$\text{Sparseness} = 1 - \frac{(\sum_{i=1}^{i=n} FR_i/n)^2}{\sum_{i=1}^{i=n} FR_i^2/n}$$

where FR_i is tone-evoked response to tone at frequency i, and n is number of frequencies used. The amplitude of neuronal response to tones was defined as the difference between mean spontaneous (0–50 ms before tone onset) and tone-evoked (0–50 ms after tone onset) firing rate and, for each neuron. Only responses to tones within 0.5 octaves of best frequency (the frequency which resulted in maximum firing rate) of each neuron were included.

Statistical Analysis

Data were analyzed using two-tailed paired t-tests in Matlab (Mathworks) following the Shapiro-Wilk test for normality. For all tests, the significance was assayed at $p < 0.05$. We compared the firing rates of neurons, computed as described above, on trials with and without laser stimulation, before (spontaneous, -50-0 ms) and after (tone-evoked, 0-50 ms) tone onset; as well as sparseness. The sample size (N = number of neurons), and statistical test results, such as p, dstat and df are reported in results for all measurements. Confidence intervals (standard error) are displayed in figures where appropriate.

Modeling

We used single-compartment Hodgkin-Huxley neuron models to create a 3-cell network consisting of a thalamic reticular nucleus (TRN) neuron, a thalamocortical neuron representing the MGB and a regular spiking neuron representing primary auditory cortex (AC; Fig. 4A). Starting from the mechanistic models of Traub et al. (2005) and Haas and Landisman (2012), we tuned cells with the following characteristics ($\bar{g}_x$ are maximal conductances with units of $[\mathrm{mS/cm^2}]$ and E_x are reversal potentials in [mV]). We used the NEURON implementation in ModelDB (Traub et al., 2003; Traub et al., 2005b), accession numbers 20756, 45539. Our simulation code is available at https://github.com/jhaaslab/trn_aud.

	$\bar{g}_L$	$\bar{g}_{Naf}$	$\bar{g}_{Kdr}$	$\bar{g}_{KA}$	$\bar{g}_{K2}$	$\bar{g}_{CaT}$	$\bar{g}_{AR}$	E_K	E_L	E_{Na}	E_{Ca}	E_{AR}
TRN	0.1	60.5	60	5	0.5	0.75	0.025	-100	-75	50	125	-40
TC	0.04	100	33.75	6	2	0.75	0.25	-95	-70	50	125	-35
RS	0.04	200	170	20	0.5	0.1	0.1	-95	-70	50	125	-35

Chemical synapses included fast inhibitory $GABA_A$ ($E_{GABAR} = -80$ mV) and excitatory AMPA ($E_{AMPAR} = 0$ mV) synapses, both with NEURON implementation of AMPA point process synapses, in which the postsynaptic potentials consist of both rise time and fall times, with the former being 0.999 of the latter (cf ModelDB accession number 45539). In our simulated network, MGB sent a feedforward excitatory AMPA synapse to TRN with $\tau_{AMPAR}^{TC\rightarrow TRN} = 2.0$ ms and $\bar{g}_{AMPAR}^{TC\rightarrow TRN} = 0.025$ μS. The TRN neuron sent feedback inhibition via a $GABA_A$ synapse to the MGB neuron, with both fast and slow fall times (3.3ms and 10ms respectively (Traub et al., 2005a)) each contributing equally to the $GABA_A$ conductance ($\bar{g}_{GABAR}^{TRN\rightarrow TC} = 0.050$ μS). Finally, MGB also sent an AMPA synapse to AC with $\tau_{AMPAR}^{TC\rightarrow RS} = 2.0$ ms and $\bar{g}_{AMPAR}^{TC\rightarrow RS} = 0.20$ μS. We set the synaptic delay to be 2.0 ms and the event detection threshold to be 25 mV.

We simulated the network in NEURON for 600 ms, with $dt = 0.005ms, V_0 = -60mV$ and saved sampled data for visualization (Fig 4B) with sampling rate of 0.1ms. To simulate spontaneous activity in MGB, we added AMPA synapses with Poisson inputs, where $\tau_{AMPAR}^{Poisson} = 1.0$ ms and $\bar{g}_{AMPAR}^{Poisson} = 0.50$ μS, to MGB at 50 Hz, to AC at 20 Hz and to TRN at 1 Hz. We used holding current to MGB at 1nA and to AC at 0.5nA.

We ran one simulation without any Poisson inputs (Fig. $4B_1$) and 50 simulations for each condition with random Poisson inputs (Fig $4B_{2\text{-}3}$, Fig 4C). In all simulations, we delivered a DC input of 10nA to MGB representing the tone inputs. We delivered a 100-ms input to TRN to represent BLA activation, at three strengths (0 nA, 0.5 nA, 0.8 nA, and 1.8 nA).

To quantify the results of simulations, we calculated the histograms of spike times, binned at 1 ms, then smoothed with a Hanning window of size 31. We normalized each rate to the maximum rate in the control condition preceding input to TRN. To calculate peak activity, we obtained the raw peak activity in the windows of tone input to MGB input for MGB and AC, then normalized those values to the control conditions. Peak-peak amplitude was taken as the difference between the raw peak activity during the tone and the mean activity during the 50 ms before the tone, also normalized to the control condition.

CHAPTER 3:

INHIBITORY NEURON TYPES OF THE TRN DIFFERENTIALLY MODULATE AUDITORY THALAMIC SOUND RESPONSES.

Adapted from: Rolón-Martínez, S., Mendoza, A., Angeloni, C.F., Diaz-Nieves, I.A., Chen, R., Haas, J.S., Geffen M.N. (2023) Inhibitory neuron types of the TRN differentially modulate auditory thalamic sound responses. In preparation.

ABSTRACT

Inhibition along the auditory pathway is crucial for the processing of acoustic information. Auditory information is transmitted to the auditory cortex (AC) via the auditory thalamus (medial geniculate body, MGB), which receives inhibitory input from the thalamic reticular nucleus (TRN). The TRN is an entirely inhibitory structure that sends dense projections to the MGB and other thalamic nuclei. The neuronal population of the TRN includes somatostatin (SST) and Parvalbumin (PV) positive cells. Prior studies in the AC show that these two inhibitory neuron types play crucial roles in auditory processing. This suggests a role of PV and SST neurons of the TRN for auditory processing within subcortical thalamic circuits. In AC, PVs and SSTs play differential roles in modulating sound processing by excitatory neurons. Here, we investigated how PV and SST neurons of the TRN anatomically project to the MGB and how inactivation of these two populations of cells modulates responses in excitatory cells of the MGB. Using viral anatomical tracing we find that PV and SST neurons project to different subdivisions of the MGB. PV neurons of the TRN project primarily to the ventral subdivision of the MGB whereas SST neurons of the TRN project primarily to the dorsal and medial subdivisions of the MGB. We also measured the effects of optogenetic silencing of PV and SST neurons of the TRN on tone evoked

responses in MGB. Surprisingly, inactivating SST neurons in the TRN suppressed tone-evoked activity in the majority of recorded neurons in the MGB (70%). By contrast, inactivation of PV cells of the TRN facilitated tone evoked responses in 29% of MGB neurons and suppressed responses in 46% of recorded MGB neurons. These findings suggest that PV and SST neurons of the TRN differentially modulate tone evoked activity in the MGB, further elucidating our understanding of cell-type specific effects in auditory processing.

3.1 INTRODUCTION

Sensory perception has been long understood to be a set of feedforward and feedback processes between the periphery, well established subcortical neuronal pathways, and the sensory cortical regions. Throughout these pathways, the interplay between excitatory and inhibitory synapses shapes how sensory information is transmitted (Blackwell & Geffen, 2017). Within the auditory system, excitatory synapses between the auditory cortex (AC) and the auditory thalamic nuclei, the medial geniculate body (MGB), play a key role in fine-tuning peripheral sensory information (Bartlett, 2013; He, 2003). Critical to this process are the inhibitory inputs from the thalamic reticular nucleus (TRN) – a thin sheet of inhibitory neurons that envelops the thalamus– to the MGB (Crabtree, 1998, 2018; Houser et al., 1980; Pinault, 2004). The two dominant sub-classes of inhibitory cells within the TRN are parvalbumin- (PV) and somatostatin- (SST) positive neurons, which differentially project to and modulate somatosensory thalamic nuclei, and are also critical subclasses of interneurons for auditory processing within the AC (Aizenberg et al., 2015; Blackwell & Geffen, 2017; Clemente-Perez, et al., 2017; Hamilton et al., 2013; E. A. Phillips & Hasenstaub, 2016; E. A. K. Phillips et al., 2017; Seybold et al., 2015). Yet it remains unknown whether and how these two sub-classes of inhibitory cells of the TRN anatomically project to and functionally modulate the excitatory neurons in the auditory thalamus. The goal of the present

study was to test the hypothesis that PV and SST neurons of the TRN anatomically target distinct sub-nuclei of the MGB and differentially modulate sound responses in MGB.

The TRN is the primary source of inhibition to the sensory thalamic nuclei. Through its inhibitory projections to excitatory relay cells, it filters relevant sensory information important for perception (Ahrens et al., 2015; Crick, 2006; Halassa et al., 2014) and supports optimal behavioral performance in sensory attentional tasks (Nakajima et al., 2019; Schmitt et al., 2017; Wimmer et al., 2015). Anatomical projections of the caudo-ventral area of the TRN, considered the auditory TRN (audTRN), target and envelop one, two or multiple subdivisions of the auditory thalamus, or the MGB (Guillery & Sherman, 2002). The MGB is functionally and anatomically subdivided into three main subnuclei: the ventral division (vMGB), the medial division (mMGB), and the dorsal division (dMGB). At a circuit level, the TRN receives excitatory information through projections from the MGB and from corticothalamic inputs of L5 and L6 cells, it then sends inhibitory projections back to the MGB (Carroll et al., 2022; Crabtree, 2018; Gentet & Ulrich, 2004; Guo et al., 2017; Lam & Sherman, 2005, 2011). This process serves as a feedback mechanism that modifies sensory information within the MGB. Furthermore, the TRN has been shown to evoke diverse effects in sound responses in the MGB. In the anesthetized rat preparation, responses to auditory stimuli in MGB were increased when TRN neurons were activated (Shosaku & Sumitomo, 1983). Neurons of the TRN that project differentially to subdivisions of the MGB also exhibit distinct bursting properties in presence of white noise (Kimura & Imbe, 2015; Shosaku & Sumitomo, 1983). These results suggest a possible cell type specific modulation of MGB neurons from distinct inhibitory neurons of the TRN.

Within the AC, PV and SST positive interneurons play differential but critical functions (Aizenberg et al., 2015; Briguglio et al., 2018; L. Y. Li et al., 2015; Moore & Wehr, 2013; Natan et al., 2015, 2017; Park & Geffen, 2019; E. A. Phillips & Hasenstaub, 2016; E. A. K. Phillips et al., 2017). These studies show that 1) SSTs, but not PVs contribute to stimulus-specific adaptation

(SSA), a phenomenon in which neurons adapt selectively to a subset of inputs presented frequently (Farley et al., 2010; Fishman & Steinschneider, 2012; Natan et al., 2015, 2017; Polterovich et al., 2018; Taaseh et al., 2011; Ulanovsky et al., 2003), and 2) PV and SST neurons differentially modulate frequency-dependent responses of excitatory neurons in AC (Natan et al., 2017; E. A. Phillips & Hasenstaub, 2016; E. A. K. Phillips et al., 2017).

In the somatosensory system, PV and SST neurons of the TRN target distinct thalamic nuclei involved in divergent thalamocortical circuits (Clemente-Perez, et al., 2017; Hoseini et al., 2021; Martinez-Garcia et al., 2020). PV and SST neurons of somatosensory TRN also have differential bursting properties and differentially modulate somatosensory behavior (Clemente-Perez, et al., 2017). Though it is shown that these cells have differential effects in AC and the somatosensory TRN, it remains unknown how PV and SST neurons of the auditory TRN project to and modulate the excitatory neurons of the MGB. Given the findings in the somatosensory system, we expect that PV and SST neurons of TRN differentially affect responses of the auditory thalamus.

In this study, our first goal was to anatomically identify how PV and SST inhibitory cells of the TRN project to the sub-nuclei of the MGB. We used viral tracing techniques to express an anterograde virus encoding a flexed fluorescent reporter in TRN of transgenic PV-Cre or SST-Cre mouse lines and traced projections to the MGB. Secondly, we tested the hypothesis that PV and SST cells of the TRN differentially modulate responses in MGB. We used viral transfection methods to drive a soma targeted inhibitory opsin in the TRN to inactivate TRN-PV or TRN-SST cells while recording neuronal activity from relay cells of the MGB of awake passively listening head-fixed mice. We found that PV and SST neurons of the TRN target distinct nuclei of the MGB and differentially modulate neuronal activity. Our study is the first to show 1) a differential anatomical projection pattern of PV and SST cells of the TRN to MGB and 2) differential modulation of MGB relay cells by PV and SST neurons of the TRN. This work reveals cell-type

specific properties of inhibition within the auditory thalamus, a structure that is key to auditory perception, and provides a framework to properly understand the function of excitatory-inhibitory interactions throughout circuits in the auditory system.

3.2 RESULTS

PV and SST neurons of the TRN project to different sub-nuclei of the MGB.

To test the hypothesis that PV and SST neurons of the TRN project differentially to the sub-divisions of the MGB, we used viral neuroanatomical tracing methods in PV-Cre and SST-Cre transgenic mice. We injected anterograde adeno-associated viruses into the TRN of PV-Cre or SST-Cre mice and traced the projections onto the MGB (**Figure 3.1A**). PV neurons of the TRN preferentially projected to the ventral sub-division of the MGB (vMGB) (**Figure 3.1B**). By contrast, SST neurons of the TRN preferentially projected to the dorsal and medial sub-divisions of the MGB (m/dMGB) (**Figure 3.1B**). We took advantage of the finding that calretinin is solely expressed in the higher-order MGB (Lu et al., 2009) to validate these findings. The virus labeled axons in MGB for neurons that receive direct inputs from TRN. Indeed, when the virus expressed in cell bodies of PV neurons in the TRN, labelled axons were located in the ventral MGB region, which was not immunolabeled by calretinin. There was little overlap in expression of the virus-driven fluorescent marker and the calretinin antibody. By contrast, axons of SST neurons of the TRN primarily targeted immunolabeled calretinin cells of m/dMGB (**Figure 3.1B**). Combined, these data demonstrate that PVs and SSTs in TRN target different subdivisions of the MGB.

Our anterograde injections targeted all the PV-Cre or SST-Cre expressing cells in the TRN; we next localized the PV and SST neurons of the TRN that directly project to MGB. To localize these neurons, we injected a retrograde adeno-associated virus in the MGB of PV-Cre and SST-Cre mice (**Figure 3.1C**). We then immunostained these brain slices to quantify the PV+ and SST+ neurons of the audTRN that project to MGB. We found that not all PV+ and SST+ neurons of the

TRN project to MGB (**Figure 3.1D**). Combined, these results show that PV and SST neurons of the TRN project to different sub-divisions of the MGB. PV cells primarily target the ventral sub-division of the MGB, or first-order MGB and SST cells primarily target the medial and dorsal sub-divisions of the MGB.

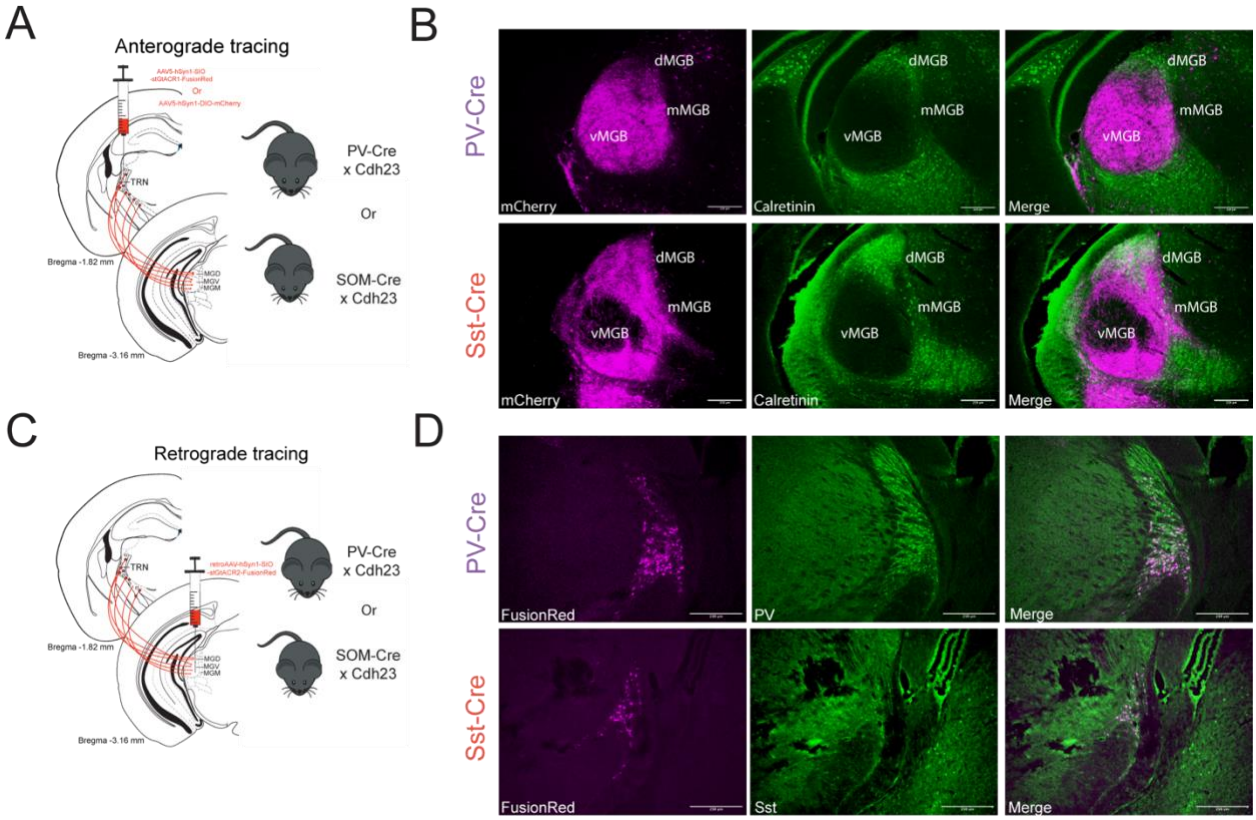

Figure 3.1. Anatomical tracing shows PV and SST neurons of the TRN project to different subnuclei of the MGB.

A. PV-cre or SST mice were injected with AAV5-hSyn1-DIO-mCherry into TRN for anterograde tracing of PV and SST cells in the TRN. **B. Top:** Projections of audTRN-PV neurons primarily target the ventral subdivision of the MGB. *Left panel*: Image showing viral expression of projections to thalamus. *Middle panel:* Image showing immunohistochemical labelling of calretinin in MGB. *Right panel*: Merged channels. Scale bar = 0.25 mm. vMGB: ventral MGB; dMGB: dorsal MGB; mMGB: medial MGB; **Bottom:** Projections of audTRN-SST neurons primarily target the medial and dorsal subdivision of the MGB. *Left panel*: Image showing viral expression of projections to thalamus. *Middle panel:* Image showing immunohistochemical labelling of calretinin in MGB. *Right panel*: Merged channels. Scale bar = 0.25 mm. vMGB: ventral MGB; dMGB: dorsal MGB; mMGB: medial MGB; **C.** PV-cre or SST mice were injected with a retrograde virus retroAAV-hSyn1-SIO-stGtACR1-FusionRed into the MGB for retrograde

tracing of PV and SST cells in the TRN that directly project to MGB. **D. Top:** audTRN-PV neurons that project to the MGB. *Left panel*: Image showing viral expression of projections to thalamus. *Middle panel:* Image showing immunohistochemical labelling of calretinin in MGB. *Right panel*: Merged channels. Scale bar = 0.25 mm. vMGB: ventral MGB; dMGB: dorsal MGB; mMGB: medial MGB; **Bottom:** audTRN-SST neurons that project to the MGB. *Left panel*: Image showing viral expression of projections to thalamus. *Middle panel:* Image showing immunohistochemical labelling of calretinin in MGB. *Right panel*: Merged channels. Scale bar = 0.25 mm. vMGB: ventral MGB; dMGB: dorsal MGB; mMGB: medial MGB. (n=4 each experiment).

Inactivation of SST neurons of the TRN primarily suppresses tone-evoked responses in excitatory relay cells of the MGB.

Previous work shows that genetically distinct TRN neurons express different physiological properties (Clemente-Perez, et al., 2017; Martinez-Garcia et al., 2020). Therefore, we hypothesized that the effects on tone-evoked responses of excitatory relay cells of the MGB would be differentially affected depending on which cell type of the TRN it receives inputs from. To test if excitatory relay cells of the MGB are differentially modulated by different TRN inputs, we first tested the effect of inhibition of SST cells of the auditory TRN on tone-evoked responses of MGB neurons. We injected a Cre-dependent soma-targeted inhibitory opsin (AV5-hSyn-SIO-stGtACR1-FusionRed) in the audTRN of SST-Cre mice. This virus only expresses in the soma of Cre-expressing SST cells, eliminating the chance of effects from backpropagating action potentials from local terminals (Mahn et al., 2018). We then implanted an optic fiber above audTRN, a headpost and a ground pin for awake *in-vivo* electrophysiological recordings. Mice passively listened to tones ranging from 3-80kHz, while we recorded and measured spiking activity of MGB neurons. In some set of trials, we inactivated audTRN-SST neurons by shining blue light via an implanted optic fiber cannula (**Figure3.2A & Figure 3.2B**). We then quantified neuronal firing

rate for both laser off and laser on conditions. As expected, when inhibiting SST neurons of the TRN we found an increase in tone-evoked firing rate (FR) of an MGB unit (**Figure 3.2C**). This facilitation of tone evoked response was consistent across preferred frequencies (**Figure 3.2C**). We calculated the tone-evoked responses during two windows of time, the early- tone on window (0-25ms of tone presentation) and the late- tone on window (25-tone offset), to assess if and how constant inhibition from TRN would affect the tone-responsiveness of MGB cells across time. We show that there is no change in the tuning in the late tone-on period (**Figure 3.2C**). Surprisingly, we also found individual units that showed suppression of neuronal activity during laser on trials (**Figure 3.2D**). As with the facilitated units, the suppression of tone evoked response was consistent across preferred frequencies (**Figure 3.2D**). These results show that inhibition of SST neurons of the audTRN have a facilitative and suppressive effect on tone evoked responses on individual MGB neurons.

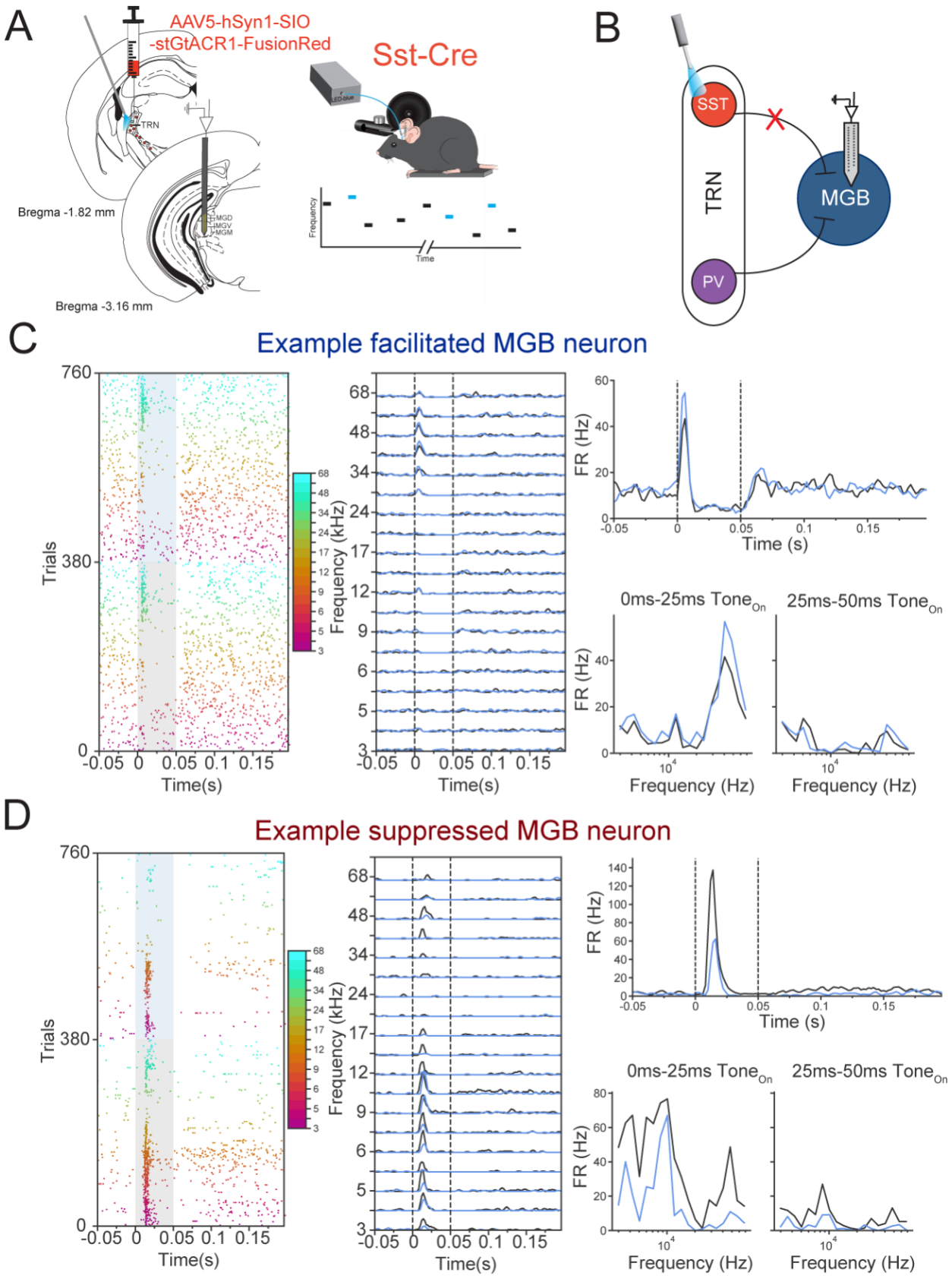
A
AAV5-hSyn1-SIO
-stGtACR1-FusionRed
Sst-Cre
TRN
Bregma -1.82 mm
MGD
MGV
MGM
Bregma -3.16 mm
LED-blue
Frequency
Time
B
SST
TRN
MGB
PV
C
Example facilitated MGB neuron
760
380
0
Trials
-0.05 0 0.05 0.1 0.15
Time(s)
68
48
34
24
17
12
9
6
5
3
Frequency (kHz)
FR (Hz)
60
40
20
0
Time (s)
0ms-25ms Tone$_{On}$
25ms-50ms Tone$_{On}$
10^4
Frequency (Hz)
D
Example suppressed MGB neuron
140
120
100
80

Figure 3.2. Suppression of SST neurons of the TRN facilitates and suppresses tone-evoked activity in MGB neurons.

A. SST mice were injected with a soma-targeted AAV5-hSyn1-DIO-stGtACR1-FusionRed into the audTRN and were implanted with an optic fiber. We recorded from MGB neurons in awake head-fixed mice. We presented a set of pure tones in light on and light off conditions. **B.** We selectively suppressed SST neurons of the audTRN while recording from thalamic relay cells of the MGB. **C.** *Left:* raster plot of an example facilitated unit; trials are ordered by frequency and laser condition. Gray box indicates laser off conditions, blue box indicating the laser on conditions. *Middle*: peri-stimulus time histogram (PSTH) of the example facilitated neuron ordered per frequency trial. *Top right*: PSTH of the facilitated example unit averaged across all trials for the laser off (black line) and laser on (blue line) conditions. *Bottom right*: (left) frequency response function for the facilitated unit during the first 25ms of tone presentation during laser off and laser on conditions and (right) the frequency response function of the unit during the late 25-50ms of tone presentation. **D.** *Left*: raster plot of an example suppressed unit; trials are ordered by frequency and laser condition. Gray box indicates laser off conditions, blue box indicating the laser on conditions. *Middle:* PSTH of the example suppressed neuron ordered per frequency trial. *Top right*: PSTH of the suppressed example unit averaged across all trials for the laser off (black line) and laser on (blue line) conditions. *Bottom right*: (left) frequency response function for the suppressed unit during the first 25ms of tone presentation during laser off and laser on conditions and (right) the frequency response function of the unit during the late 25-50ms of tone presentation.

Inactivation of PV neurons of the TRN facilitates and suppresses tone-evoked responses in excitatory relay cells of the MGB.

Studies in the TRN show that PV cells have different intrinsic properties than those of SST cells of the TRN (Clemente-Perez, et al., 2017), we therefore hypothesized that PV cells of the TRN would affect MGB neurons in a different way to SST neurons. We tested the effect of inhibition of PV cells of the auditory TRN on tone-evoked responses of MGB neurons. As described above, we injected a Cre-dependent soma-targeted inhibitory opsin in the audTRN of PV-Cre mice, implanted an optic fiber above audTRN, a headpost and a ground pin for awake *in-vivo* electrophysiological recordings. We recorded and measured spiking activity of MGB neurons while inactivating audTRN-PV neurons by shining blue light via an implanted optic fiber cannula (**Figure 3.3A & Figure 3.3B**). We quantified neuronal firing rates for both laser off and laser on conditions. When inhibiting PV neurons of the TRN found an increase in tone-evoked firing rate (FR) of MGB neurons which was consistent across all frequencies (**Figure 3.3C**). Similar to the effects of optogenetically inhibiting SST neurons, we also found individual units in which there was a suppression of neuronal activity during laser on trials (**Figure 3.3D**). The suppression of tone evoked response was also consistent across all frequencies (**Figure 3.3D**). These results suggest that PV neurons of the audTRN can both directly suppress neuronal responses in MGB, and likely via a reciprocal connection with SSTs of the TRN and with each other, enhance the response firing rate.

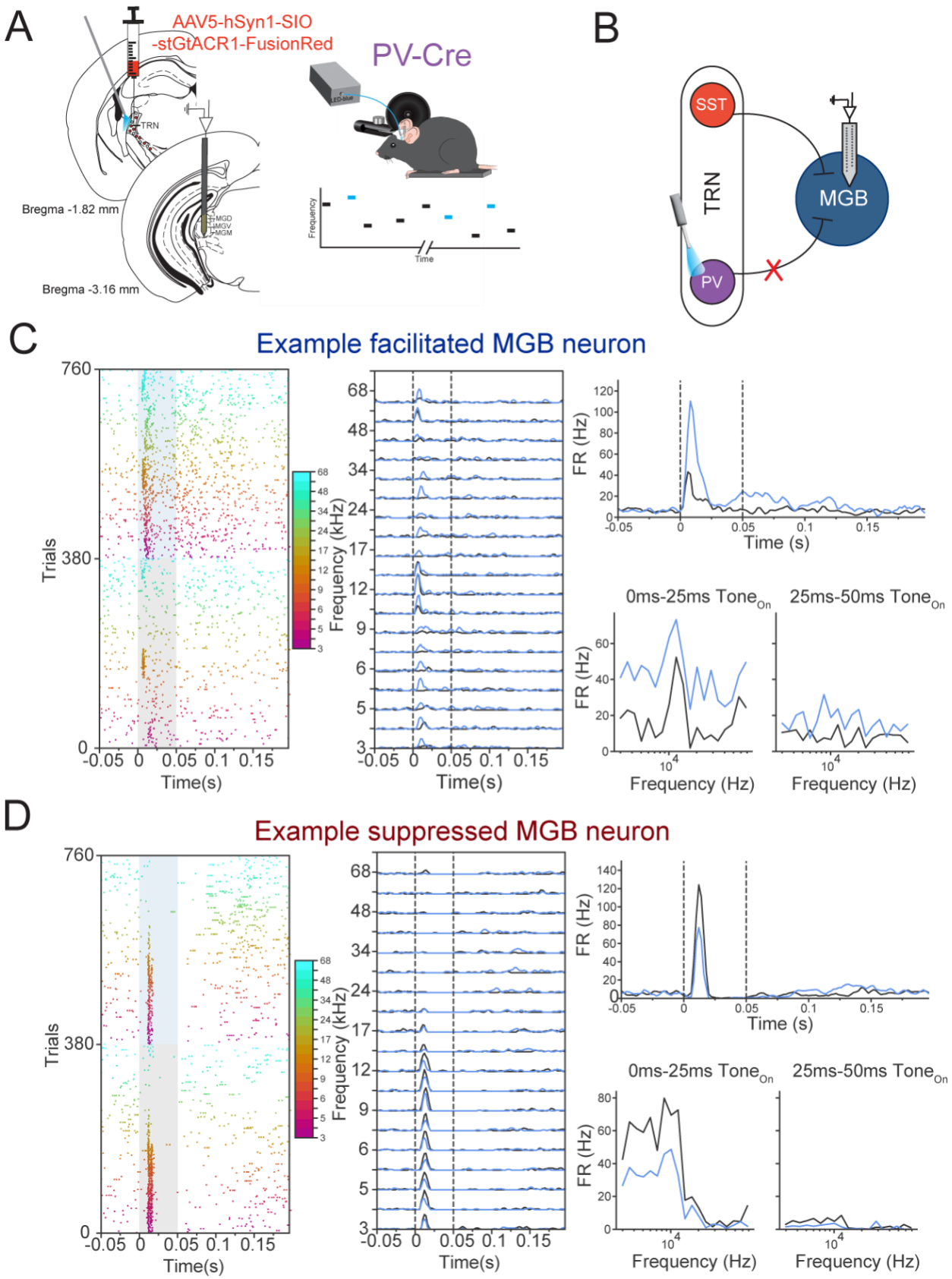
A
AAV5-hSyn1-SIO
-stGtACR1-FusionRed
PV-Cre
TRN
Bregma -1.82 mm
Bregma -3.16 mm
MGD
MGV
MGM
Frequency
Time
B
SST
TRN
MGB
PV
C
Example facilitated MGB neuron
Trials
Time(s)
Frequency (kHz)
FR (Hz)
Time (s)
0ms-25ms Tone On
25ms-50ms Tone On
Frequency (Hz)
D
Example suppressed MGB neuron
Trials
Time(s)
Frequency (kHz)
FR (Hz)
Time (s)
0ms-25ms Tone On
25ms-50ms Tone On
Frequency (Hz)

Figure 3.3. Suppression of PV neurons of the TRN facilitates and suppresses tone-evoked activity in MGB neurons.

A. PV-cre mice were injected with a soma-targeted AAV5-hSyn1-DIO-stGtACR1-FusionRed into the audTRN and were implanted with an optic fiber. We recorded from MGB neurons in awake head-fixed mice. We presented a set of pure tones in light on and light off conditions. **B.** We selectively suppressed PV neurons of the audTRN while recording from thalamic relay cells of the MGB. **C.** *Left*: raster plot of an example facilitated unit; trials are ordered by frequency and laser condition. Gray box indicates laser off conditions, blue box indicating the laser on conditions. *Middle*: PSTH of the example facilitated neuron ordered per frequency trial. *Top right*: PSTH of the facilitated example unit averaged across all trials for the laser off (black line) and laser on (blue line) conditions. *Bottom right*: (left) frequency response function for the facilitated unit during the first 25ms of tone presentation during laser off and laser on conditions and (right) the frequency response function of the unit during the late 25-50ms of tone presentation. **D.** *Left*: raster plot of an example suppressed unit; trials are ordered by frequency and laser condition. Gray box indicates laser off conditions, blue box indicating the laser on conditions. *Middle*: PSTH of the example suppressed neuron ordered per frequency trial. *Top right*: PSTH of the suppressed example unit averaged across all trials for the laser off (black line) and laser on (blue line) conditions. *Bottom right*: (left) frequency response function for the suppressed unit during the first 25ms of tone presentation during laser off and laser on conditions and (right) the frequency response function of the unit during the late 25-50ms of tone presentation.

Inactivation of SST neurons of the TRN suppresses tone-evoked responses in 70% of excitatory thalamic relay cells of the MGB.

Given these previously described results, we wanted to analyze tone-evoked responses at the population level to further understand how widespread this facilitation and suppression is within cells of the MGB. When inhibiting audTRN-SST neurons, we found that there is only a very small subset of MGB relay cells who exhibit facilitation of their tone-evoked responses (2% of tone-responsive units) (**Figure 3.4B**). Strikingly, the majority of MGB units show suppression of their tone-evoked responses (70% of tone-responsive units) (**Figure 3.4B**). We also found a subset of tone-responsive neurons that were not significantly affected by the laser manipulation (25% of tone-responsive units) (**Figure 3.4B**). For the neurons in the facilitated tone-evoked activity group, inactivation of audTRN-SST neurons significantly increases tone evoked firing rate during the first 25ms of the tone presentation and during the remaining 25ms of tone presentation, and as expected there was no effect on spontaneous activity (**Figure 3.4D**). In the suppressed tone-evoked activity group, inactivation of audTRN-SST neurons significantly reduces tone evoked firing rate during the first 25ms of the tone presentation and during the remaining 25ms of tone presentation, and as expected there was no effect on spontaneous activity (**Figure 3.4D**). We then separated each sub-group and plotted their frequency response functions. For the facilitated sub-group, we observed that inhibition of audTRN-SST produced no significant changes in tuning (**Figure 3.4E**). The population of MGB neurons that had suppressed tone-evoked firing rates had a significant downward shift in the frequency response function during the first 25ms of the tone presentation and the remaining 25ms of tone presentation (**Figure 3.4F**).

To examine frequency selectivity of neurons–how specific are neuronal responses to a particular stimulus–we calculated the sparseness index. A value closer to 1 indicates that the unit responds narrowly to a set of stimuli and a value closer to 0 indicates that units will respond to a

broader range of stimuli. We found that inactivation of SST neurons of audTRN did not affect sparseness in the facilitated group, however it significantly increased the sparseness index in the suppressed group (**Figure 3.4E-F & Figure 3.6D-E**). Together, these results indicate that SST neurons of the TRN contribute to how narrowly or broadly tuned MGB cells are to auditory stimuli.

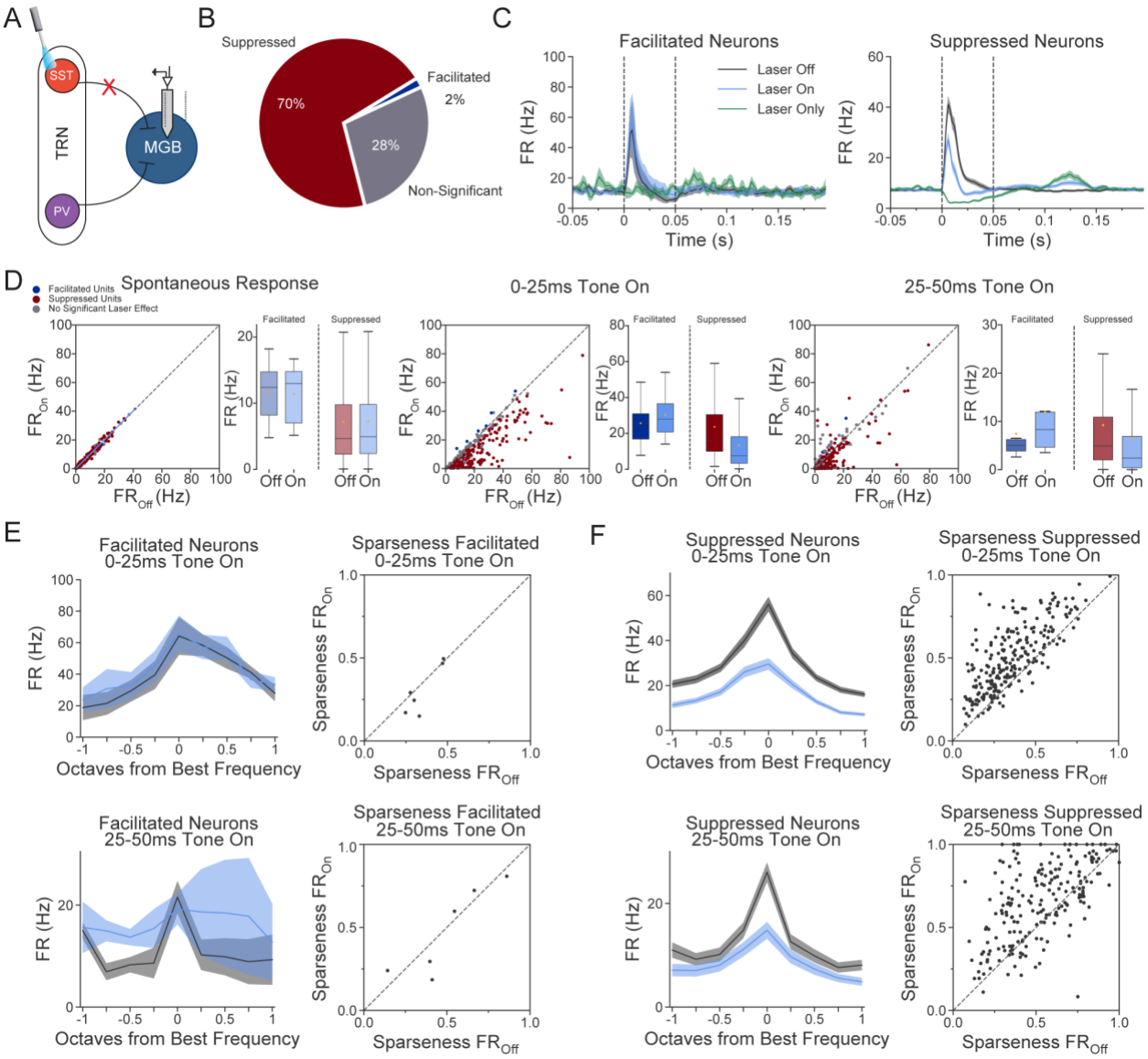

Figure 3.4. Suppression of SST neurons of the TRN suppresses tone-evoked activity in the majority of recorded MGB neurons.

A. SST-cre mice were injected with a soma-targeted AAV5-hSyn1-DIO-stGtACR1-FusionRed into the audTRN. We recorded from MGB neurons in awake head-fixed mice while we presented a set of pure tones in light on and light off conditions. **B.** Pie chart breaking down the effect of audTRN-SST inactivation in neurons of the MGB. We find that 70% of recorded units had suppressed tone-evoked responses (red slice), only 2% of recorded units had facilitated tone-evoked responses (navy blue slice), and 28% of tone-responsive units were not affected by laser manipulation (gray

slice). **C.** Mean PSTH of all recorded units grouped by their tone evoked responses. *Left*: Units with facilitated tone responses following audTRN-SST inhibition during laser-only trials (green line), tone-only trials (black line), and tone- and laser-on trials (light blue line). *Right*: Units with suppressed tone responses following audTRN-SST inhibition during laser-only trials, tone-only trials, and tone- and laser-on trials (light blue line). **D.** *Left*: scatter and boxplot of the mean FR in laser off and laser on conditions for facilitated (navy blue) and suppressed (red) units during spontaneous activity. *Middle*: scatter and boxplot of the mean FR in laser off and laser on conditions for facilitated (navy blue) and suppressed (red) units during the first 0-25ms of tone presentation. *Right*: scatter and boxplot of the mean FR in laser off and laser on conditions for facilitated (navy blue) and suppressed (red) units during the last 25-50ms of tone presentation. **E.** *Top left*: Mean frequency response function centered at best frequency (0 octaves = BF) for units with facilitated tone evoked responses in both the laser on and laser off trials during the initial 0-25ms of tone presentation. Shaded areas represent SEM±. *Top right*: Scatter plot showing the sparseness index during the first 0-25ms of tone presentation during laser off and laser on trials. *Bottom left:* Mean frequency response function centered at best frequency (0 octaves = BF) for units with facilitated tone evoked responses in both the laser on and laser off trials during the remaining 25-50msms of tone presentation. Shaded areas represent SEM±. *Bottom right*: Scatter plot showing the sparseness index during the remaining 25-50ms of tone presentation during laser off and laser on trials. **F.** *Top left:* Mean frequency response function centered at best frequency (0 octaves = BF) for units with suppressed tone evoked responses in both the laser on and laser off trials during the initial 0-25ms of tone presentation. Shaded areas represent SEM±. *Top right*: Scatter plot showing the sparseness index during the first 0-25ms of tone presentation during laser off and laser on trials. *Bottom left:* Mean frequency response function centered at best frequency (0 octaves = BF) for units with suppressed tone evoked responses in both the laser on and laser off trials during the remaining 25-50msms of tone

presentation. Shaded areas represent SEM±. *Bottom right*: Scatter plot showing the sparseness index during the remaining 25-50ms of tone presentation during laser off and laser on trials. (N = 328; n=4).

Inactivation of PV neurons of the TRN facilitates tone-evoked responses in 26% of MGB cells and suppresses tone-evoked responses in 46% of excitatory thalamic relay cells of the MGB.

To examine if PV and SST inhibition contribute to tone-evoked responses in MGB, we then analyze tone-evoked responses of MGB neurons at the population data following audTRN-PV suppression (**Figure 3.5A**). When we suppressed audTRN-PV neurons, we found that there is a higher percent of MGB neurons that exhibit facilitation of their tone-evoked responses compared to audTRN-SST inhibition (26% of tone-responsive units) (**Figure 3.5B**). Surprisingly still, there was also a high number of MGB units that had suppressed tone-evoked responses (46% of tone-responsive units) (**Figure 3.5B**). We also found a subset of tone-responsive neurons that were not significantly affected by the laser manipulation (25% of tone-responsive units) (**Figure 3.5B**). In MGB neurons with facilitated tone-evoked responses, inactivation of audTRN-PV neurons significantly increased tone evoked firing rate during the first 25ms of the tone presentation 25-50ms of tone presentation and had no effect on spontaneous activity (**Figure 3.4D**). Inactivation of audTRN-PV neurons significantly reduced tone evoked firing rate during the first 25ms of the tone presentation, 25-50ms of tone presentation, and had no effect on spontaneous activity (**Figure 3.5D**). Suppression of audTRN-SST produced significant changes in tuning for both the facilitated- and suppressed-activity groups; with a significant shift upwards and a significant shift downwards in the frequency response function, respectively (**Figure 3.5E & Figure 3.5F**). Interestingly, the population of MGB neurons that had facilitated tone-evoked

responses decreased the response to the best frequency (BF: 0 octaves), but still had a significant increase in the response to the side frequencies (**Figure 3.5E**).

We found that suppression of PV neurons of audTRN significantly affected sparseness in both subgroups. Following audTRN-PV inhibition, MGB neurons that experience facilitated tone-evoked responses, had a significant decrease in the sparseness index, making these units more broadly tuned (**Figure 3.5E, Figure 3.6E-F**). The suppressed tone-evoked response group had a significant increase in the sparseness index, making these neurons more narrowly tuned following audTRN-PV inhibition (**Figure 3.5F, Figure 3.6E-F**). These results indicates that PV neurons of the TRN contribute to how narrowly or broadly tuned MGB cells are to auditory stimuli in an output dependent manner.

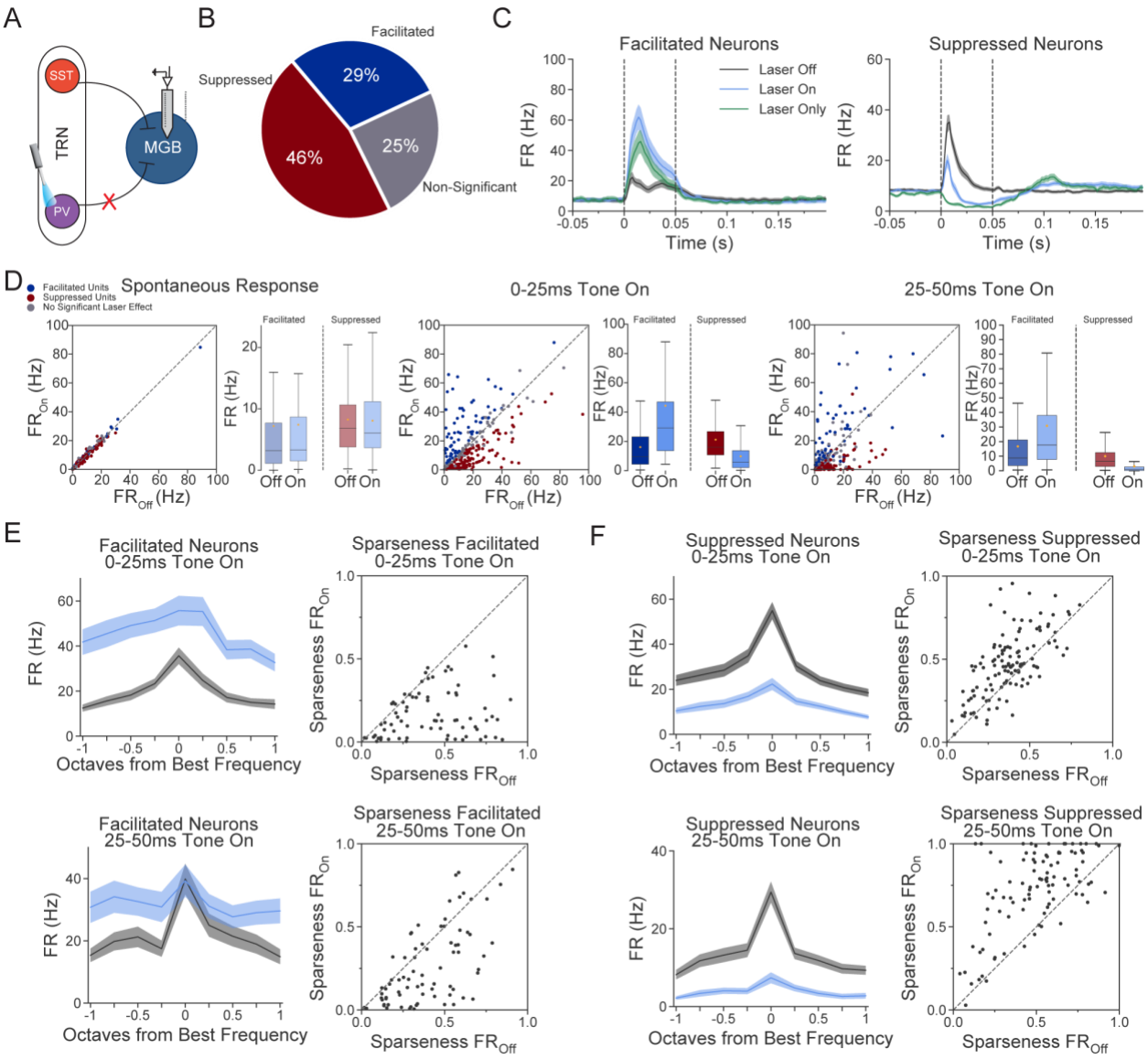

Figure 3.5. Suppression of PV neurons of the TRN suppresses and facilitates tone-evoked activity in MGB neurons.

A. PV-cre mice were injected with a soma-targeted AAV5-hSyn1-DIO-stGtACR1-FusionRed into the audTRN. We recorded from MGB neurons in awake head-fixed mice while we presented a set of pure tones in light on and light off conditions. **B.** Pie chart breaking down the effect of audTRN-PV inactivation in neurons of the MGB. We find that 46% of recorded units had suppressed tone-evoked responses (red slice), 29% of recorded units had facilitated tone-evoked responses (navy blue slice), and 25% of tone-responsive units were not affected by laser manipulation (gray slice).

C. Mean PSTH of all recorded units grouped by their tone evoked responses. *Left*: Units with facilitated tone responses following audTRN-PV inhibition during laser-only trials (green line), tone-only trials (black line), and tone- and laser-on trials (light blue line). *Right*: Units with suppressed tone responses following audTRN-PV inhibition during laser-only trials, tone-only trials, and tone- and laser-on trials (light blue line). **D.** *Left*: scatter and boxplot of the mean FR in laser off and laser on conditions for facilitated (navy blue) and suppressed (red) units during spontaneous activity. *Middle*: scatter and boxplot of the mean FR in laser off and laser on conditions for facilitated (navy blue) and suppressed (red) units during the first 0-25ms of tone presentation. *Right*: scatter and boxplot of the mean FR in laser off and laser on conditions for facilitated (navy blue) and suppressed (red) units during the last 25-50ms of tone presentation. **E.** *Top left*: Mean frequency response function centered at best frequency (0 octaves = BF) for units with facilitated tone evoked responses in both the laser on and laser off trials during the initial 0-25ms of tone presentation. Shaded areas represent SEM±. *Top right*: Scatter plot showing the sparseness index during the first 0-25ms of tone presentation during laser off and laser on trials. *Bottom left*: Mean frequency response function centered at best frequency (0 octaves = BF) for units with facilitated tone evoked responses in both the laser on and laser off trials during the remaining 25-50msms of tone presentation. Shaded areas represent SEM±. *Bottom right*: Scatter plot showing the sparseness index during the remaining 25-50ms of tone presentation during laser off and laser on trials. **F.** *Top left*: Mean frequency response function centered at best frequency (0 octaves = BF) for units with suppressed tone evoked responses in both the laser on and laser off trials during the initial 0-25ms of tone presentation. Shaded areas represent SEM±. *Top right*: Scatter plot showing the sparseness index during the first 0-25ms of tone presentation during laser off and laser on trials. *Bottom left*: Mean frequency response function centered at best frequency (0 octaves = BF) for units with suppressed tone evoked responses in both the laser on and laser off trials during the remaining 25-50msms of tone

presentation. Shaded areas represent SEM±. *Bottom right*: Scatter plot showing the sparseness index during the remaining 25-50ms of tone presentation during laser off and laser on trials. (N = 237; n=4).

PV and SST neurons of the TRN affect frequency tuning of MGB neurons differentially.

Work in the auditory cortex (AC) shows that inhibition of PV and SST interneurons produce changes in gain and tuning of excitatory pyramidal cells of AC (Natan et al., 2017; E. A. Phillips & Hasenstaub, 2016; E. A. K. Phillips et al., 2017). Given the lack of robust local inhibitory networks within the MGB (Ito et al., 2011), we hypothesized that PV and SST neurons of the TRN modulate gain and tuning of relay cells of the MGB. To test this hypothesis, we ran a linear regression model on the frequency response functions of MGB cells during inactivation of PV or SST cells of the TRN. We calculated the slopes and the intercepts of the frequency response functions; wherein changes in the slopes account for changes in gain and changes in the intercepts account for changes in tuning (Natan et al., 2017; E. A. Phillips & Hasenstaub, 2016). We found that when inactivating audTRN-PV or audTRN-SST the median slopes and y-intercepts are below 0 (slope coefficient) and above 1 (y-intercepts) in both facilitated and suppressed tone-evoked response groups (**Figure 3.6A-B**).

To further understand PV and SST dynamics on MGB neurons, we also measured time-to-peak responses in both groups. We found that time-to-peak significantly increases and decreases in the facilitated-tone evoked response and suppressed-tone evoked response groups respectively when inhibiting PV neurons of the audTRN (**Figure 3.6C-D**). However, there was no change in the time-to-peak response of MGB neurons upon inhibition of SST audTRN cells. The effects of sparseness were similar between PV and SST inhibition, both facilitated and suppressed groups had a decrease sparseness index and an increase in sparseness index

respectively (**Figure 3.6E-F)** Together these results showcase the diversity of effects on tuning and firing properties in cells of the MGB following inhibition of PV and SST neurons of the audTRN.

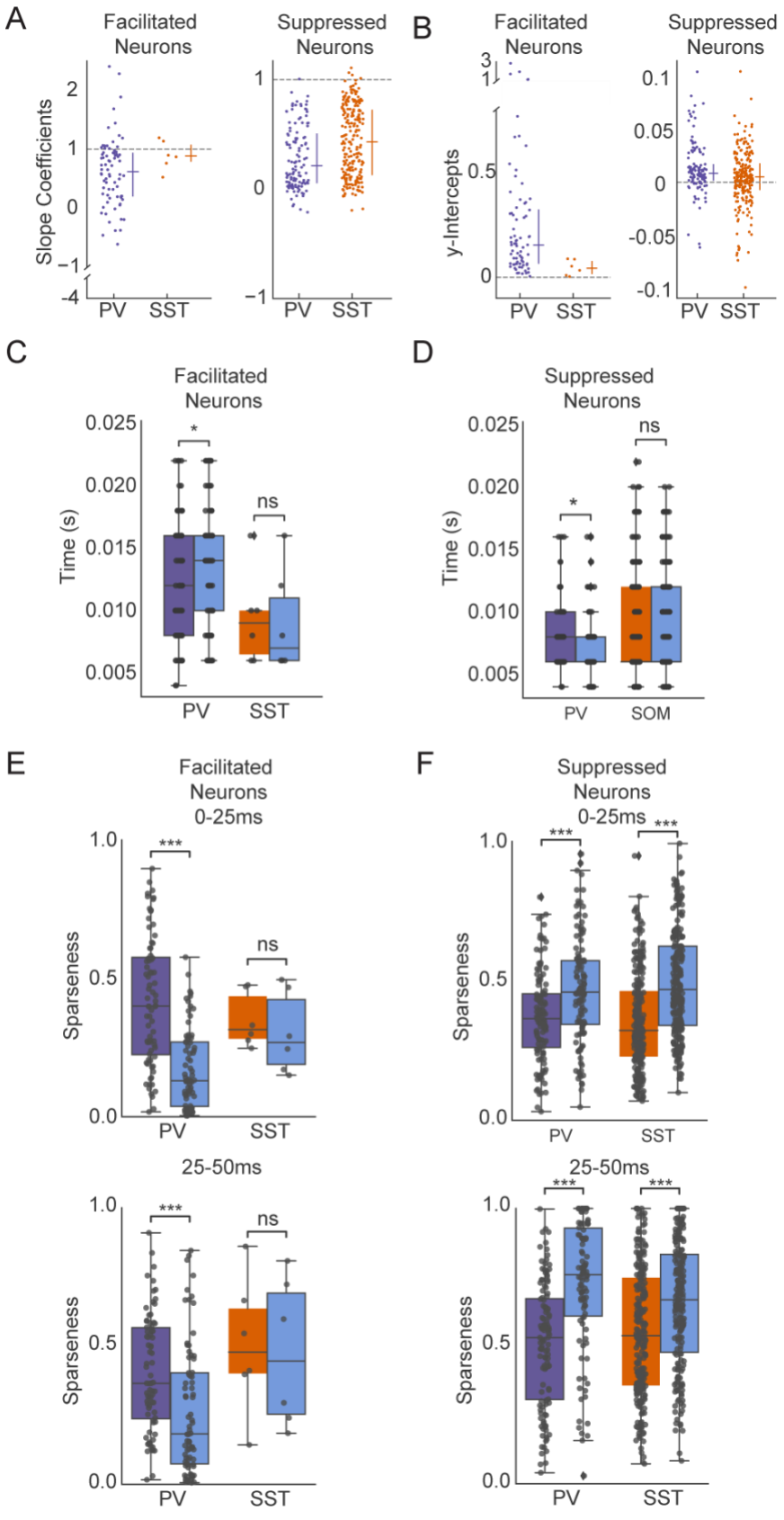
A
Facilitated Neurons
Suppressed Neurons
Slope Coefficients
PV
SST
B
Facilitated Neurons
Suppressed Neurons
y-Intercepts
PV
SST
C
Facilitated Neurons
Time (s)
*
ns
PV
SST
D
Suppressed Neurons
Time (s)
*
ns
PV
SOM
E
Facilitated Neurons
0-25ms
Sparseness
***
ns
PV
SST
25-50ms
Sparseness
***
ns
PV
SST
F
Suppressed Neurons
0-25ms
Sparseness
***
***
PV
SST
25-50ms
Sparseness
***
***
PV
SST

Figure 3.6. Effects of suppression of SST and PV neurons of the TRN on tuning and intrinsic properties of the MGB.

A. *Left*: slope coefficients for MGB neurons with facilitated tone evoked responses following audTRN-PV suppression (purple) and audTRN-SST suppression (orange). *Right*: slope coefficients for MGB neurons with suppressed tone evoked responses following audTRN-PV suppression and audTRN-SST suppression. Purple or orange horizontal lines indicate median, purple or orange vertical lines indicate interquartile range. **B.** *Left*: y-intercepts for MGB neurons with facilitated tone evoked responses following audTRN-PV suppression (purple) and audTRN-SST suppression (orange). *Right*: y-intercepts for MGB neurons with suppressed tone evoked responses following audTRN-PV suppression and audTRN-SST suppression. Purple or orange horizontal lines indicate median, purple or orange vertical lines indicate interquartile range. **C.** Boxplot of time to peak latency in units with facilitated tone responses following audTRN-PV (purple) or audTRN-SST (orange) inhibition. Laser-on conditions are represented by blue boxplot. **D.** Boxplot of time to peak latency in units with suppressed tone responses following audTRN-PV (purple) or audTRN-SST (orange) inhibition. Laser-on conditions are represented by blue boxplot. **E.** *Top*: Boxplot of sparseness index in units with facilitated tone responses following audTRN-PV (purple) or audTRN-SST (orange) inhibition during the first 0-25ms of tone presentation. Laser-on conditions are represented by blue boxplot. *Bottom*: Boxplot of sparseness index in units with facilitated tone responses following audTRN-PV (purple) or audTRN-SST (orange) inhibition during the last 25-50ms of tone presentation. Laser-on conditions are represented by blue boxplot. **E.** *Top*: Boxplot of sparseness index in units with suppressed tone responses following audTRN-PV (purple) or audTRN-SST (orange) inhibition during the first 0-25ms of tone presentation. Laser-on conditions are represented by blue boxplot. *Bottom*: Boxplot of sparseness index in units with suppressed tone responses

following audTRN-PV (purple) or audTRN-SST (orange) inhibition during the last 25-50ms of tone presentation. Laser-on conditions are represented by blue boxplot.

3.3 DISCUSSION

The TRN is the main source of inhibitory information to all the sensory thalamic structures (Houser et al., 1980; Oertel et al., 1983; Pinault & Deschênes, 1998). The TRN–though entirely GABAergic (Houser et al., 1980)–is not homogenous in its molecular or genetic composition; cells within the TRN showcase a variety of genetic profiles, physiological properties, and distinct anatomical distributions (Clemente-Perez, et al., 2017; Y. Li et al., 2020; Martinez-Garcia et al., 2020; Pinault, 2004). Showcasing the anatomical complexity within the TRN, a recent single-cell transcriptomic analysis has shown that the TRN's distinct anatomical pattern of cells is in fact a result of expression of negatively correlated transcriptomic genetic profiles (Y. Li et al., 2020). Furthermore, this differential anatomical distribution of TRN neurons is not limited to their topographical locations within the TRN, it also extends to how they project to their anatomical targets. Distinct populations of cells in the TRN project to hierarchically distinct thalamic areas; for example, PV cells target primary or first-order thalamic nuclei and SST cells primarily targeting secondary or higher-order thalamic regions (Clemente-Perez, et al., 2017; Y. Li et al., 2020). Consistent with recent studies from the somatosensory system, we show that PV neurons of the TRN primarily project to the primary or first-order auditory thalamic sub-region (ventral MGB) and SST neurons of the TRN primarily project to the second-order or higher-order auditory thalamic sub-regions (dorsal & medial MGB) (**Figure 3.1**). Our anatomical data suggests that this differential output pattern of PV and SST neurons of the TRN to hierarchically distinct sensory thalamic regions is conserved across sensory modalities and may provide insights on the complexity of input-output relationships between the TRN and other brain regions.

In the present study, we found that inactivation of two distinct sub-populations of TRN neurons has diverging effects in tone-responses of MGB neurons. We show that upon inactivation

of PV and SST neurons of the TRN there is facilitation of tone-responses in the smaller fraction of recorded MGB neurons (**Figure 3.3 & Figure 3.4**). Surprisingly however, the majority of the MGB neurons have suppressed tone-responses upon inactivation of PV and SST neurons of the TRN. These results indicate a more nuanced role of TRN function on MGB neurons than a straightforward inhibitory projection. Previous research shows that TRN neurons evoke diverse effects on sound responses within the MGB. Neurons of the TRN that differentially project to subdivisions of the MGB exhibit distinct bursting properties in the presence of white noise (Kimura et al., 2005, 2007, 2012; Simm et al., 2017). TRN neurons projecting to the vMGB exhibit a greater number of spikes and shorter interspike-intervals than TRN neurons that project to dMGB (Kimura & Imbe, 2015). Research in the somatosensory system similarly shows distinct bursting properties of PVs and SSTs of the TRN (Clemente-Perez, et al., 2017). Furthermore, recent studies show the physiological differences between shell and core neuronal populations in TRN (Y. Li et al., 2020; Martinez-Garcia et al., 2020). It is possible that the different results we report in response to inhibition of sub-populations of TRN cells in tone-responses in MGB correspond to their genetic profile and anatomical location; with low bursting core-like neurons providing excitatory feedback to shell-like neurons when they are inhibited. Though it has been previously reported that there are no GABAergic connections between reticular cells in the slice preparation (Hou et al., 2016), our data might also suggest an intricate microcircuitry of synapses between cell types within the TRN. The TRN is composed of gap junctions and synaptic connections (Crabtree, 2018; Pinault, 2004). It is also possible that gap junctions play a major role in shell-like cells providing feedback and not in the core-like cells. These two possibilities would explain the two different response profiles our data shows when inhibiting PV and SST neurons of the TRN. Our data shows that the TRN is a convoluted structure based on its input-output circuitry.

Given these varying internal physiological effects, we asked whether these different cell types have differential effects on tuning in the MGB. We hypothesized that distinct neuron types of the TRN would drive differential physiological effects on auditory thalamic sound tuning. Though there are a variety of molecular distinct cell types within the TRN, in this study we focused on the two major inhibitory cell types known for shaping auditory responses in auditory cortical brain regions–PV and SST neurons. Within the auditory cortex, PV and SST neurons differentially affect tuning of excitatory cortical neurons (Natan et al., 2017; E. A. Phillips & Hasenstaub, 2016; E. A. K. Phillips et al., 2017). We therefore hypothesized that PV and SST neurons of the TRN will have similar diverging effects on tuning in excitatory relay cells of the MGB. Our data shows that inactivation of both PV and SST neurons of the TRN results in a divisive change in gain of MGB frequency response functions, but no cell type drives a larger effect in this change in gain (**Figure 3.4**). However, when comparing the effects of inactivation of PV and SST neurons of the TRN in tuning of the MGB relay cells, optogenetic manipulation of PV had a significantly larger effect in tuning than when inactivating the SST neuronal population (**Figure 3.4**). These diverging effects in the frequency response functions of the MGB relay cells suggests that PV but not SST neurons of the TRN are critical for shaping auditory information at the level of the thalamus.

The TRN is a functionally complex structure, playing key roles in attention, sleep spindles, pain, whisking behaviors, and sensory filtering (Clemente-Perez, et al., 2017; Iavarone et al., 2023; J. Liu et al., 2023; Nakajima et al., 2019; Visocky et al., 2022). Recent studies explore the effect of PV neurons of the TRN in sleep spindles as well as pain reduction (Iavarone et al., 2023; J. Liu et al., 2023). Our results can add to this complex set of behaviors given that these two neuron types show different response, perhaps one cell type is required over the other for certain types of behaviors. Previously, studies involving attention have ablated the entirety of the TRN. Less is known on how the different molecular and genetic complexity of the TRN plays a role in behavior. We hypothesize that PV neurons are more likely to play key roles in more complex

auditory processing that involved the lemniscal auditory pathway. These results are consistent with the literature that shows that PV neurons of the TRN are more likely to be involved in primary functions of brain regions, for example in the whisking system of Whereas SST neurons are likely involved in behaviors that require other auditory responses such as associative learning, somatosensory integration, etc.

Together our results provide a greater insight into the complexity of the TRN and its function in sensory processing. Therefore, the question of how other inhibitory cell types within the TRN anatomically project to auditory thalamic regions, remains unknown.

3.4 MATERIALS AND METHODS

Animals.

We performed all experimental procedures in accordance with NIH guidelines on use and care of laboratory animals and by approval of the Institutional Animal Care and Use Committee at the University of Pennsylvania (protocol number 803266). Care was taken to minimize any pain, discomfort, or distress of the animals during and following experiments. Experiments were performed in adult male (n = 12) and female (n = 12) mice aged 3-8 months and weighing 20-32g. The mouse lines used in this study were crosses between Cdh23 mice (B6.CAST-Cdh23^{Ahl+}/Kjn; RRID:IMSR_JAX:002756)—a transgenic line that has a targeted point reversion in the Cdh23 gene which protects mice from age-related hearing loss (Johnson et al., 2017)—and PV-Cre mice (B6.129P2-Pvalb$^{tm1(cre)Arbr}$/J; RRID:IMSR_JAX:017320) or SST-Cre mice (SST$^{tm2.1(cre)Zjh}$/J; RRID:IMSR_JAX:013044). Mice were housed at 28°C on a reversed 12hr light-dark cycle with ad libitum access to food and water. Experiments were performed during the animals' dark cycle and housed individually in an enriched environment after major surgery. Euthanasia was performed by infusion of a ketamine (300mg/kg) and dexmedetomidine (3mg/kg) cocktail or prolonged

exposure to CO2. Both methods are consistent with the recommendations of the American Veterinary Medical Association (AVMA) Guidelines on Euthanasia.

Surgical Procedures.

Mice were induced to a surgical plane with 3% isoflurane in oxygen and secured in a stereotaxic frame. Animals were then maintained in an anesthetic plane with 1-2% isoflurane in oxygen and kept at a body temperature of 36°C with the use of a homeothermic blanket. Prior to any surgical procedure, mice were administered subcutaneous injections of sustained release buprenorphine (1mg/kg) for analgesia, dexamethasone (0.2mg/kg) for reduction of swelling, and bupivacaine (2mg/kg), for local anesthesia. Mice received a subcutaneous injection of an antibiotic, enrofloxacin (Baytril; 5mg/kg), for 3 days as part of their post-operative care.

Viral Injections.

Approximately 21 days prior to electrophysiological recordings or transcardial perfusions, we performed small (0.5mm in diameter) unilateral craniotomies using a micromotor drill (Foredom)–under aseptic conditions–over audTRN or MGB. Glass syringes–attached to a syringe pump (Pump 11 Elite, Harvard Apparatus)–were backfilled with modified viral vectors, placed over the brain region of interest, and used to inject virus at 60nL/min. Glass syringes were made using a micropipette puller (P-97, Sutter Instruments) from glass capillaries (Harvard Apparatus, 30-0038) with tip openings ranging from 30µm-40µm in diameter. Following injections, syringes were left in place for 15-20min before retraction. Craniotomies were then covered with bone wax (Fine Science Tools) or a removable silicone plug (Kwik-Cast, World Precision Instruments). audTRN coordinates: -1.80mm posterior to bregma, ±2.25mm lateral to bregma, -2.90mm below the pial surface. MGB coordinates: -3.30mm posterior to bregma, ±2.00mm lateral to bregma, -2.90mm below the pial surface. Viral spread was confirmed post-mortem.

Viral Vectors.

For soma-targeted inhibition of PV or SST neurons of the audTRN we injected 400nL of AAV5_hSyn1-SIO-stGtACR1-FusionRed (full titer, Addgene 105678-AAV5). For anterograde tracing of PV or SST neurons of the audTRN and control experiments we injected 400nL of AAV5-hSyn-DIO-mCherry (full titer, Addgene 50459-AAV5). For retrograde tracing of PV or SST neurons of the audTRN we injected 500nL of retroAAV_hSyn1-SIO-stGtACR2-FusionRed (full titer, Addgene 105677-AAVrg) or retroAAV-hSyn-DIO-EGFP (full titer, Addgene 50457-AAVrg).

Fiber Optic Cannula & Headpost Implantation.

Following virus injections, fiber optic cannulas (Prizmatix: 3mm in length, 1.25mm in diameter, Ø200µm core, 0.66NA) were implanted above audTRN at a 20° angle, -1.80mm posterior to bregma, ±3.25mm lateral to bregma, and -2.50mm below the pial surface. A small craniotomy was made over the left frontal lobe and a ground pin was implanted. Craniotomies were sealed with Kwik-Cast (World Precision Instruments). The cannula, ground pin and a custom-made stainless-steel headpost (eMachine shop) were then secured with dental cement (C&B Metabond, Parkell) and dental acrylic (Lang Dental).

Tissue Processing.

After allowing time for proper viral expression or following electrophysiological recordings, mice were deeply anesthetized with a cocktail of ketamine and dexmedetomidine (see Animals) and transcardially perfused with 1X PBS followed by 4% paraformaldehyde (PFA) in PBS. Brains were extracted and post-fixed in 4% PFA overnight at 4°C. Following post-fixation, tissue was cryoprotected in 30% sucrose for at least 24hrs at 4°C until sectioning. Brain sections of 40µm-50µm in thickness were cut on a cryostat (Leica CM1860) and collected for

immunohistochemistry or imaging of viral expression. For imaging of viral expression or probe location, 50µm-thick sections were mounted on gelatin-coated glass slides and coverslipped using ProLong Diamond Antifade Mounting media with DAPI (Catalog # P36971, Invitrogen). For immunohistochemistry, 40µm-thick sections were collected in 12-well plates filled with 1X PBS (~5-10 sections per well). Slides were imaged using a fluorescent microscope (Olympys BX43) or a confocal microscope (Zeiss LSM 800).

Immunohistochemistry.

Free-floating 40µm-thick brain sections were first washed in 1X PBS (3 x 10min washes). To increase membrane permeability, sections were microwaved for approximately 10 seconds and then incubated in a solution of 0.3% Triton X-100 in 1X PBS (hereinafter referred to as PBT) for 30 min at room temperature. The sections were then incubated in a blocking solution consisting of 3% normal goat serum in PBT (hereinafter referred to as PBTG) for 30min at room temperature. Following incubation with PBTG, sections were incubated in primary antibody solution which consisted of the following antibodies diluted in PBTG: (1) 1:500 mouse monoclonal anti-Parvalbumin (Swant, PV-235; RRID:AB_10000343), (2) 1:500 rabbit polyclonal anti-Somatostatin (Immunostar, 20067); RRID: AB_572264), and (3) 1:1000 rabbit polyclonal anti-Calretinin (Swant, Calretinin-7697; RRID:AB_2721226). Incubation in primary solution was done overnight at 4°C on a shaker (Fisher Scientific); well plates were covered with parafilm and a plastic lid. Following the incubation period with primary antibody solution, sections were washed in PBT (3 x 10min washes). Sections were then incubated in secondary antibodies conjugated to fluorescent markers diluted in PBTG for 2hrs at room temperature; well plates were covered with aluminum foil to block light. Secondary antibodies used were: (1) Alexa Fluor Plus 488 Goat anti-Mouse IgG (H+L) (for PV stain; catalog # A32723, Invitrogen; RRID: AB_2633275), (2) Alexa Fluor Plus 488 Goat anti-Rat IgG (H+L) (for SST stain; Catalog #

A48262, Invitrogen; RRID: AB_2896330), and (2) Alexa Fluor Plus 488 Goat anti-Rabbit IgG (H+L) (for Calretinin stain; Catalog # A32731, Invitrogen; RRID: AB_2633280). The sections were subsequently washed in 1X PBS (3 x 10min washes). Sections were then mounted on gelatin-coated glass slides, coverslipped using ProLong Diamond Antifade Mounting media with DAPI (Catalog # P36971, Invitrogen) and left to curate at room temperature for at least 24hrs prior to imaging on a flat surface. Slides were then imaged using a fluorescent microscope (Olympys BX43) or a confocal microscope (Zeiss LSM 800).

Acoustic Stimuli.

Stimuli were generated using custom MATLAB code and were sampled at 200kHz with a 32-bit resolution. Acoustic stimuli were delivered through a speaker (Multicomp by Newark, MCPCT-G5100-4139) positioned in the direction of the animals' ear contralateral to the recording site. To assess stimulus-locked auditory responses, we used a set of click trains made up of 5 broadband noise bursts at a rate of 1Hz. The noise bursts were 25ms long and presented at a rate of 10Hz for a total of 500ms. To assess frequency tuning in our neuronal population, we generated a set of 19 pure tones of logarithmically spaced frequencies ranging between 3kHz and 80kHz at 70dB SPL sound pressure. Each tone was 50ms long with a 1ms cosine squared ramp, repeated 40 times with an inter-stimulus-interval of 300ms and presented in a pseudo-random order. 20 of those 40 tone repetitions were accompanied by a continuous laser pulse with a 1ms cosine squared ramp starting at tone onset and ending at tone offset (50ms long; for details on laser stimuli see Optogenetic Inactivation).

Optogenetic Inactivation and Calibration.

To inactivate populations of neurons, we injected a soma-targeted inhibitory opsin in the audTRN of PV- and SST-Cre mice (see Viral Injections and Viral Vectors). Laser-only recordings

were achieved by delivering continuous (1ms cosine squared ramp) laser pulses of different durations (10ms, 25ms, 50ms, and 100ms) through an implanted fiber-optic cannula via a fiber-coupled blue LED (460nm, Prizmatix, Optogenetics-LED-Blue). Frequency tuning $Laser_{On}$ trials were achieved by delivering a continuous 50ms pulse with a 1ms squared ramp.

To reduce variability in the effects of optogenetic manipulation across mice, we developed a procedure to calibrate the LED source prior to each recording session. Once the probe was in its final depth for recording, we presented alternating click trains (see Acoustic Stimuli) wherein each trial consisted of a click train without LED stimulation followed by a click train paired with LED stimulation with 20 different intensities (LED driving voltage ranged from 0 to 5V) while recording neural responses. This stimulus set was presented 10 times for each intensity value and neural responses were sorted offline using Kilosort2. To calculate if each unit was significantly sound responsive and discard noise clusters, we computed a Wilcoxon sign-rank test between the sound responses during the LED-off click trains and a baseline period of activity. Excluded units from further analysis are those whose P-values exceeded a Bonferroni-corrected α-level of $0.05/n_{clusters}$. We then calculated the number of spikes during the LED_{off} click train trials (n_{OFF}) and during the LED_{on} click train trials (n_{ON}) and computed the percent change in the response (r_{PC}) for each light intensity:

$$r_{PC} = \frac{n_{ON} - n_{OFF}}{n_{OFF}} * 100$$

Using a logistic function, we fit the response function as a function of the LED voltage,

$$y = a + \frac{b}{1 + e^{-(x-c)d}}$$

where a determines the y-offset of the response, b determines the range of the response, c determines the x-offset, and d the gain of the response. With this fit equation, we found the voltage values that elicited a 100% increase (2-fold change) in neural spiking and used that value for the rest of the stimulus presented in each individual recording session. Some sessions did not show a

2-fold increase with LED manipulation; for these sessions we used maximum LED power for all stimuli.

Acute Electrophysiological Recordings.

All electrophysiological recordings were carried out in a double-walled acoustic-isolation booth (Industrial Acoustics). At least 21 days post-viral injection, animals were anesthetized (see Surgical Procedures) and a small craniotomy (1mm in diameter) was performed using a micromotor drill (Foredom) over MGB (for coordinates see Viral Injections). Mice were then clamped into a custom-base and allowed to recover from anesthesia for at least 30min. Following their recovery time, we vertically (0° on stereotaxic arm) lowered a 32-channel silicon probe (NeuroNexus: A1x32-Poly2-10mm-50s-177) to a depth of ~3.5mm from the pial surface using a motorized micromanipulator (Scientifica) attached to a stereotaxic arm (Kopf) at a rate of 1-2μm/s. While we lowered the probe, a train of brief broadband noise clicks were played (see Acoustic Stimuli), if we observed stimulus-locked responses, we determined the probe was in a sound-responsive area. The probe was coated in lipophilic far-red dye (Vybrant DiD, Invitrogen), to determine recording sites post-hoc (see Tissue Processing). Recordings that did not display stimulus-licked responses or were not determined to be in MGB, were not used in this analysis. Once the probe reached the target recording depth, it was left to settle in the brain for at least 30min prior to recording. Neural signals were amplified via an Intan headstage (RHD 32ch, Intan Technologies), recorded at a rate of 30kHz using an OpenEphys acquisition board and GUI (Siegle et al., 2017) and digitized with an SPI cable. Signals were filtered between 500 and 6000Hz, offset corrected, and re-referenced to the median of all active channels. Recorded neural data was spike sorted using KiloSort2 (Pachitariu et al., 2023) and manually corrected using phy2. Upon manual correction, units were classified as either single- or multi- units; if units exhibited a clear refractory period, they were labeled single units, otherwise they were classified as multi-units.

Both single-units and multi-units were included in all analyses (for number of units used see Table 1). Approximately 3 recording sessions were achieved from each individual mouse at different recording sites.

Neural Response Analysis.

Following manual spike sorting, units included in this analysis were selected based on their sound responsive profiles. To select sound-responsive units, we used the find_peaks function from SciPy's Python Library and set the minimum peak height to the mean of the baseline activity–calculated as the average firing rate 50ms prior to tone onset–+3 standard deviations of each unit. If units did not display peaks above this set criteria during the presentation of the tone in laser-Off conditions–calculated as the average firing rate during the first 25ms of tone presentation across all laser-off trials–they were labeled as non-sound responsive units and excluded from further analysis. Spontaneous firing rate was computed as the average firing rate during a time window of 50ms prior to tone onset ($FR_{Spontaneous}$) for both laser-Off and laser-On trials. Tone-evoked firing rate (FR_{Evoked}) was calculated as the average firing rate for the first 25ms (0-25ms) of the total tone duration (50ms). Late tone-evoked firing rate was calculated ($FR_{EvokedLate}$) was calculated as the average firing rate from 25ms to tone offset (25ms-50ms). Offset responses (FR_{Offset}) were calculated as the average firing rate during a 150ms time-window after tone offset. Laser only responses were calculated as the average firing rate during laser presentation. We calculated the difference in the response between laser-Off and laser-On by subtracting the mean normalized firing rate during the first 25ms of tone presentation in the laser-Off trials and the mean normalized firing rate during the first 25ms of tone presentation in the laser-On trials. To calculate frequency response functions, we averaged the firing rate during early-tone presentation (0-25ms) for all the trials of the individual 19 frequencies in both laser-Off and laser-On conditions and centered them to their best frequency.

Best frequency is defined as the frequency that elicited the highest change in firing rate compared to baseline activity. Linear fits were calculated by using SciKit Learns Linear Regression Model (Python Library) on the mean firing rate of each cell for every repeat of each of the 19 frequencies. Using the outputs of this model, we extracted the slope and the y-intercepts of the fit for each unit's frequency response function.

Statistical Analysis.

We assessed normality of the data using a Shapiro-Wilk tests using Scipy's Stats Python Library`. For paired data that violated the assumption of normality, p values were calculated using a Wilcoxon sign-rank tests using Scipy's Stats Python Library. For non-paired data that violated the assumption of normality, p values were calculated using a Wilcoxon rank-sum tests using Scipy's Stats Python Library. The standard error of the mean was used to calculate error bars (±SEM). Symbols: * indicates p values <0.05, ** indicates p values < 0.01, and *** indicates p values <0.001.

CHAPTER 4:

CONCLUSIONS

In this dissertation we discussed how thalamic circuit mechanisms are crucial for sensory perception and relevant to sensory behaviors like fear conditioning, which are shown to be altered in patients with neuropsychiatric diseases. With the TRN being a key player in mediating and filtering proper sensory information. In Chapter 2 we focused on showcasing the role of the TRN in mediating sound evoked responses from the BLA, the fear center of the brain, to the auditory thalamus and cortex. Anatomically, we confirmed a direct projection from the BLA to the TRN and we tested its functional role. We found that optogenetic activation of BLA-TRN projections amplifies tone evoked responses in both the auditory thalamus and auditory cortex. These results confirm that the TRN is a crucial structure in the auditory pathway, as it mediates auditory information from auditory behavioral association areas, such as the BLA. However, not much is known about how the TRN modulates auditory within the auditory thalamus.

In chapter 3 we further explored how the TRN plays a role in circuit mechanisms in the auditory pathway. We focused on the inhibitory-excitatory circuit between the TRN and the auditory thalamus, the MGB. The TRN is a complex structure; functionally and anatomically. It is composed of varying cell types all of which have distinct anatomical projections and physiological properties. We show for the first time, that anatomical projections of two major cell types in the TRN, PV and SST neurons, target different subdivisions of the MGB. Our data shows that PV neurons of the TRN primarily target ventral MGB, or first-order auditory thalamus, and that SST-TRN neurons primarily target medial and dorsal MGB, or higher-order auditory thalamus. We then explored whether and how these two differential cell types functionally affect auditory information processing in the MGB. We found that releasing the MGB neurons of

inhibition from SST neurons of the TRN via optogenetic inhibition, caused a suppression of tone evoked responses in most of the units we recorded from. Only 2% of units recorded had an increase in tone evoked responses when released from audTRN-SST inhibition. We also found a significant decrease in the frequency response function and a significant increase in sparseness of recorded MGB neurons that had suppressed tone-evoked activity following audTRN-SST inhibition. These results suggests that inhibiting audTRN-SST narrows tuning of MGB neurons. We then tested the effects of releasing inhibition from the other major cell type within the TRN, the PV cells. We found similar but different results than when we inhibited audTRN-SST neurons. Firstly, we found that releasing inhibition from PV neurons facilitates the tone-evoked responses in 29% of recorded MGB units. A much higher proportion of cells than when we inhibited audTRN-SST cells. However, most of the cells (46%) still exhibited suppressed tone-evoked responses to auditory stimuli. Inhibiting audTRN-PV cells caused a shift upwards and a shift downwards of frequency response functions in neurons that exhibited facilitated and suppressed tone evoked responses, respectively. Furthermore, in the MGB units where there was facilitation of the response to tones, there was a significant decrease in sparseness, whereas in MGB units where there was suppression of responses to tones there was a significant increase in sparseness. This suggests that audTRN-PV neurons are key players in the tuning of MGB neurons. Interestingly, when we inhibited audtTRN-PV neurons we found that MGB cells that exhibited facilitated responses to tones had a faster time-to-peak response than in tone only trials. Concurrently, inhibition of audTRN-PV neurons caused a decrease in time-to-peak of MGB neurons that exhibited suppressed tone evoked responses during disinhibition.

These results are surprising given that the TRN is the primary source of inhibition to the MGB, however they provide insights at the complexity of thalamic inhibitory-excitatory circuit mechanisms. They suggest a more nuanced role of thalamic reticular cell types in the processing of auditory information. They might also uncover unknown circuit dynamics within cells of the

TRN that might further explain the crucial role of the TRN as the gatekeeper of relevant sensory information for sensory processing.

Limitations of the study & other considerations.

We used a combination of viral anatomical tracing, optogenetics and awake *in-vivo* electrophysiological recordings to study the functional role of inhibitory neurons of the TRN in modulating sound responses in MGB and cortex. Viral tracing and optogenetic techniques allow us to express and manipulate specific types of cells with the use of transgenic animals. *In-vivo* awake recordings provide the ability to record neurons in an alert state and with little to no circuit disruption. However, when we discuss cell-type specific mechanisms, and interactions between feedforward and feedback structures, we must be mindful of the amount of feedback information that any given region of interest is receiving. Within the auditory thalamus, the TRN provides most of the inhibitory information to MGB, however the MGB also receives feedback from corticothalamic cells in L5/L6 of AC as well as input from other association areas such as the BLA (Guo et al., 2017; Lee & Sherman, 2010; Winer, 2005). It is possible that the suppressive effects we observe when we disinhibit MGB from a specific cell type of the TRN, is the result of fast feedback inhibition from another region of the brain. Future studies using high-density channel probes to record from multiple brain areas simultaneously can further our understanding of inhibitory circuit mechanisms. For example, one can think of using Neuropixel probes to record from the TRN-MGB-AC at the same time while simultaneously optogenetically manipulating 1) corticothalamic feedback 2) TRN-MGB inhibitory synapses or 3) collateral inputs from MGB to the TRN. This experiment would allow to record simultaneous effects on neural responses along the auditory pathway.

One proposed mechanism we discuss in this dissertation is the possibility of intra-TRN synapses between PV and SST cells. Much like cortical regions where PV and SST interneurons have reciprocal connections to one another (Blackwell & Geffen, 2017). There have not been any

GABAergic synapses found in the adult rodent TRN in slice preparations (Hou et al., 2016). A limitation of the study by Hou, et. al, is that it was performed *in-vitro*, therefore there exists the possibility that intra-TRN GABAergic synapses do occur in the *in-vivo* preparation. Reports of dendro-dendritic synapses have been reported in the TRN of the cat (Deschênes et al., 1985). Similarly in the cat TRN, it has been reported that excitatory collateral inputs from thalamic relay nuclei drive excitatory input onto TRN cells and therefore activating TRN cells (Yen et al., 1985). Furthermore, the TRN is a physiologically complex structure that also contains electrical synapses in the form of gap junctions in addition to chemical synapses (Crabtree, 2018). A limitation in the experiments described in this dissertation is lack of control of driving inputs to the PV or SST neurons of the TRN from other regions of the brain. It is possible that the suppression effects in tone responsive units of the MGB is a direct result of fast feedback arising from excitatory MGB collaterals, intra-TRN dendro-dendritic synapses, or other regions of GABAergic inputs to the TRN like the basal forebrain, substantia nigra or lateral hypothalamus (Asanuma, 1989; Asanuma & Porter, 1990; Herrera et al., 2015; Paré et al., 1990). Indeed, one can think of performing an extensive anatomical tracing study to precisely identify possible sources of GABAergic input to PV and SST cells involved in the auditory pathway. Rabies tracing in the somatosensory TRN reveals that PV and SST neurons receive input from differential brain areas (Clemente-Perez, et al., 2017), however no similar study has been performed in the auditory region of the TRN. This can reveal possible sources of feedback inhibitory inputs to the TRN that might drive the tone evoked suppression we observe.

A key aspect to keep in mind in the interpretation of these results is that the TRN is a complex structure with cell types that vary in intrinsic physiological properties. As discussed in Chapter 1, PV and SST neurons of the ssTRN have differential physiological properties, with PV neurons showing higher levels of bursting than SST cells (Clemente-Perez, et al., 2017). Concurrent findings in TRN edge-zone and core-zone cells and the genetically distinct *Spp1*$^{+}$ and

Ecel1$^+$, show that core-zone and *Spp1*$^+$ which both receive input from FO thalamus are more likely to fire rebound bursts following hyperpolarization. However, edge-zone and *Ecel1*$^+$ fail to produce or have very few rebound bursts (Y. Li et al., 2020; Martinez-Garcia et al., 2020). This can lead to speculation on how optogenetic manipulation during different stages of firing of TRN neurons can affect the synaptic properties. It would be of interest to study circuit mechanisms while recording the states of the TRN cells while optogenetically manipulating the circuit. It would give greater insight on the importance of cellular mechanisms in inhibitory circuits.

The experiments described in Chapter 2 and Chapter 3 use a set of simple auditory stimuli. Pure tone pips, ranging in frequencies from low to high with varying lengths in time. There is a lot of scientific value for using simple vs. complex auditory stimuli. Simple tone pips provide for thorough analysis of sound response profiles, effects of circuit manipulations, etc. In this dissertation we have been able to extract key physiological findings when manipulating the MGB-audTRN pathway, like frequency tuning, time of peak response, changes in firing rate, etc., from single pure tone pip stimuli. However, the TRN and MGB are both highly functional brain regions involved in many behaviors. The TRN has been shown to be a critical structure for the formation of sleep spindles, regulation of seizures, whisking behaviors, pain, etc. More importantly it has been shown to play a key role in attention tasks. In tasks where mice were presented with conflicting cues, with the TRN was suppressed, animals were worse at correctly identifying the attention target (Nakajima et al., 2019; Wimmer et al., 2015). However, little is known about the contributions of PV and SST cells of the TRN to attentional tasks. In the auditory cortex, PV and SST are involved in crucial auditory behaviors like stimulus-specific adaptation and fear behaviors. Understanding whether and how PV and SST neurons of the TRN contribute to auditory attention tasks, like signal-in-noise tasks can provide further insight on the "gatekeeper" theory of the TRN. One can speculate that mice performing a simple go-no-go signal-in-noise behavior task in which mice must lick for a water reward when they hear a target in noise and not

lick when the signal is not present, will lick to the no-go stimulus more often when PV or SST neurons of the audTRN are optogenetically silenced.

In Chapter 3 we show an interesting anatomical projection pattern of PV and SST neurons of the TRN to the MGB. With PV neurons primarily targeting ventral FO-MGB and SST neurons primarily targeting dorsal and medial HO-MGB. Recent studies have shown the contributions of HO-MGB to associative behavior memory tasks (Pardi et al., 2020). It would be interesting to investigate if SST neurons of the TRN selectively play a role in behaviors that require HO-MGB. Whether and how disruption of inhibitory cell types of the TRN affects behavioral outputs of the MGB has been yet to be explored. Function goes hand in hand with anatomy, therefore these projection patterns must convey sensory modality dependent information to thalamic relay cells and must play a larger role in thalamic circuits than previously understood.

Final Conclusions

The results described in this dissertation establish, for the first time, a critical role of the inhibitory cell types of the TRN in the auditory pathway. The TRN has canonically been understood to be the primary source of inhibition to the auditory thalamus, yet surprisingly little has been done to further understand the circuit mechanisms between the two structures. Moreso in a cell type specific manner, which has been shown to have differential effects in other sensory modalities. Our findings open new avenues to investigate how inhibitory-excitatory auditory thalamic circuits shape sensory information in auditory behaviors like signal in noise or attention tasks. This body of work provides a foundation to further understand cell-type specific circuit mechanisms between inhibitory-excitatory networks in the auditory system.

REFERENCES

Adolphs, R., Tranel, D., Damasio, H., & Damasio, A. (1994). Impaired recognition of emotion in facial expressions following bilateral damage to the human amygdala. *Nature*, *372*(6507), 669–672. https://doi.org/10.1038/372669a0

Ahrens, S., Jaramillo, S., Yu, K., Ghosh, S., Hwang, G. R., Paik, R., Lai, C., He, M., Huang, Z. J., & Li, B. (2015). ErbB4 regulation of a thalamic reticular nucleus circuit for sensory selection. *Nature Neuroscience*, *18*(1), 104–111. https://doi.org/10.1038/nn.3897

Aizenberg, M., & Geffen, M. N. (2013). Bidirectional effects of aversive learning on perceptual acuity are mediated by the sensory cortex. *Nature Neuroscience*, *16*(8), 994–996. https://doi.org/10.1038/nn.3443

Aizenberg, M., Mwilambwe-Tshilobo, L., Briguglio, J. J., Natan, R. G., & Geffen, M. N. (2015). Bidirectional Regulation of Innate and Learned Behaviors That Rely on Frequency Discrimination by Cortical Inhibitory Neurons. *PLoS Biology*, *13*(12), 1–32. https://doi.org/10.1371/journal.pbio.1002308

Amaral, D. G., & Price, J. L. (1984). Amygdalo-cortical projections in the monkey (Macaca fascicularis). *Journal of Comparative Neurology*, *230*(4), 465–496. https://doi.org/10.1002/cne.902300402

Anderson, A. K., & Phelps, E. A. (2001). Lesions of the human amygdala impair enhanced perception of emotionally salient events. *Nature*, *411*(6835), 305–309. https://doi.org/10.1038/35077083

Anderson, L. A., Christianson, G. B., & Linden, J. F. (2009). Stimulus-specific adaptation occurs in the auditory thalamus. *The Journal of Neuroscience : The Official Journal of the*

Society for Neuroscience, *29*(22), 7359–7363. https://doi.org/10.1523/JNEUROSCI.0793-09.2009

Anderson, L. A., & Linden, J. F. (2011). Physiological differences between histologically defined subdivisions in the mouse auditory thalamus. *Hearing Research*, *274*(1–2), 48–60. https://doi.org/10.1016/j.heares.2010.12.016

Antunes, F. M., & Malmierca, M. S. (2011). Effect of auditory cortex deactivation on stimulus-specific adaptation in the medial geniculate body. *The Journal of Neuroscience : The Official Journal of the Society for Neuroscience*, *31*(47), 17306–17316. https://doi.org/10.1523/JNEUROSCI.1915-11.2011

Antunes, F. M., & Malmierca, M. S. (2021). Corticothalamic Pathways in Auditory Processing: Recent Advances and Insights From Other Sensory Systems. *Frontiers in Neural Circuits*, *15*. https://www.frontiersin.org/articles/10.3389/fncir.2021.721186

Antunes, F. M., Nelken, I., Covey, E., & Malmierca, M. S. (2010). Stimulus-Specific Adaptation in the Auditory Thalamus of the Anesthetized Rat. *PLoS ONE*, *5*(11), 14071. https://doi.org/10.1371/journal.pone.0014071

Asanuma, C. (1989). Axonal arborizations of a magnocellular basal nucleus input and their relation to the neurons in the thalamic reticular nucleus of rats. *Proceedings of the National Academy of Sciences*, *86*(12), 4746–4750. https://doi.org/10.1073/pnas.86.12.4746

Asanuma, C., & Porter, L. L. (1990). Light and electron microscopic evidence for a GABAergic projection from the caudal basal forebrain to the thalamic reticular nucleus in rats. *The Journal of Comparative Neurology*, *302*(1), 159–172. https://doi.org/10.1002/cne.903020112

Bakin, J. S., & Weinberger, N. M. (1990). Classical conditioning induces CS-specific receptive field plasticity in the auditory cortex of the guinea pig. *Brain Research*, *536*(1), 271–286. https://doi.org/10.1016/0006-8993(90)90035-A

Bartlett, E. L. (2013). The organization and physiology of the auditory thalamus and its role in processing acoustic features important for speech perception. *Brain and Language*, *126*(1), 29–48. https://doi.org/10.1016/j.bandl.2013.03.003

Belén Pardi, M., Vogenstahl, J., Dalmay, T., Spanò, T., Pu, D. L., Naumann, L. B., Kretschmer, F., Sprekeler, H., & Letzkus, J. J. (2020). A thalamocortical top-down circuit for associative memory. *Science*, *370*(6518), 844–848. https://doi.org/10.1126/SCIENCE.ABC2399/SUPPL_FILE/ABC2399_PARDI_SM.PDF

Bickford, M. (2016). Thalamic Circuit Diversity: Modulation of the Driver/Modulator Framework. *Frontiers in Neural Circuits*, *9*. https://www.frontiersin.org/articles/10.3389/fncir.2015.00086

Blackwell, J. M., & Geffen, M. N. (2017). Progress and challenges for understanding the function of cortical microcircuits in auditory processing. *Nature Communications*, *8*(1), 2165. https://doi.org/10.1038/s41467-017-01755-2

Boatman, J. A., & Kim, J. J. (2006). A thalamo-cortico-amygdala pathway mediates auditory fear conditioning in the intact brain. *European Journal of Neuroscience*, *24*(3), 894–900. https://doi.org/10.1111/j.1460-9568.2006.04965.x

Briguglio, J. J., Aizenberg, M., Balasubramanian, V., & Geffen, M. N. (2018). Cortical neural activity predicts sensory acuity under optogenetic manipulation. *Journal of Neuroscience*, *38*(8), 2094–2105. https://doi.org/10.1523/JNEUROSCI.2457-17.2017

Brown, J. W., Taheri, A., Kenyon, R. V., Berger-Wolf, T. Y., & Llano, D. A. (2020). Signal Propagation via Open-Loop Intrathalamic Architectures: A Computational Model. *ENeuro*, *7*(1), ENEURO.0441-19.2020. https://doi.org/10.1523/ENEURO.0441-19.2020

Butler, B., & Lomber, S. (2013). Functional and structural changes throughout the auditory system following congenital and early-onset deafness: Implications for hearing restoration. *Frontiers in Systems Neuroscience*, *7*. https://www.frontiersin.org/articles/10.3389/fnsys.2013.00092

Cambiaghi, M., Grosso, A., Likhtik, E., Mazziotti, R., Concina, G., Renna, A., Sacco, T., Gordon, J. A., & Sacchetti, B. (2016). Higher-Order Sensory Cortex Drives Basolateral Amygdala Activity during the Recall of Remote, but Not Recently Learned Fearful Memories. *Journal of Neuroscience*, *36*(5), 1647–1659. https://doi.org/10.1523/JNEUROSCI.2351-15.2016

Campeau, S., & Davis, M. (1995). Involvement of the central nucleus and basolateral complex of the amygdala in fear conditioning measured with fear-potentiated startle in rats trained concurrently with auditory and visual conditioned stimuli. *The Journal of Neuroscience : The Official Journal of the Society for Neuroscience*, *15*(3 Pt 2), 2301–2311.

Carroll, B. J., Sampathkumar, V., Kasthuri, N., & Sherman, S. M. (2022). Layer 5 of cortex innervates the thalamic reticular nucleus in mice. *Proceedings of the National Academy of Sciences of the United States of America*, *119*(38). https://doi.org/10.1073/PNAS.2205209119

Chavez, C. M., McGaugh, J. L., & Weinberger, N. M. (2009). The basolateral amygdala modulates specific sensory memory representations in the cerebral cortex. *Neurobiology of Learning and Memory*, *91*(4), 382–392. https://doi.org/10.1016/J.NLM.2008.10.010

Clem, R. L., & Huganir, R. L. (2010). Calcium-permeable AMPA receptor dynamics mediate fear memory erasure. *Science (New York, N.Y.)*, *330*(6007), 1108–1112. https://doi.org/10.1126/science.1195298

Clemente-Perez, A., Makinson, S. R., Higashikubo, B., Brovarney, S., Cho, F. S., Urry, A., Holden, S. S., Wimer, M., Dávid, C., Fenno, L. E., Acsády, L., Deisseroth, K., & Paz, J. T. (2017). Distinct Thalamic Reticular Cell Types Differentially Modulate Normal and Pathological Cortical Rhythms. *Cell Reports*, *19*(10), 2130–2142. https://doi.org/10.1016/j.celrep.2017.05.044

Collins, D. R., & Paré, D. (2000). Differential fear conditioning induces reciprocal changes in the sensory responses of lateral amygdala neurons to the CS(+) and CS(-). *Learning & Memory (Cold Spring Harbor, N.Y.)*, *7*(2), 97–103.

Crabtree, J. W. (1998). Organization in the auditory sector of the cat's thalamic reticular nucleus. *Journal of Comparative Neurology*, *390*(2), 167–182. https://doi.org/10.1002/(sici)1096-9861(19980112)390:2<167::aid-cne1>3.0.co;2-%23

Crabtree, J. W. (2018). Functional diversity of thalamic reticular subnetworks. *Frontiers in Systems Neuroscience*, *12*, 41. https://doi.org/10.3389/FNSYS.2018.00041/BIBTEX

Crick, F. (2006). Function of the thalamic reticular complex: The searchlight hypothesis. *Proceedings of the National Academy of Sciences*, *81*(14), 4586–4590. https://doi.org/10.1073/pnas.81.14.4586

Descheˆnes, M., Madariaga-Domich, A., & Steriade, M. (1985). Dendrodendritic synapses in the cat reticularis thalami nucleus: A structural basis for thalamic spindle synchronization. *Brain Research*, *334*(1), 165–168. https://doi.org/10.1016/0006-8993(85)90580-3

Farley, B. J., Quirk, M. C., Doherty, J. J., & Christian, E. P. (2010). Stimulus-Specific Adaptation in Auditory Cortex Is an NMDA-Independent Process Distinct from the Sensory Novelty Encoded by the Mismatch Negativity. *Journal of Neuroscience*, *30*(49), 16475–16484. https://doi.org/10.1523/JNEUROSCI.2793-10.2010

Ferrarelli, F., & Tononi, G. (2011). The thalamic reticular nucleus and schizophrenia. *Schizophrenia Bulletin*, *37*(2), 306–315. https://doi.org/10.1093/schbul/sbq142

Fishman, Y. I., & Steinschneider, M. (2012). Searching for the mismatch negativity in primary auditory cortex of the awake monkey: Deviance detection or stimulus specific adaptation? *Journal of Neuroscience*, *32*(45), 15747–15758. https://doi.org/10.1523/JNEUROSCI.2835-12.2012

Gentet, L. J., & Ulrich, D. (2003). Strong, reliable and precise synaptic connections between thalamic relay cells and neurones of the nucleus reticularis in juvenile rats. *The Journal of Physiology*, *546*(Pt 3), 801–811. https://doi.org/10.1113/jphysiol.2002.032730

Gentet, L. J., & Ulrich, D. (2004). Electrophysiological characterization of synaptic connections between layer VI cortical cells and neurons of the nucleus reticularis thalami in juvenile rats. *The European Journal of Neuroscience*, *19*(3), 625–633. https://doi.org/10.1111/j.1460-9568.2004.03168.x

Ghosh, S., & Chattarji, S. (2015). Neuronal encoding of the switch from specific to generalized fear. *Nature Neuroscience*, *18*(1), 112–120. https://doi.org/10.1038/nn.3888

Goosens, K. A., & Maren, S. (2001). Contextual and auditory fear conditioning are mediated by the lateral, basal, and central amygdaloid nuclei in rats. *Learning & Memory (Cold Spring Harbor, N.Y.)*, *8*(3), 148–155. https://doi.org/10.1101/lm.37601

Grewe, B. F., Gründemann, J., Kitch, L. J., Lecoq, J. A., Parker, J. G., Marshall, J. D., Larkin, M. C., Jercog, P. E., Grenier, F., Li, J. Z., Lüthi, A., & Schnitzer, M. J. (2017). Neural ensemble dynamics underlying a long-term associative memory. *Nature*, *543*(7647), 670–675. https://doi.org/10.1038/nature21682

Gribkova, E. D., Ibrahim, B. A., & Llano, D. A. (2018). A novel mutual information estimator to measure spike train correlations in a model thalamocortical network. *Journal of Neurophysiology*, *120*(6), 2730–2744. https://doi.org/10.1152/jn.00012.2018

Grimm, S., & Escera, C. (2012). Auditory deviance detection revisited: Evidence for a hierarchical novelty system. *International Journal of Psychophysiology*, *85*, 88–92. https://doi.org/10.1016/j.ijpsycho.2011.05.012

Grosso, A., Cambiaghi, M., Concina, G., Sacco, T., & Sacchetti, B. (2015). Auditory cortex involvement in emotional learning and memory. *Neuroscience*, *299*, 45–55. https://doi.org/10.1016/j.neuroscience.2015.04.068

Guillery, R. W., Feig, S. L., & Lozsádi, D. A. (1998). Paying attention to the thalamic reticular nucleus. *Trends in Neurosciences*, *21*(1), 28–32. https://doi.org/10.1016/S0166-2236(97)01157-0

Guillery, R. W., & Sherman, S. M. (2002). Review Thalamic Relay Functions and Their Role in Corticocortical Communication: Generalizations from the Visual System. In *Neuron* (Vol. 33, pp. 163–175).

Guo, W., Clause, A. R., Barth-Maron, A., & Polley, D. B. (2017). A Corticothalamic Circuit for Dynamic Switching between Feature Detection and Discrimination. *Neuron*, *95*(1), 180-194.e5. https://doi.org/10.1016/j.neuron.2017.05.019

Haas, J. S., & Landisman, C. E. (2012). State-Dependent Modulation of Gap Junction Signaling by the Persistent Sodium Current. *Frontiers in Cellular Neuroscience*, *5*, 31. https://doi.org/10.3389/fncel.2011.00031

Halassa, M. M., Chen, Z., Wimmer, R. D., Brunetti, P. M., Zhao, S., Zikopoulos, B., Wang, F., Brown, E. N., & Wilson, M. A. (2014). State-dependent architecture of thalamic reticular subnetworks. *Cell*, *158*(4), 808–821. https://doi.org/10.1016/j.cell.2014.06.025

Hamilton, L. S., Sohl-Dickstein, J., Huth, A. G., Carels, V. M., Deisseroth, K., & Bao, S. (2013). Optogenetic Activation of an Inhibitory Network Enhances Feedforward Functional Connectivity in Auditory Cortex. *Neuron*, *80*(4), 1066–1076. https://doi.org/10.1016/j.neuron.2013.08.017

He, J. (2003). Corticofugal modulation of the auditory thalamus. *Experimental Brain Research*, *153*(4), 579–590. https://doi.org/10.1007/s00221-003-1680-5

Herrera, C. G., Cadavieco, M. C., Jego, S., Ponomarenko, A., Korotkova, T., & Adamantidis, A. (2015). Hypothalamic feedforward inhibition of thalamocortical network controls arousal and consciousness. *Nature Neuroscience*, *19*(2), 290–298. https://doi.org/10.1038/nn.4209

Hirsch, J. A., Wang, X., Sommer, F. T., & Martinez, L. M. (2015). How Inhibitory Circuits in the Thalamus Serve Vision. *Annual Review of Neuroscience*, *38*(1), 309–329. https://doi.org/10.1146/annurev-neuro-071013-014229

Hoseini, M. S., Higashikubo, B., Cho, F. S., Chang, A. H., Clemente-Perez, A., Lew, I., Ciesielska, A., Stryker, M. P., & Paz, J. T. (2021). Gamma rhythms and visual information in mouse v1 specifically modulated by somatostatin+ neurons in reticular thalamus. *ELife*, *10*, 1–24. https://doi.org/10.7554/ELIFE.61437

Hou, G., Smith, A. G., & Zhang, Z.-W. (2016). Lack of intrinsic GABAergic connections in the thalamic reticular nucleus of the mouse. *Journal of Neuroscience*, *36*(27), 7246–7252.

Houser, C. R., Vaughn, J. E., Barber, R. P., & Roberts, E. (1980). GABA neurons are the major cell type of the nucleus reticularis thalami. *Brain Research*, *200*(2), 341–354. https://doi.org/10.1016/0006-8993(80)90925-7

Huguenard, J. R. (1996). Low-Threshold Calcium Currents in Central Nervous System Neurons. *Annual Review of Physiology*, *58*(1), 329–348. https://doi.org/10.1146/annurev.ph.58.030196.001553

Iavarone, E., Simko, J., Shi, Y., Bertschy, M., García-Amado, M., Litvak, P., Kaufmann, A.-K., O'Reilly, C., Amsalem, O., Abdellah, M., Chevtchenko, G., Coste, B., Courcol, J.-D., Ecker, A., Favreau, C., Fleury, A. C., Van Geit, W., Gevaert, M., Guerrero, N. R., … Hill, S. L. (2023). Thalamic control of sensory processing and spindles in a biophysical somatosensory thalamoreticular circuit model of wakefulness and sleep. *Cell Reports*, *42*(3), 112200. https://doi.org/10.1016/j.celrep.2023.112200

Ito, T., Bishop, D. C., & Oliver, D. L. (2011). Expression of glutamate and inhibitory amino acid vesicular transporters in the rodent auditory brainstem. *Journal of Comparative Neurology*, *519*(2), 316–340. https://doi.org/10.1002/CNE.22521

Janak, P. H., & Tye, K. M. (2015). From circuits to behaviour in the amygdala. *Nature*. https://doi.org/10.1038/nature14188

Jhang, J., Lee, H., Kang, M. S., Lee, H. S., Park, H., & Han, J. H. (2018). Anterior cingulate cortex and its input to the basolateral amygdala control innate fear response. *Nature Communications*, *9*(1). https://doi.org/10.1038/s41467-018-05090-y

Johansen, J. P., Hamanaka, H., Monfils, M. H., Behnia, R., Deisseroth, K., Blair, H. T., & LeDoux, J. E. (2010). Optical activation of lateral amygdala pyramidal cells instructs associative fear learning. *Proceedings of the National Academy of Sciences of the United States of America*, *107*(28), 12692–12697. https://doi.org/10.1073/pnas.1002418107

Johnson, K. R., Tian, C., Gagnon, L. H., Jiang, H., Ding, D., & Salvi, R. (2017). Effects of Cdh23 single nucleotide substitutions on age-related hearing loss in C57BL/6 and 129S1/Sv mice and comparisons with congenic strains. *Scientific Reports*, *7*, 44450. https://doi.org/10.1038/srep44450

Jones, E. G. (1975). Some aspects of the organization of the thalamic reticular complex. *Journal of Comparative Neurology*, *162*(3), 285–308. https://doi.org/10.1002/cne.901620302

Kim, U., Sanchez-Vives, M. V., & McCormick, D. A. (1997). Functional Dynamics of GABAergic Inhibition in the Thalamus. *Science*, *278*(5335), 130–134. https://doi.org/10.1126/science.278.5335.130

Kimura, A. (2014). Diverse subthreshold cross-modal sensory interactions in the thalamic reticular nucleus: Implications for new pathways of cross-modal attentional gating function. *European Journal of Neuroscience*, *39*(9), 1405–1418. https://doi.org/10.1111/ejn.12545

Kimura, A., Donishi, T., Okamoto, K., & Tamai, Y. (2005). Topography of projections from the primary and non-primary auditory cortical areas to the medial geniculate body and thalamic reticular nucleus in the rat. *Neuroscience*, *135*(4), 1325–1342. https://doi.org/10.1016/j.neuroscience.2005.06.089

Kimura, A., Donishi, T., Sakoda, T., Hazama, M., & Tamai, Y. (2003). Auditory thalamic nuclei projections to the temporal cortex in the rat. *Neuroscience*, *117*(4), 1003–1016. https://doi.org/10.1016/S0306-4522(02)00949-1

Kimura, A., & Imbe, H. (2015). Anatomically structured burst spiking of thalamic reticular nucleus cells: Implications for distinct modulations of sensory processing in lemniscal and non-lemniscal thalamocortical loop circuitries. *European Journal of Neuroscience*, *41*(10), 1276–1293. https://doi.org/10.1111/ejn.12874

Kimura, A., Imbe, H., Donishi, T., & Tamai, Y. (2007). Axonal projections of single auditory neurons in the thalamic reticular nucleus: Implications for tonotopy-related gating function and cross-modal modulation. *European Journal of Neuroscience*, *26*(12), 3524–3535. https://doi.org/10.1111/j.1460-9568.2007.05925.x

Kimura, A., Yokoi, I., Imbe, H., Donishi, T., & Kaneoke, Y. (2012). Auditory thalamic reticular nucleus of the rat: Anatomical nodes for modulation of auditory and cross-modal sensory processing in the loop connectivity between the cortex and thalamus. *The Journal of Comparative Neurology*, *520*(7), 1457–1480. https://doi.org/10.1002/cne.22805

Kumar, S., Kriegstein, K. von, Friston, K., & Griffiths, T. D. (2012). Features versus Feelings: Dissociable Representations of the Acoustic Features and Valence of Aversive Sounds. *Journal of Neuroscience*, *32*(41), 14184–14192. https://doi.org/10.1523/JNEUROSCI.1759-12.2012

Lam, Y. W., & Sherman, S. M. (2005). Mapping by laser photostimulation of connections between the thalamic reticular and ventral posterior lateral nuclei in the rat. *Journal of Neurophysiology*, *94*(4), 2472–2483. https://doi.org/10.1152/jn.00206.2005

Lam, Y. W., & Sherman, S. M. (2011). Functional organization of the thalamic input to the thalamic reticular nucleus. *Journal of Neuroscience*, *31*(18), 6791–6799. https://doi.org/10.1523/JNEUROSCI.3073-10.2011

Landisman, C. E., Long, M. A., Beierlein, M., Deans, M. R., Paul, D. L., & Connors, B. W. (2002). Electrical Synapses in the Thalamic Reticular Nucleus. *Journal of Neuroscience*, *22*(3), 1002–1009. https://doi.org/10.1523/JNEUROSCI.22-03-01002.2002

LeDoux, J. E., Cicchetti, P., Xagoraris, A., & Romanski, L. M. (1990). The lateral amygdaloid nucleus: Sensory interface of the amygdala in fear conditioning. *The Journal of Neuroscience : The Official Journal of the Society for Neuroscience*, *10*(4), 1062–1069. https://doi.org/10.1523/JNEUROSCI.10-04-01062.1990

Lee, C. C. (2015). Exploring functions for the non-lemniscal auditory thalamus. *Frontiers in Neural Circuits*, *9*, 69. https://doi.org/10.3389/fncir.2015.00069

Lee, C. C., & Sherman, S. M. (2010). Drivers and Modulators in the Central Auditory Pathways. *Frontiers in Neuroscience*, *4*, 79. https://doi.org/10.3389/neuro.01.014.2010

Lennartz, R. C., & Weinberger, N. M. (1992). Frequency-Specific Receptive Field Plasticity in the Medial Geniculate Body Induced by Pavlovian Fear Conditioning Is Expressed in the Anesthetized Brain. *Behavioral Neuroscience*, *106*(3), 484–497.

Lerner, T. N., Ye, L., & Deisseroth, K. (2016). *Leading Edge Primer Communication in Neural Circuits: Tools, Opportunities, and Challenges*. https://doi.org/10.1016/j.cell.2016.02.027

Letzkus, J. J., Wolff, S. B. E., Meyer, E. M. M., Tovote, P., Courtin, J., Herry, C., & Lüthi, A. (2011). A disinhibitory microcircuit for associative fear learning in the auditory cortex. *Nature*, *480*(7377), 331–335. https://doi.org/10.1038/nature10674

Li, L. Y., Xiong, X. R., Ibrahim, L. A., Yuan, W., Tao, H. W., & Zhang, L. I. (2015). Differential Receptive Field Properties of Parvalbumin and Somatostatin Inhibitory Neurons in Mouse Auditory Cortex. *Cerebral Cortex*, *25*(7), 1782–1791. https://doi.org/10.1093/cercor/bht417

Li, W., Howard, J. D., Parrish, T. B., & Gottfried, J. A. (2008). *Aversive Learning Enhances Perceptual and Cortical Discrimination of Indiscriminable Odor Cues*. *964*(March), 1842–1846.

Li, Y., Lopez-Huerta, V. G., Adiconis, X., Levandowski, K., Choi, S., Simmons, S. K., Arias-Garcia, M. A., Guo, B., Yao, A. Y., Blosser, T. R., Wimmer, R. D., Aida, T., Atamian, A., Naik, T., Sun, X., Bi, D., Malhotra, D., Hession, C. C., Shema, R., … Feng, G. (2020). Distinct subnetworks of the thalamic reticular nucleus. *Nature*, *583*. https://doi.org/10.1038/s41586-020-2504-5

Liu, J., Chen, D. H., Li, X. S., Xu, C. Y., & Hu, T. (2023). Activating PV-positive neurons in ventral thalamic reticular nucleus reduces pain sensitivity in mice. *Brain Research*, *1799*. https://doi.org/10.1016/J.BRAINRES.2022.148174

Liu, P.-F., Wang, Y., Xu, L., Xiang, A.-F., Liu, M.-Z., Zhu, Y.-B., Jia, X., Zhang, R., Li, J.-B., Zhang, L., & Mu, D. (2022). Modulation of itch and pain signals processing in ventrobasal thalamus by thalamic reticular nucleus. *IScience*, *25*(1), 103625. https://doi.org/10.1016/j.isci.2021.103625

Lu, E., Llano, D. A., & Sherman, S. M. (2009). Different distributions of calbindin and calretinin immunostaining across the medial and dorsal divisions of the mouse medial geniculate body. *Hearing Research*, *257*(1–2), 16–23. https://doi.org/10.1016/J.HEARES.2009.07.009

Mahn, M., Gibor, L., Patil, P., Cohen-Kashi Malina, K., Oring, S., Printz, Y., Levy, R., Lampl, I., & Yizhar, O. (2018). High-efficiency optogenetic silencing with soma-targeted anion-conducting channelrhodopsins. *Nature Communications*, *9*(1), Article 1. https://doi.org/10.1038/s41467-018-06511-8

Makinson, C. D., & Huguenard, J. R. (2015). Attentional flexibility in the thalamus: Now we're getting SOMwhere. *Nature Neuroscience*, *18*(1), 2–4. https://doi.org/10.1038/nn.3902

Maren, S. (2000). Auditory fear conditioning increases CS-elicited spike firing in lateral amygdala neurons even after extensive overtraining. *European Journal of Neuroscience*, *12*(11), 4047–4054. https://doi.org/10.1046/j.1460-9568.2000.00281.x

Martinez-Garcia, R. I., Voelcker, B., Zaltsman, J. B., Patrick, S. L., Stevens, T. R., Connors, B. W., Cruikshank, S. J., & Carney, N. D. (2020). Two dynamically distinct circuits drive inhibition in the sensory thalamus. *Nature*, *583*. https://doi.org/10.1038/s41586-020-2512-5

Mascagni, F., McDonald, A. J., & Coleman, J. R. (1993). Corticoamygdaloid and corticocortical projections of the rat temporal cortex: A Phaseolus vulgaris leucoagglutinin study. *Neuroscience*, *57*(3), 697–715. https://doi.org/10.1016/0306-4522(93)90016-9

McKernan, M. G., & Shinnick-Gallagher, P. (1997). Fear conditioning induces a lasting potentiation of synaptic currents in vitro. *Nature*, *390*(6660), 607–611. https://doi.org/10.1038/37605

Moore, A. K., & Wehr, M. (2013). Parvalbumin-expressing inhibitory interneurons in auditory cortex are well-tuned for frequency. *Journal of Neuroscience*, *33*(34), 13713–13723. https://doi.org/10.1523/JNEUROSCI.0663-13.2013

Murray Sherman, S. (2016). Thalamus plays a central role in ongoing cortical functioning. *Nature Neuroscience VOLUME*, *19*(4). https://doi.org/10.1038/nn.4269

Nabavi, S., Fox, R., Proulx, C. D., Lin, J. Y., Tsien, R. Y., & Malinow, R. (2014). Engineering a memory with LTD and LTP. *Nature*, *511*. https://doi.org/10.1038/nature13294

Nakajima, M., Schmitt, L. I., & Halassa, M. M. (2019). Prefrontal Cortex Regulates Sensory Filtering through a Basal Ganglia-to-Thalamus Pathway. *Neuron*, *103*(3), 445-458.e10. https://doi.org/10.1016/j.neuron.2019.05.026

Natan, R. G., Briguglio, J. J., Mwilambwe-Tshilobo, L., Jones, S. I., Aizenberg, M., Goldberg, E. M., & Geffen, M. N. (2015). Complementary control of sensory adaptation by two types of cortical interneurons. *ELife*, *4*. https://doi.org/10.7554/eLife.09868

Natan, R. G., Rao, W., & Geffen, M. N. (2017). Cortical Interneurons Differentially Shape Frequency Tuning following Adaptation. *Cell Reports*, *21*(4), 878–890. https://doi.org/10.1016/j.celrep.2017.10.012

Oertel, W. H., Graybiel, A. M., Mugnaini, E., Elde, R. P., Schmechel, D. E., & Kopin, I. J. (1983). Coexistence of glutamic acid decarboxylase- and somatostatin-like immunoreactivity in neurons of the feline nucleus reticularis thalami. *Journal of Neuroscience*, *3*(6), 1322–1332. https://doi.org/10.1523/JNEUROSCI.03-06-01322.1983

Ohman, A., Flykt, A., & Esteves, F. (2001). Emotion drives attention_Snakes in the grass.pdf. *Journal of Experiemntal Psychology: General*, *130*(3), 466–478. https://doi.org/10.1037/AXJ96-3445.130.3.466

Oliver, D. L., & Huerta, M. F. (1992). Inferior and Superior Colliculi. In D. B. Webster, A. N. Popper, & R. R. Fay (Eds.), *The Mammalian Auditory Pathway: Neuroanatomy* (pp. 168–221). Springer. https://doi.org/10.1007/978-1-4612-4416-5_5

Pachitariu, M., Sridhar, S., & Stringer, C. (2023). *Solving the spike sorting problem with Kilosort* (p. 2023.01.07.523036). bioRxiv. https://doi.org/10.1101/2023.01.07.523036

Padmala, S., & Pessoa, L. (2008). Affective Learning Enhances Visual Detection and Responses in Primary Visual Cortex. *Journal of Neuroscience*, *28*(24), 6202–6210. https://doi.org/10.1523/JNEUROSCI.1233-08.2008

Paré, D., Hazrati, L. N., Parent, A., & Steriade, M. (1990). Substantia nigra pars reticulata projects to the reticular thalamic nucleus of the cat: A morphological and electrophysiological study. *Brain Research*, *535*(1), 139–146. https://doi.org/10.1016/0006-8993(90)91832-2

Paré, D., & Quirk, G. J. (2017). When scientific paradigms lead to tunnel vision: Lessons from the study of fear. *Npj Science of Learning*, *2*(1), 6. https://doi.org/10.1038/s41539-017-0007-4

Park, Y., & Geffen, M. N. (2019). A Unifying Mechanistic Model of the Auditory Cortex with Inhibitory Subtypes. *BioRxiv*, 626358. https://doi.org/10.1101/626358

Pham, T., & Haas, J. S. (2018). Electrical synapses between inhibitory neurons shape the responses of principal neurons to transient inputs in the thalamus: A modeling study. *Scientific Reports*, *8*(1), Article 1. https://doi.org/10.1038/s41598-018-25956-x

Phelps, E. A., Ling, S., & Carrasco, M. (2006). Emotion Facilitates Perception and Potentiates the Perceptual Benefits of Attention. *Psychological Science*, *17*(4), 292–299. https://doi.org/10.1111/j.1467-9280.2006.01701.x

Phillips, E. A., & Hasenstaub, A. R. (2016). Asymmetric effects of activating and inactivating cortical interneurons. *ELife*, *5*(OCTOBER2016). https://doi.org/10.7554/eLife.18383

Phillips, E. A. K., Schreiner, C. E., & Hasenstaub, A. R. (2017). Cortical Interneurons Differentially Regulate the Effects of Acoustic Context. *Cell Reports*, *20*(4), 771–778. https://doi.org/10.1016/j.celrep.2017.07.001

Phillips, M. L., Drevets, W. C., Rauch, S. L., & Lane, R. (2003). Neurobiology of emotion perception II: Implications for major psychiatric disorders. *Biological Psychiatry*, *54*(5), 515–528. https://doi.org/10.1016/S0006-3223(03)00171-9

Pinault, D. (2004). The thalamic reticular nucleus: Structure, function and concept. *Brain Research Reviews*, *46*(1), 1–31. https://doi.org/10.1016/J.BRAINRESREV.2004.04.008

Pinault, D., & Deschênes, M. (1998). Projection and innervation patterns of individual thalamic reticular axons in the thalamus of the adult rat: A three-dimensional, graphic, and morphometric analysis. *Journal of Comparative Neurology*, *391*(2), 180–203. https://doi.org/10.1002/(SICI)1096-9861(19980209)391:2<180::AID-CNE3>3.0.CO;2-Z

Polterovich, A., Jankowski, M. M., & Nelken, I. (2018). Deviance sensitivity in the auditory cortex of freely moving rats. *PLoS ONE*, *13*(6), e0197678. https://doi.org/10.1371/journal.pone.0197678

Quirk, G. J., Armony, J. L., & LeDoux, J. E. (1997). Fear conditioning enhances different temporal components of tone-evoked spike trains in auditory cortex and lateral amygdala. *Neuron*, *19*(3), 613–624. https://doi.org/10.1016/S0896-6273(00)80375-X

Quirk, G. J., Repa, J. C., & LeDoux, J. E. (1995). Fear conditioning enhances short-latency auditory responses of lateral amygdala neurons: Parallel recordings in the freely behaving rat. *Neuron*, *15*(5), 1029–1039. https://doi.org/10.1016/0896-6273(95)90092-6

Resnik, J., & Paz, R. (2015). Fear generalization in the primate amygdala. *Nature Neuroscience*, *18*(2), Article 2. https://doi.org/10.1038/nn.3900

Resnik, J., Sobel, N., & Paz, R. (2011). *Auditory aversive learning increases discrimination thresholds*. *14*(6). https://doi.org/10.1038/nn.2802

Rogan, M. T., Stäubli, U. V., & LeDoux, J. E. (1997). Fear conditioning induces associative long-term potentiation in the amygdala. *Nature*, *390*(6660), 604–607. https://doi.org/10.1038/37601

Romanski, L. M., Clugnet, M.-C., Bordi, F., & LeDoux, J. E. (1993). Somatosensory and auditory convergence in the lateral nucleus of the amygdala. *Behavioral Neuroscience*, *107*, 444–450. https://doi.org/10.1037/0735-7044.107.3.444

Romanski, L. M., & LeDoux, J. E. (1992). Equipotentiality of thalamo-amygdala and thalamo-cortico-amygdala circuits in auditory fear conditioning. *The Journal of Neuroscience : The Official Journal of the Society for Neuroscience*, *12*(11), 4501–4509.

Romanski, L. M., & Ledoux, J. E. (1993). Information cascade from primary auditory cortex to the amygdala: Corticocortical and corticoamygdaloid projections of temporal cortex in the rat. *Cerebral Cortex*, *3*(6), 515–532. https://doi.org/10.1093/cercor/3.6.515

Rudy, B., Fishell, G., Lee, S., & Hjerling-Leffler, J. (2011). Three groups of interneurons account for nearly 100% of neocortical GABAergic neurons. *Developmental Neurobiology*, *71*(1), 45–61. https://doi.org/10.1002/dneu.20853

Sacco, T., & Sacchetti, B. (2010). Role of secondary sensory cortices in emotional memory storage and retrieval in rats. *Science (New York, N.Y.)*, *329*(5992), 649–656. https://doi.org/10.1126/science.1183165

Schmitt, L. I., Wimmer, R. D., Nakajima, M., Happ, M., Mofakham, S., & Halassa, M. M. (2017). Thalamic amplification of cortical connectivity sustains attentional control. *Nature*, *545*(7653), 219–223. https://doi.org/10.1038/nature22073

Seybold, B. A., Phillips, E. A. K., Schreiner, C. E., & Hasenstaub, A. R. (2015). Inhibitory Actions Unified by Network Integration. *Neuron*, *87*(6), 1181–1192. https://doi.org/10.1016/J.NEURON.2015.09.013

Sherman, S. M., & Guillery, R. W. (1998). On the actions that one nerve cell can have on another: Distinguishing "drivers" from "modulators." *Proceedings of the National Academy of Sciences*, *95*(12), 7121–7126. https://doi.org/10.1073/pnas.95.12.7121

Shosaku, A., & Sumitomo, I. (1983). Auditory neurons in the rat thalamic reticular nucleus. *Experimental Brain Research*, *49*(3), 432–442. https://doi.org/10.1007/BF00238784

Siegle, J. H., López, A. C., Patel, Y. A., Abramov, K., Ohayon, S., & Voigts, J. (2017). Open Ephys: An open-source, plugin-based platform for multichannel electrophysiology. *Journal of Neural Engineering*, *14*(4), 045003. https://doi.org/10.1088/1741-2552/aa5eea

Simm, G. M., de Ribaupierre, F., de Ribaupierre, Y., & Rouiller, E. M. (2017). Discharge properties of single units in auditory part of reticular nucleus of thalamus in cat. *Journal of Neurophysiology*, *63*(5), 1010–1021. https://doi.org/10.1152/jn.1990.63.5.1010

Taaseh, N., Yaron, A., & Nelken, I. (2011). Stimulus-Specific Adaptation and Deviance Detection in the Rat Auditory Cortex. *PLoS ONE*, *6*(8), e23369. https://doi.org/10.1371/journal.pone.0023369

Traub, R. D., Contreras, D., & Whittington, M. A. (2005). Combined Experimental/Simulation Studies of Cellular and Network Mechanisms of Epileptogenesis In Vitro and In Vivo. *Journal of Clinical Neurophysiology*, *22*(5), 330. https://doi.org/10.1097/01.WNP.0000179967.76990.25

Turner, B. H., & Herkenham, M. (1991). Thalamoamygdaloid Projections in the Rat: A Test of the Amygdala's Role in Sensory Processing. *THE JOURNAL OF COMPARATIVE NEUROLOGY*, *313295325*.

Ulanovsky, N., Las, L., & Nelken, I. (2003). Processing of low-probability sounds by cortical neurons. *Nature Neuroscience*, *6*(4), 391–398. https://doi.org/10.1038/nn1032

Villa, A. E. P. (1990). Physiological differentiation within the auditory part of the thalamic reticular nucleus of the cat. *Brain Research Reviews*, *15*(1), 25–40. https://doi.org/10.1016/0165-0173(90)90010-L

Visocky, V., Morris, B. J., Dunlop, J., Brandon, N., Sakata, S., & Pratt, J. A. (2022). Site-specific inhibition of the thalamic reticular nucleus induces distinct modulations in sleep architecture. *European Journal of Neuroscience*, *n/a*(n/a). https://doi.org/10.1111/ejn.15908

Weinberger, N. M. (2004). Specific long-term memory traces in primary auditory cortex. *Nature Reviews Neuroscience*, *5*(4), 279–290. https://doi.org/10.1038/nrn1366-c3

Willis, A. M., Slater, B. J., Gribkova, E. D., & Llano, D. A. (2015). Open-loop organization of thalamic reticular nucleus and dorsal thalamus: A computational model. *Journal of Neurophysiology*, *114*(4), 2353–2367. https://doi.org/10.1152/jn.00926.2014

Wimmer, R. D., Schmitt, L. I., Davidson, T. J., Nakajima, M., Deisseroth, K., & Halassa, M. M. (2015). Thalamic control of sensory selection in divided attention. *Nature*, *526*(7575), 705–709. https://doi.org/10.1038/nature15398

Winer, J. A. (1992). The Functional Architecture of the Medial Geniculate Body and the Primary Auditory Cortex. In D. B. Webster, A. N. Popper, & R. R. Fay (Eds.), *The Mammalian*

Auditory Pathway: Neuroanatomy (pp. 222–409). Springer. https://doi.org/10.1007/978-1-4612-4416-5_6

Winer, J. A. (2005). Decoding the auditory corticofugal systems. *Hearing Research*, *207*(1), 1–9. https://doi.org/10.1016/j.heares.2005.06.007

Wood, K. C., Angeloni, C. F., Oxman, K., Clopath, C., & Geffen, M. N. (2022). Neuronal activity in sensory cortex predicts the specificity of learning in mice. *Nature Communications*, *13*(1), Article 1. https://doi.org/10.1038/s41467-022-28784-w

Wood, K. C., Blackwell, J. M., & Geffen, M. N. (2017). Cortical inhibitory interneurons control sensory processing. *Current Opinion in Neurobiology*, *46*, 200–207. https://doi.org/10.1016/j.conb.2017.08.018

Yang, Y., Liu, D. Q., Huang, W., Deng, J., Sun, Y., Zuo, Y., & Poo, M. M. (2016). Selective synaptic remodeling of amygdalocortical connections associated with fear memory. *Nature Neuroscience*. https://doi.org/10.1038/nn.4370

Yen, C. T., Conley, M., Hendry, S. H., & Jones, E. G. (1985). The morphology of physiologically identified GABAergic neurons in the somatic sensory part of the thalamic reticular nucleus in the cat. *The Journal of Neuroscience: The Official Journal of the Society for Neuroscience*, *5*(8), 2254–2268. https://doi.org/10.1523/JNEUROSCI.05-08-02254.1985

Young, A., & Wimmer, R. D. (2017). Implications for the thalamic reticular nucleus in impaired attention and sleep in schizophrenia. *Schizophrenia Research*, *180*, 44–47. https://doi.org/10.1016/j.schres.2016.07.011

Yu, X.-J., Xu, X.-X., He, S., & He, J. (2009). Change detection by thalamic reticular neurons. *Nature Neuroscience*, *12*(9), 1165–1170. https://doi.org/10.1038/nn.2373

Yukie, M. (2002). Connections between the amygdala and auditory cortical areas in the macaque monkey. *Neuroscience Research*, *42*(3), 219–229. https://doi.org/10.1016/S0168-0102(01)00325-X

Zikopoulos, B., & Barbas, H. (2012). Pathways for Emotions and Attention Converge on the Thalamic Reticular Nucleus in Primates. *Journal of Neuroscience*, *32*(15), 5338–5350. https://doi.org/10.1523/JNEUROSCI.4793-11.2012

Znamenskiy, P., & Zador, A. M. (2013). Corticostriatal neurons in auditory cortex drive decisions during auditory discrimination. *Nature*, *497*(7450), 482–485. https://doi.org/10.1038/nature12077